

# Manganese catalysed synthesis of polyketones using hydrogen borrowing approach.

KULYABIN, P., MAGDYSYUK, O., NADEN, A.B., DAWSON, D.M.,  
PANCHOLI, K., WALKER, M., VASSALLI, M. and KUMAR, A.

2024

# Manganese Catalysed Synthesis of Polyketones Using Hydrogen Borrowing Approach

Pavel Kulyabin,<sup>†</sup> Oxana V. Magdysyuk,<sup>†</sup> Aaron B Naden,<sup>†</sup> Daniel M Dawson,<sup>†</sup> Ketan Pancholi,<sup>δ</sup> Matthew Walker,<sup>γ</sup> Massimo Vassalli,<sup>ζ</sup> and Amit Kumar<sup>†\*</sup>

<sup>†</sup>EaStCHEM, School of Chemistry, University of St Andrews, North Haugh, St Andrews, KY16 9ST, UK.

<sup>δ</sup> The Sir Ian Wood Building, Robert Gordon University, Garthdee Rd, Garthdee, Aberdeen, AB10 7GE, UK.

<sup>γ</sup>Centre for the Cellular Microenvironment, Advanced Research Centre, University of Glasgow, Glasgow, G116EW, UK.

<sup>ζ</sup> James Watt School of Engineering, University of Glasgow, Glasgow G12 8QQ, UK.

E-mail: [ak336@st-andrews.ac.uk](mailto:ak336@st-andrews.ac.uk)

**KEYWORDS.** *Manganese, pincer, polyketones, 1,4-diacetylbenzene, diol, dehydration, dehydrogenation, hydrogen borrowing*

**ABSTRACT:** We report here a new method to make polyketones from the coupling of diketones and diols using a manganese pincer complex. The methodology allows us to access a new type of polyketone (polyarylalkylketone) containing aryl, alkyl, and ether functionalities bridging the gap between the two classes of commercially available polyketones – aliphatic polyketones and polyaryletherketones. Using this methodology, twelve new polyketones have been synthesized and characterised using various analytical techniques to understand their chemical, physical, morphological, and mechanical properties. Based on previous reports and our studies, we suggest that the polymerization occurs via a hydrogen-borrowing mechanism that involves the dehydrogenation of diols to dialdehyde followed by aldol condensation of dialdehyde with diketones to form chalcone derivatives and their subsequent hydrogenation to form polyarylalkylketones.

## INTRODUCTION

Polyketones are high-performance thermoplastics with a wide range of applications in the automotive, electronics, electrical and medical industries.<sup>1,2</sup> Compared with the structure of polyolefins, polyketones contain additional  $C=O$  groups in the polymer backbone chains which due to its polarity imparts excellent mechanical properties, crystallinity, hydrophilicity, and surface properties.<sup>3</sup> Compared with polyamides, polyketones lack the  $NH$  group in the polymer backbone chain which makes it much less hygroscopic and less sensitive to moisture. Despite the excellent properties of polyketones, this class of polymer is relatively less studied. Aliphatic polyketones (POKs) are made from the reaction of palladium catalysed coupling of ethene and propene with CO (Figure 1A). Although the seminal reports on the synthesis of aliphatic polyketones (POK) date back to 1940s and 1950s using nickel,<sup>4-6</sup> and

1980s using palladium,<sup>7</sup> it was only in 1996 that POK was first commercialized by the Shell. However, the product was discontinued in 2000 due to reasons such as low demand, and difficulty in polymer processing. Nevertheless, due to the demand of the POK, the product was relaunched in 2015 by Hyosung (a company in South Korea). Another class of polyketones is aromatic polyketones that also contain ether linkages and is known as polyaryletherketone (PAEK).<sup>8</sup> The most common types of polymers from this class are polyetheretherketone (PEEK) and polyetherketoneketone (PEKK). These polymers have been commercialized since the 1980s and exhibit exceptional mechanical properties and chemical resistance. Their performance is considered the highest among all thermoplastics and as a result they are used in demanding applications such as aerospace, oil and gas drilling, and medical implants.<sup>1,2</sup> Nevertheless, these polymers are difficult to process and there is an ongoing need to develop new materials of this class bearing higher processability and keeping similar levels of thermal and mechanical properties. Additionally, in comparison to aliphatic polyketones (POK), aromatic polyketones or polyaryletherketones (PAEK) are around ten times more expensive due to the use of more expensive feedstock/reagents. For example, polyetheretherketone (PEEK) is made from the nucleophilic substitution of 4,4'-difluorobenzophenone by the disodium salt of hydroquinone in the presence of a polar aprotic solvent such as diphenylsulfone at 300 °C (Figure 1B). Similarly, PEKK (polyetherketoneketone) can be made via electrophilic polycondensation of diphenyl ether with mixtures of terephthaloyl chloride in the presence of AlCl<sub>3</sub> catalyst (Figure 1C). Another drawback of these methodologies is limited substrate scope due to the lack of commercial or inexpensive functional monomers of this type. It is noteworthy that polyaryletherketones have been considered for several emerging applications in the recent past such as in the containment vessel for nuclear power plants,<sup>9,10</sup> cryogenic hydrogen storage,<sup>11</sup> and separators for batteries.<sup>12</sup> Thus, there is a need to develop new methods to access diverse polyaryletherketones that could offer excellent thermal, physical, and mechanical properties and can be produced and processed economically.

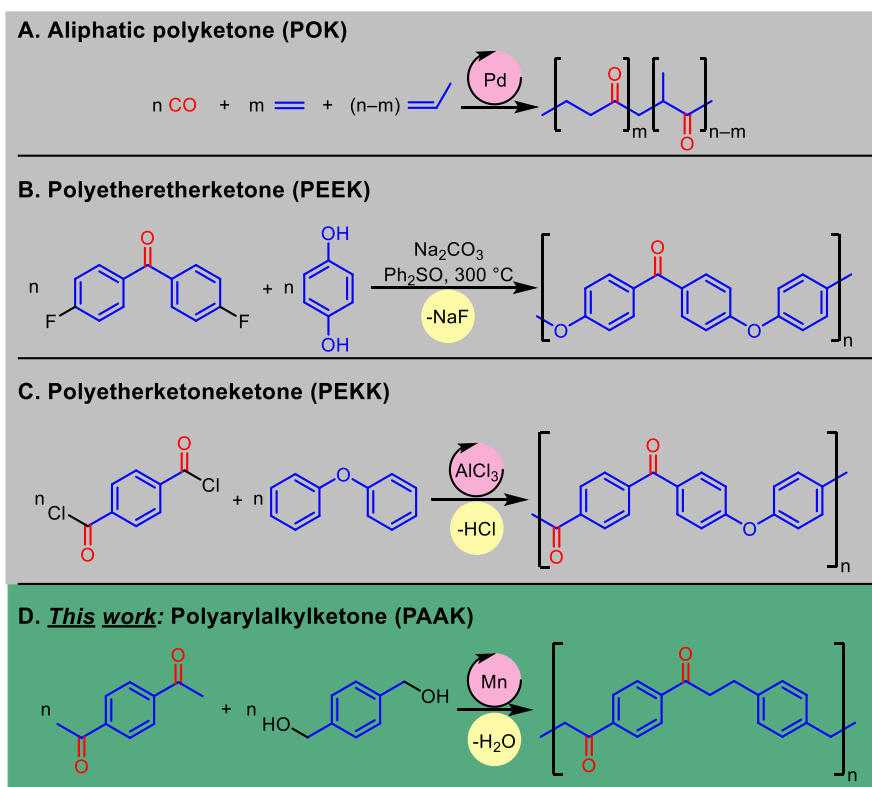


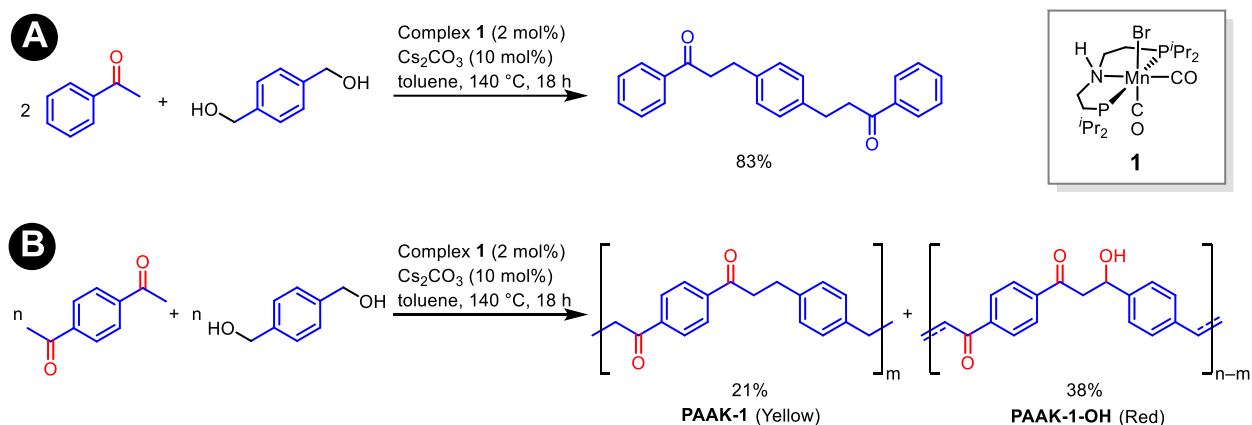
**Figure 1.** Methods for the synthesis of previously reported polyketones – aliphatic polyketone (POK), polyetheretherketone (PEEK), polyetherketoneketone (PEKK), and the polyketone reported herein – polyaryllalkylketone (PAAK).

It has been suggested in the past that the presence of alkyl chains in the aliphatic ketones provides the necessary flexibility for desirable processing whereas the presence of aromatic groups in polyaryletherketones (PAEK) provides exceptional mechanical properties.<sup>13</sup> Therefore, we hypothesize that a polyketone containing both aryl and alkyl groups - polyaryllalkylketone (PAAK) can fill the gap between aliphatic and aromatic polyketones and might provide a polymer that can be easily processed and have excellent mechanical properties at the same time.

The concept of *acceptorless dehydrogenative* (where H<sub>2</sub> gas is released as a byproduct) and *borrowing hydrogen* (where the released H<sub>2</sub> is utilized to hydrogenate an intermediate in the reaction) catalysis is an atom-economic approach for the synthesis of organic compounds.<sup>14</sup> The area has led to the discovery of several green transformations to make prevalent functional groups/compounds such as alcohols,<sup>15–17</sup> hydroxy phosphines,<sup>18</sup> ketones,<sup>19,20</sup> esters,<sup>21</sup> amides,<sup>22–24</sup> carboxylic acids,<sup>25</sup> carbamates,<sup>26,27</sup> ureas,<sup>28–30</sup> amines,<sup>31,32</sup> acetals,<sup>33</sup> imines,<sup>34,35</sup> and heterocycles.<sup>36</sup> These strategies have also been utilized for the synthesis of polymers such as polyesters<sup>37,38</sup> and polyamides,<sup>38–40</sup> and more recently polyureas<sup>41–44</sup> and polyethylenimines<sup>45</sup> by us and others. Directly relevant to this report is the C-alkylation of ketones using a number of transition metal-based catalysts such as ruthenium, manganese, and iron as recently reviewed by several groups.<sup>46–52</sup> Despite several reports on this chemical transformation, the study has remained limited to the synthesis of small molecules. We envisioned that this concept might allow us to make the hypothesised polyaryllalkylketones (PAAK) from the metal catalysed coupling of

diacetylbenzene and diols for the first time (Figure 1D). Since some diols can be prepared from renewable feedstocks, this approach can also allow us to make semi-renewable aromatic polyketones for the first time.

## RESULTS AND DISCUSSION

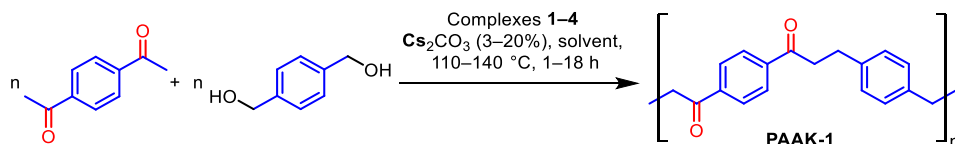


**Scheme 1.** Coupling of acetophenone (A) or 1,4-diacetylbenzene (B) with 1,4-benzenedimethanol in the presence of the precatalyst **1**.

We started our investigation by studying a model reaction - coupling of acetophenone (0.4 M) with 1,4-benzenedimethanol (0.2 M) in the presence of 2 mol% complex **1** and 10 mol% Cs<sub>2</sub>CO<sub>3</sub> in toluene (140 °C, 18 h). The choice of our initial catalytic conditions was inspired by previous reports<sup>46</sup> on the transition-metal catalysed C-alkylation of ketones using alcohols especially the one by Beller where reactions in toluene were as effective as that in 1,4-dioxane and *tert*-amyl alcohol.<sup>53</sup> Remarkably, this led to the formation of the expected diketone in 83% yield which was characterised by NMR and IR spectroscopy (Scheme 1A). Motivated by this initial result, we studied the coupling of 1,4-diacetylbenzene (0.2 M) with 1,4-benzenedimethanol (0.2 M) under identical reaction conditions. The reaction led to the isolation of a mixture of yellow (21% yield) and red (38% yield) solids that could be physically separated (Scheme 1B). Both these solids were found to be insoluble in common solvents such as toluene, DCM, acetone, chloroform, THF, chlorobenzene, water, DMF, DMSO, and trifluoroacetic acid because of which we could not employ solution-state NMR spectroscopy or GPC (Gel Permeation Chromatography) to analyse the chemical structure of these materials. The IR spectrum of the yellow solid showed signals at 3049 and 2922 cm<sup>-1</sup> corresponding to aromatic and aliphatic C-H stretching frequencies (Figure S4, see ESI). The presence of aromatic rings was further confirmed by signals at 1601 and 1508 cm<sup>-1</sup> characteristic of aromatic C=C stretches. A sharp signal at 1674 cm<sup>-1</sup> characteristic of an aromatic C=O (ketone) stretching frequency was observed. These spectral assignments are suggestive of the structure of the polymer to be **PAAK-1** and are also in agreement with a reported polyketone made from the reaction of styrene and CO that contained phenyl groups, CH<sub>2</sub> linkages, and ketone groups.<sup>54</sup> This was further corroborated by a solid-state <sup>13</sup>C CP MAS NMR spectrum that showed signals at δ 29-70, 128-151, and 199 ppm characteristic of alkyl, aryl, and ketone regions confirming the structure of **PAAK-1** (Figure 2B). The IR spectrum of the red solid looked very similar to that of the yellow solid except for the two distinctive signals at 1605, and 1373

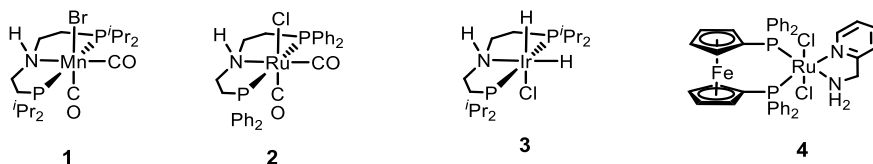
cm<sup>-1</sup> which are attributed to olefinic C=C and C–O bonds respectively (Figure S4, see ESI). Additionally, a much broader signal at 3348 cm<sup>-1</sup> corresponding to the O–H stretch was also observed. Based on these observations, we suggest that the red solid is a polyaryalkylketone with some double bonds and O–H groups characterized to be **PAAK-1-OH**. We hypothesized that the elimination of water from **PAAK-1-OH** might be facilitated by the presence of a proton source in the reaction mixture that would convert the hydroxy group into a better leaving group (water) or by using a polar protic solvent. Indeed, performing the reaction in *tert*-amyl alcohol (*t*AmOH) solvent resulted in the selective formation of **PAAK-1** in 89% yield (Table 1, entry 1, Figure 2A). Performing the same reaction in the presence of ruthenium<sup>55,56</sup> and iridium<sup>52</sup> complexes **2-4**, which have been previously reported for the catalytic dehydrogenative transformations led to relatively lower yields of **PAAK-1** (Table 1, entries 2-4). We then studied the effect of various catalytic conditions e.g. concentration of starting materials and base, size of the reaction vessel to the yield of the reaction (see Table S1 in the ESI for full details). Interestingly, using 1 mol% complex **1** also led to the isolation of **PAAK-1** in 85% yield (entry 5). Further reducing the catalytic loading to 0.5 mol% led to a lower but still very good, isolated yield (70%) of **PAAK-1** (entry 6). Considering the insolubility of **PAAK-1**, we speculated that the use of a higher amount of solvent could result in the formation of a higher molecular weight polymer leading to higher thermal stability. Indeed, conducting a reaction at 0.1 M concentration of 1,4-diacetylbenzene and 1,4-benzenedimethanol led to the formation of **PAAK-1** in 85% yield which is similar to that conducted at 0.2 M concentration (entry 1) although a higher *T*<sub>d</sub> (decomposition temperature, 373 °C) was observed in case of 0.1 M concentration in comparison to that of 0.2 M concentration (*T*<sub>d</sub> = 356 °C) supporting our hypothesis (entries 5, and 7). Decreasing the concentration further to 0.05 M did not make any significant difference in the yield or *T*<sub>d</sub> of the isolated polymer in comparison to that of 0.1 M (entry 8). Changing the size of the reaction vessel from 100 mL to 15 mL did not make any significant difference in the yield and thermal stability of the polymer (entry 9). Increasing the amount of Cs<sub>2</sub>CO<sub>3</sub> to 20 mol% (entry 10) led to a slight increment in yield (90%) whereas decreasing the amount of Cs<sub>2</sub>CO<sub>3</sub> reduced the yield (80%, entry 11) suggesting the significance of base in the coupling process.

**Table 1.** Optimisation of catalytic conditions for the coupling of 1,4-diacetylbenzene and 1,4-benzenedimethanol.<sup>a</sup>



Entry	Complex (mol%)	Conc.	Cs <sub>2</sub> CO <sub>3</sub> (mol%)	Time (h)	Yield <sup>b</sup> , %	<i>T</i> <sub>d</sub> <sup>c</sup> , °C
1 <sup>d</sup>	<b>1</b> (2 mol%)	0.2 M	10%	18	89	338
2 <sup>d</sup>	<b>2</b> (2 mol%)	0.2 M	10%	18	< 5	n.d.
3 <sup>d</sup>	<b>3</b> (2 mol%)	0.2 M	10%	18	51	353
4 <sup>d</sup>	<b>4</b> (2 mol%)	0.2 M	10%	18	17	n.d.
5 <sup>d</sup>	<b>1</b> (1 mol%)	0.2 M	10%	18	87	356
6 <sup>d</sup>	<b>1</b> (0.5 mol%)	0.2 M	10%	18	70	348

7	<b>1</b> (1 mol%)	0.1 M	10%	18	85	373
8 <sup>e</sup>	<b>1</b> (1 mol%)	0.05 M	10%	18	86	342
9 <sup>f</sup>	<b>1</b> (1 mol%)	0.1 M	10%	18	73	342
10	<b>1</b> (1 mol%)	0.1 M	20%	18	90	369
11	<b>1</b> (1 mol%)	0.1 M	3%	18	80	335
12 <sup>g</sup>	<b>1</b> (1 mol%)	0.1 M	10%	18	67	328
13	<b>1</b> (1 mol%)	0.1 M	10%	2	89	363
14	<b>1</b> (1 mol%)	0.1 M	10%	1	81	343
15	None	0.1 M	10%	18	<10	396
16	<b>1</b> (1 mol%)	0.1 M	none	18	none	n.d.
17	Mn(CO) <sub>5</sub> Br (1 mol%)	0.1 M	10%	18	< 5	n.d.
18	Mn(CO) <sub>5</sub> Br (1 mol%) + PPh <sub>3</sub> (3 mol%)	0.1 M	10%	18	< 5	n.d.



<sup>a</sup>General reaction conditions: 1,4-diacetylbenzene (0.5 mmol), 1,4-benzenedimethanol (0.5 mmol), 100 mL ampule with J-Young's valve, temperature 140 °C, *t*AmOH. <sup>b</sup>All yields are isolated yields. <sup>c</sup>T<sub>d</sub> stands for the decomposition temperature calculated from TGA (thermogravimetric analysis) as a temperature of 10% weight loss. n.d. stands for not detected. <sup>d</sup>1 mmol of 1,4-diacetylbenzene and 1,4-benzenedimethanol were used. <sup>e</sup>10 mL of *t*AmOH were used. <sup>f</sup>Reaction in 15 mL pressure vessel. <sup>g</sup>Reaction at 110 °C.

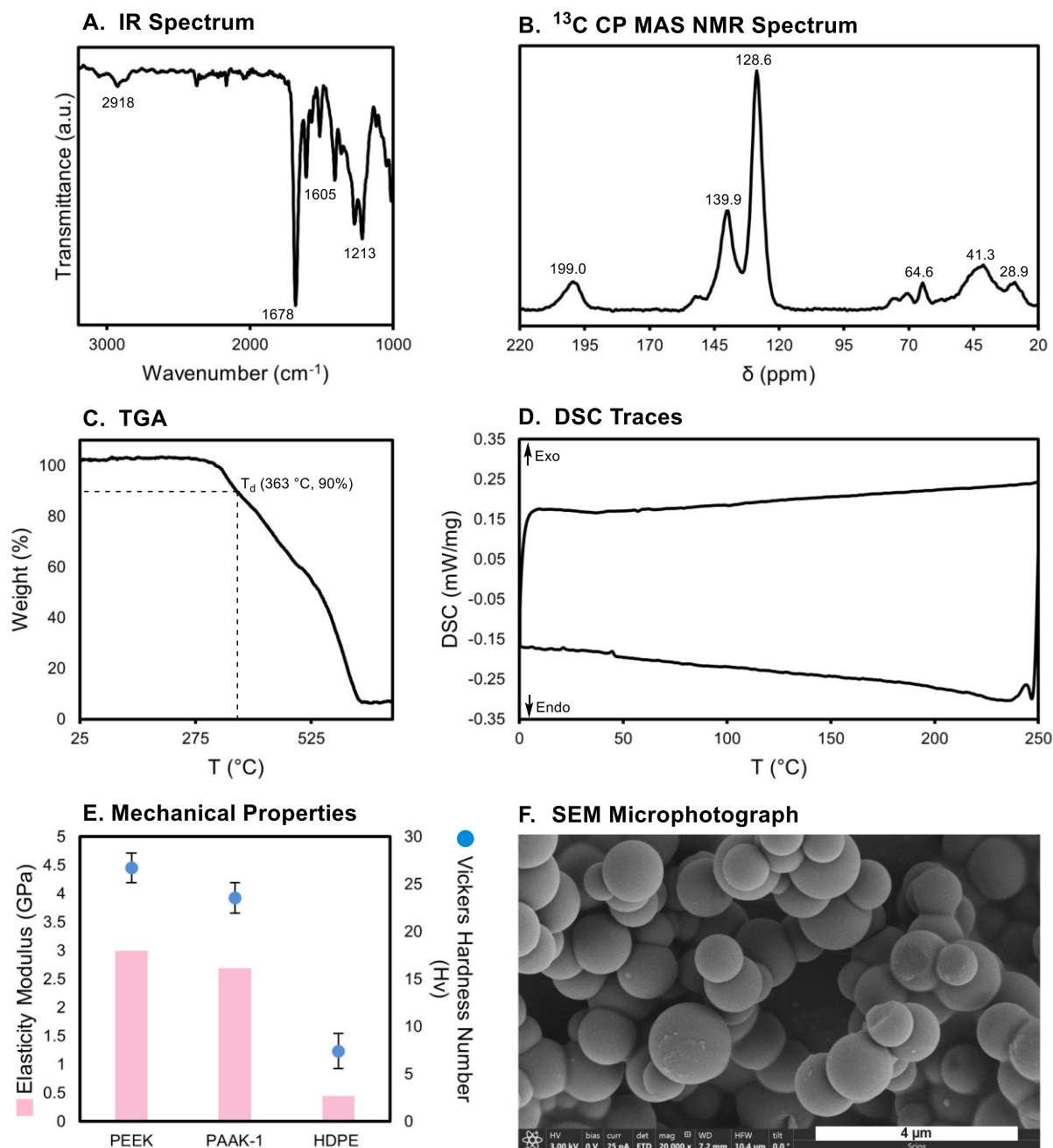
Lowering the temperature to 110 °C reduced the yield to 67% (entry 12). Interestingly, studying the time profile of the reaction suggested that the reaction reaches completion in 2 h leading to 89% yield of the **PAAK-1** whereas 81% yield is obtained in 1 h (entries 13, 14). Finally, when the reaction was conducted in the absence of complex **1** and by using just Cs<sub>2</sub>CO<sub>3</sub> (10 mol%), a solid was isolated in <10% yield (entry 15). Based on the IR spectrum and thermal studies of the isolated material, we suggest that the obtained product is a polymer resulting from the self-condensation of 1,4-diacetylbenzene (see ESI, Figure S43-44). Interestingly, no conversion of any starting material was obtained when the reaction was conducted just in the presence of complex **1** without using any base (entry 16). Additionally, conducting the reaction in the presence of Mn(CO)<sub>5</sub>Br (1 mol%) and the combination of Mn(CO)<sub>5</sub>Br (1 mol%) + PPh<sub>3</sub> (3 mol%) resulted in only less than 5% yield of the polyketone material (entries 17, 18) suggesting that the manganese-MACHO pincer complex (**1**) is important in the catalytic process. Thus, the optimised catalytic conditions are: complex **1** (1 mol%), Cs<sub>2</sub>CO<sub>3</sub> (10 mol%), 1,4-diacetylbenzene (0.1 M), 1,4-benzenedimethanol (0.1 M), 140 °C, 2h, *t*AmOH (entry 13).

Thermal properties of the polymer were investigated by TGA (Thermogravimetric Analysis) and DSC (Differential Scanning Calorimetry) which revealed that the **PAAK-1** is a thermoset plastic with a decomposition temperature of 363 °C (T<sub>d</sub>, 10% weight loss) as no melting temperature could be observed (Figures 2C, D). This is similar to a polyketone containing both aromatic and aliphatic chains prepared using another method and was found to be a

thermoset.<sup>57</sup> This was further confirmed by the powder XRD study that revealed that the polymer is amorphous in nature (Figure S38, ESI).

To get some understanding of the mechanical properties of the synthesized polyketone (**PAAK-1**), we processed the polymer using hot-compression to prepare a film of 2 mm thickness which was used to study the load-displacement curve using nanoindentation (Section 2, ESI). The elasticity modulus and Vickers hardness of the **PAAK-1** were measured to be 2.7 GPa and 23.6 HV (Figure 2E). For comparison, the nanoindentation study was conducted on a commercial sample of PEEK and HDPE (High-Density Polyethylene) under identical conditions. Remarkably, the elasticity modulus and Vickers hardness number of the **PAAK-1** were found to be comparable with the commercial sample of PEEK (3 GPa, and 26.7 HV), and higher than those measured for the HDPE (0.45 GPa, and 7.4 HV). These numbers are also consistent with previous reports in the literature on the measurement of elasticity modulus and Vickers hardness of commercial PEEK and HDPE.<sup>58-60</sup>

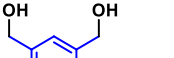
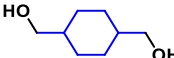
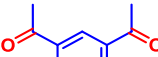
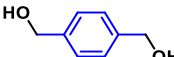
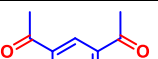
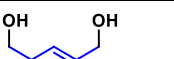
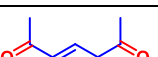
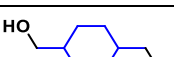
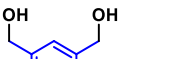
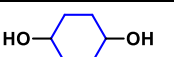
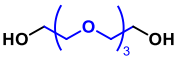
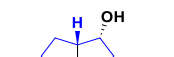
The morphology of polymers plays important roles in polymer processing and their applications and spherical particles are desirable for various processing techniques such as selective laser sintering which is used for 3-D printing or additive manufacturing which can also be used to process polyketones.<sup>61</sup> Polyketones can also be used in engineered powder as was recently demonstrated by an electronics manufacturing company, Jabil Inc., which has launched PK5000 for additive manufacturing. This polyketone has desirable chemical and mechanical properties such as high-impact strength, and high abrasion resistance in comparison to nylons.<sup>62,63</sup> A study of the morphology of **PAAK-1** (made using Table 1, entry 8) using SEM (Scanning Electron Microscope) showed granular structures composed of small spherical particles of size around 1.3 - 1.5  $\mu\text{m}$  (Figure 2F).



**Figure 2.** Characterization of PAAK-1. **A**, Infrared spectrum (ATR-FTIR). **B**, <sup>13</sup>C CP MAS NMR spectrum. **C**, Mass loss as a function of temperature. **D**, DSC plot. **E**, Elasticity modulus and Vickers Hardness Number of commercial PEEK, polyketone **PAAK-1**, and HDPE. **F**, SEM microphotograph.

Having optimized the reaction conditions for the synthesis of **PAAK-1** (polyaryllalkylketone), we studied the substrate scope of our methodology to understand the structure property relationships. As described in Table 2 (entry 2), the coupling of 1,4-diacetylbenzene and 1,3-benzenedimethanol led to the formation of the corresponding polyaryllalkylketone in a 77% yield. However, a lower yield of polyketone (41%) was obtained from the coupling of 1,4-diacetylbenzene and

**Table 2.** Substrate scope for the synthesis of polyketones from diketones and diols.

$n \text{ } \begin{array}{c} \text{O} \quad \text{O} \\ \parallel \quad \parallel \\ \text{R} \end{array} + n \text{ HO-CH}_2\text{-R}'\text{-CH}_2\text{-OH} \xrightarrow[2-18 \text{ h, } 140 \text{ }^\circ\text{C, tAmOH}]{\text{1 (1 mol\%), base (10-100 mol\%)}} \left[ \begin{array}{c} \text{O} \quad \text{O} \\ \parallel \quad \parallel \\ \text{R} \end{array} \text{-CH}_2\text{-CH}_2\text{-R}'\text{-CH}_2\text{-CH}_2 \right]_n + \text{H}_2\text{O}$						
Entry	Diketone	Diol	Yield (%)	T <sub>d</sub> (°C)	Morphology	Crystallinity
1. <sup>a</sup>			89 95 <sup>d</sup>	363 397 <sup>d</sup>	Spherical (size ~1.5 μm)	Amorphous
2. <sup>a</sup>			77	351	Spherical (size ~0.5 μm)	Amorphous (unknown crystalline component) <sup>e</sup>
3. <sup>a,b</sup>			41	369	Spherical (size ~3 μm)	Amorphous (unknown crystalline component)
4. <sup>a</sup>			98	321	Spherical agglomerates (0.2-2 μm)	Amorphous (unknown crystalline component) <sup>e</sup>
5. <sup>a</sup>			97	338	Spherical agglomerates (0.1-2 μm)	Amorphous (unknown crystalline component) <sup>e</sup>
6. <sup>a,b</sup>			99	357	Spherical agglomerates (0.1-1 μm)	Amorphous
7. <sup>a</sup>			89 99 <sup>d</sup>	362 371 <sup>d</sup>	Spherical (size ~2 μm)	Amorphous (unknown crystalline component) <sup>e</sup>
8. <sup>a</sup>			79	365	Spherical (size ~1 μm)	Amorphous (unknown crystalline component) <sup>e</sup>
9. <sup>a,b</sup>			71 99 <sup>d</sup>	383 384 <sup>d</sup>	Non-homogeneous agglomerates	Amorphous (unknown crystalline component) <sup>e</sup>
10. <sup>c</sup>			57	363	Spherical (size ~2 μm)	Amorphous
11. <sup>c</sup>			52	375	Non-homogeneous agglomerates	Amorphous
12. <sup>c</sup>			64	381	Non-homogeneous agglomerates	Amorphous

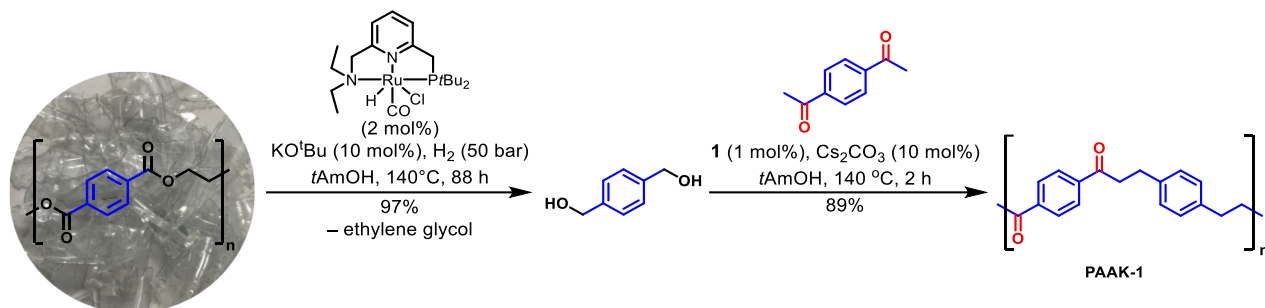
<sup>a</sup>Reaction conditions: diketone (0.5 mmol), diol (0.5 mmol), **1** (2.5 mg, 0.005 mmol), Cs<sub>2</sub>CO<sub>3</sub> (16.5 mg, 0.05 mmol) in 100 mL J-Young's flask, temperature 140 °C, 2 h. All yields are isolated yields. <sup>b</sup>18 h. <sup>c</sup>tBuOK (56 mg, 0.5 mmol), 18 h. All yields are isolated yields. T<sub>d</sub> corresponds to the temperature of 10% weight loss. <sup>d</sup>Reaction conducted in the presence of H<sub>2</sub> (Section 1.8, ESI). <sup>e</sup>The unknown crystalline component did not match with either starting

1,4-cyclohexanedimethanol (entry 3). Remarkably, excellent yields of polyketones were obtained from the coupling of 1,3-diacetylbenzene with various diols (entries 4-6). To introduce ether functionality as in the case of polyaryletherketones (PAEKs), we used 4-acetylphenyl ether as a diketone feedstock. Remarkably, we were able to couple 4-acetylphenyl ether with various aromatic and aliphatic diols to make polyketones in moderate to excellent yields as described in Table 2, entries 7–12. Of particular significance is the use of D-Isosorbide as a diol (entry 12) which is a commercially available sugar derivative and can also be made from cellulose making the corresponding polyketone to be semi-renewable.<sup>64</sup> The polymers were characterized by IR spectroscopy, and <sup>13</sup>C CP MAS solid state NMR spectroscopy that showed signals corresponding to C=O, aromatic, and aliphatic groups (see ESI, section 1.5). The decomposition temperatures ( $T_d$ ), calculated as a temperature of 10% weight loss from TGA (thermogravimetric analysis), were found to be in the range of 321–383 °C as described in Table 2. This was lower than what was recorded for a commercial PEEK sample ( $T_d$  = 557 °C, see ESI, Figure S141). The morphology of polyketones for most cases showed agglomerates of spherical particles of size in the range of 0.2–3  $\mu$ m as described in Table 2. In some cases, the particle sizes were more uniform (e.g. entry 1) than others (e.g. entry 4) whereas in some cases non-homogeneous agglomerates were observed. The powder XRD studies showed that all the polymers are amorphous in nature with some polymers containing unidentified components of crystallinity (Table 2, also see ESI for full details, section 1.14).

We envisioned that since the product precipitates out from the reaction medium whereas the catalyst is likely to remain soluble, presents an opportunity to test the recyclability of the catalyst. After the reaction conducted as described in Table 2, entry 7 (coupling of 4-acetylphenyl ether, 0.5 mmol and 1,4-benzendimethanol, 0.5 mmol that led to the isolation of PAAK-7 in 89% yield), the *t*AmOH solution was transferred to another Young's flask containing 4-acetylphenyl ether (0.5 mmol), 1,4-benzendimethanol (0.5 mmol), and Cs<sub>2</sub>CO<sub>3</sub> (10 mol%). The reaction mixture was then refluxed at 140 °C for 2 h. This resulted in the isolation of PAAK-7 in 55% yield showing an identical IR spectrum to the polymer isolated in the first batch (see Figure S126 in the ESI). Interestingly, when the recycling study was performed without adding base in the second stage, no precipitate was observed suggesting the involvement of base in steps other than generating the active species from the precatalyst **1**. The role of the base in lowering the barriers for the (de)hydrogenation reactions catalysed by analogous pincer complexes has been reported in the past.<sup>65,66</sup>

In pursuit of methods to make (semi)renewable plastics, we envisioned if a polyketone can be made from a diol sourced from the depolymerisation of waste plastic such as PET (polyethylene terephthalate). To achieve this, we carried out a two-step process where PET waste (sourced from a plastic bottle) was hydrogenatively depolymerised in a pressure reactor using the Milstein's ruthenium PNN catalyst (**5**, 2 mol%, and KO<sup>t</sup>Bu, 10 mol%) in *t*AmOH solvent to form 1,4-benzenedimethanol and ethylene glycol in approximately quantitative yields as confirmed by the <sup>1</sup>H NMR spectroscopy. Analogous reaction on the hydrogenative depolymerisation of PET has been reported by Robertson,<sup>67</sup> and Klankermayer.<sup>68</sup> The mixture of 1,4-benzendimethanol and *t*AmOH were then separated from ethylene glycol by extraction in DCM/water to which 1,4-diacetylbenzene, manganese complex **1** (1 mol%), and Cs<sub>2</sub>CO<sub>3</sub> (10 mol%) were added and the reaction mixture was heated for 2 h at 140 °C as described in Table 2. This led to the isolation of **PAAK-1** in 85% yield (Scheme 2). The reaction where 1,4-benzenedimethanol was not separated from ethylene glycol led

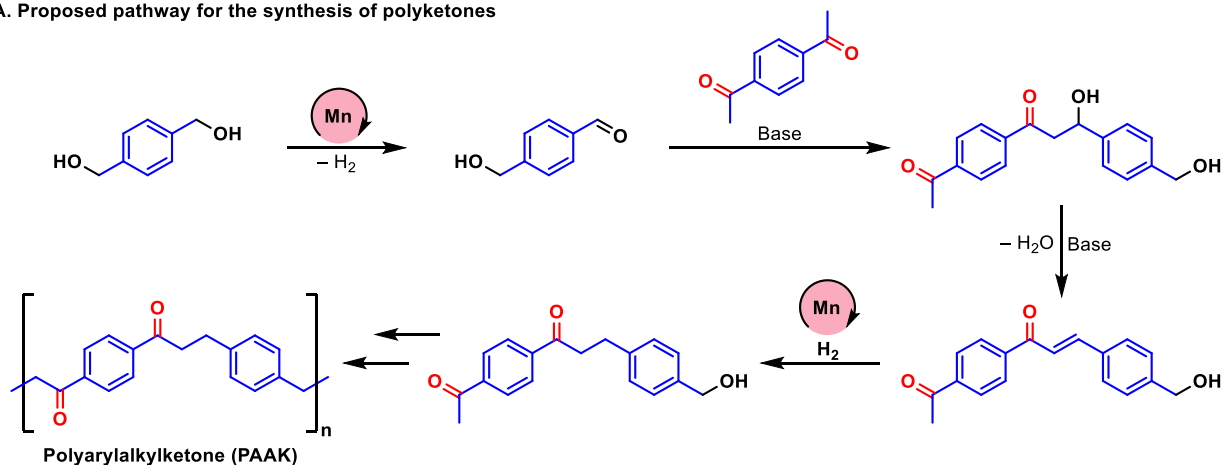
to the formation of a polyketone in only 21% yield that contained hydroxyl groups and double bonds according to the IR spectroscopy.



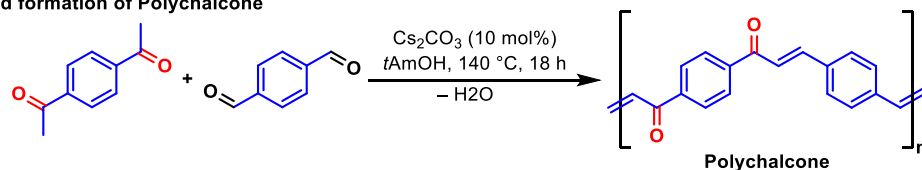
**Scheme 2.** Synthesis of polyketone **PAAK-1** from 1,4-benzendimethanol produced from the hydrogenation of a waste plastic bottle.

Mechanisms for the coupling of ketone and alcohols to form alkylated ketones using analogous pincer complexes have been studied using both experiments and DFT computation.<sup>69,70</sup> Based on the previous studies, we suggest that the reaction proceeds via a “hydrogen-borrowing” mechanism involving (i) metal-catalysed dehydrogenation of alcohol to aldehyde, (ii) base-catalysed aldol condensation of aldehyde with ketone to form a chalcone type derivative, and (iii) metal-catalysed hydrogenation of C=C bond to form an alkylated ketone. The continuation of the process leads to the formation of polyketones as outlined in Figure 2A. We conducted a few experiments to verify this proposal. Analysis of the mother liquor upon precipitation of polymer in case of Table 1, entry 6 by NMR spectroscopy showed the presence of phenylcarbonyl, phenylenemethanol, and 1-phenyl-ethanol end groups and 1,3-diphenylpropanone fragments (Figure S46, S47 in the ESI). No volatile oligomers were detected by GC-MS. These intermediates support the mechanism outlined in Figure 2A. Additionally, performing a reaction of terephthalaldehyde with 1,4-diacetylbenzene in the presence of 20 mol% Cs<sub>2</sub>CO<sub>3</sub> led to the formation of polychalcone in 93% yield (Figure 3B). This suggests our proposal that Cs<sub>2</sub>CO<sub>3</sub> is sufficient to catalyse the aldol condensation steps whereas manganese is needed for the catalytic (de)hydrogenation steps. As described in the mechanism (Figure 3A), a stoichiometric evolution of hydrogen gas is not observed as it gets consumed in the subsequent hydrogenation step. In most cases, we observe less than 1 mL of gas. Analysis of this gas by the GC (Thermal Conductivity Detector) confirmed it to be pure H<sub>2</sub> supporting our mechanistic proposal (Figure S127, see ESI). Furthermore, we also demonstrated that the precatalyst **1** is capable of the hydrogenation of C=C in chalcone by removing H<sub>2</sub> from the diol under the optimised reaction conditions making dihydrochalcone in 46% yield (Figure 3C). We then hypothesized that conducting the catalytic reactions in the presence of hydrogen atmosphere (1 bar) might ensure the hydrogenation of any remaining C=C bond in the polyketone chain and improve the yield and thermal properties of the polymers. Indeed, performing the synthesis of **PAAK-1** in the presence of a hydrogen atmosphere (1 bar) resulted in a higher yield (95% vs 89%) and higher thermal stability (T<sub>d</sub> = 397 °C vs 363 °C) as described in Table 2, entry 1 (Section 1.8, ESI). A similar result was obtained for PAAK-7 (Table 2, entry 7).

### A. Proposed pathway for the synthesis of polyketones



### B. Base-catalysed formation of Polychalcone



### C. Hydrogenation of *trans*-chalcone under reaction condition

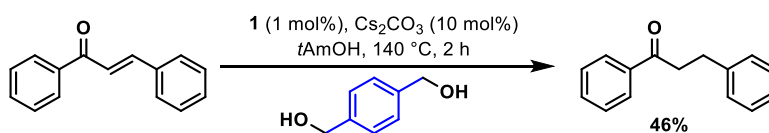


**Figure 3.** Proposed pathway for the synthesis of polyketones (A), and control experiments (B,C) .

## CONCLUSIONS

In conclusion, we have demonstrated the synthesis of a new class of polyketones called polyarylalylketones (PAAK) using the hydrogen-borrowing concept that has not been used for the synthesis of polyketones before. The present methodology allows us to access polyketones with aryl and alkyl functionalities with the potential of having properties in between aliphatic polyketones and aromatic polyketones (polyaryletherketones). Among the studied catalysts, the manganese pincer complex **1** was found to be the best precatalyst for this process affording high yields using 0.5-1.0 mol% catalytic loading and in the reaction time as low as 2 h. Using the reported methodology, we have been able to synthesize 12 new polyketones in moderate to excellent yields from different diketones and diols including a renewable diol and an example where the diol was produced from the hydrogenation of PET (sourced from waste plastic bottles). Due to the insolubility that is characteristic of polyketones, the isolated polymers were characterised by IR and solid-state NMR spectroscopy, powder XRD, SEM, TGA, and DSC studies. Additionally, the elasticity modulus and Vickers hardness numbers for the **PAAK-1** estimated by the nanoindentation studies were found to be comparable with a commercial sample of PEEK and higher than a commercial HDPE sample. Based on previous studies and conducted experiments herein, we suggest that the polymerization occurs via the hydrogen-borrowing mechanism as outlined in Figure 2A.

## ACKNOWLEDGEMENTS

This research is funded by a UKRI Future Leaders Fellowship (MR/W007460/1). We gratefully acknowledge funding from the EPSRC through grants EP/L017008/1, EP/R023751/1 and EP/T019298/1. We also thank Dr. Julia Payne for her assistance in initial powder XRD studies.

## REFERENCES

- (1) Qin, L.; Yao, S.; Zhao, J.; Zhou, C.; Oates, T. W.; Weir, M. D.; Wu, J.; Xu, H. H. K. Review on Development and Dental Applications of Polyetheretherketone-Based Biomaterials and Restorations. *Materials*. 2021.
- (2) Vavasori, A.; Ronchin, L. Polyketones: Synthesis and Applications. In *Encyclopedia of Polymer Science and Technology*; 2017; pp 1–41.
- (3) Sommazzi, A.; Garbassi, F. Olefin-Carbon Monoxide Copolymers. *Prog. Polym. Sci.* **1997**, *22*, 1547–1605.
- (4) Ballauf, F., Bayer, O. and Leichmann, L., G. *Pat. No. 863,711, 1941*.
- (5) Reppe, W. and Mangini, A., G. *Pat. No. 880,297, 1948*.
- (6) Reppe, W. and Mangini, A. *US Pat. No. 2,577,208, 1951*.
- (7) Sen, A.; Lai, T. W. Novel Palladium(II)-Catalyzed Copolymerization of Carbon Monoxide with Olefins. *J. Am. Chem. Soc.* **1982**, *104*, 3520–3522.
- (8) Maloo, L. M.; Toshniwal, S. H.; Reche, A.; Paul, P.; Wanjari, M. B. A Sneak Peek Toward Polyaryletherketone (PAEK) Polymer: A Review. *Cureus* **2022**, *14*, e31042.
- (9) Ding, R.; Xu, L.; Li, J.; Liao, J.; Wang, J.; Wang, Z.; Ma, H. Investigation and Life Expectancy Prediction on Poly(Ether-Ether-Ketone) Cables for Thermo-Oxidative Aging in Containment Dome of Nuclear Power Plant. *Polym. Test.* **2021**, *103*, 107362.
- (10) Teng, R.; Wang, H.; Qu, M.; Zhou, G. Synthesis of Amorphous Poly (Aryl Ether Ketone) Resin

- and Its Anti-Irradiation Properties under Gamma Ray. *ChemistrySelect* **2023**, *8*, e202204784.
- (11) Flanagan, M.; Grogan, D. M.; Goggins, J.; Appel, S.; Doyle, K.; Leen, S. B.; Ó Brádaigh, C. M. Permeability of Carbon Fibre PEEK Composites for Cryogenic Storage Tanks of Future Space Launchers. *Compos. Part A Appl. Sci. Manuf.* **2017**, *101*, 173–184.
- (12) Li, D.; Shi, D.; Feng, K.; Li, X.; Zhang, H. Poly (Ether Ether Ketone) (PEEK) Porous Membranes with Super High Thermal Stability and High Rate Capability for Lithium-Ion Batteries. *J. Memb. Sci.* **2017**, *530*, 125–131.
- (13) Yonezawa, N.; Okamoto, A. Synthesis of Wholly Aromatic Polyketones. *Polym. J.* **2009**, *41*, 899–928.
- (14) Gunanathan, C.; Milstein, D. Applications of Acceptorless Dehydrogenation and Related Transformations in Chemical Synthesis. *Science* **2013**, *341*.
- (15) El-Sepelgy, O.; Matador, E.; Brzozowska, A.; Rueping, M. C-Alkylation of Secondary Alcohols by Primary Alcohols through Manganese-Catalyzed Double Hydrogen Autotransfer. *ChemSusChem* **2019**, *12*, 3099–3102.
- (16) Tang, J.; He, J.; Zhao, S.-Y.; Liu, W. Manganese-Catalyzed Chemoselective Coupling of Secondary Alcohols, Primary Alcohols and Methanol. *Angew. Chem. Int. Ed.* **2023**, *62*, e202215882.
- (17) Polidano, K.; Williams, J. M. J.; Morrill, L. C. Iron-Catalyzed Borrowing Hydrogen  $\beta$ -C(Sp<sup>3</sup>)-Methylation of Alcohols. *ACS Catal.* **2019**, *9*, 8575–8580.
- (18) Sun, F.; Chen, X.; Wang, S.; Sun, F.; Zhao, S.-Y.; Liu, W. Borrowing Hydrogen  $\beta$ -Phosphinomethylation of Alcohols Using Methanol as C1 Source by Pincer Manganese Complex. *J. Am. Chem. Soc.* **2023**, *145*, 25545–25552.
- (19) Trincado, M.; Böskén, J.; Grützmacher, H. Homogeneously Catalyzed Acceptorless Dehydrogenation of Alcohols: A Progress Report. *Coord. Chem. Rev.* **2021**, *443*, 213967.
- (20) Budweg, S.; Junge, K.; Beller, M. Catalytic Oxidations by Dehydrogenation of Alkanes, Alcohols and Amines with Defined (Non)-Noble Metal Pincer Complexes. *Catal. Sci. Technol.* **2020**, *10*, 3825–3842.
- (21) Zhang, J.; Leitus, G.; Ben-David, Y.; Milstein, D. Facile Conversion of Alcohols into Esters and

- Dihydrogen Catalyzed by New Ruthenium Complexes. *J. Am. Chem. Soc.* **2005**, *127*, 10840–10841.
- (22) Gunanathan, C.; Ben-David, Y.; Milstein, D. Direct Synthesis of Amides from Alcohols and Amines with Liberation of H<sub>2</sub>. *Science* **2007**, *317*, 790–792.
- (23) Daw, P.; Kumar, A.; Espinosa-Jalapa, N. A.; Ben-David, Y.; Milstein, D. Direct Synthesis of Amides by Acceptorless Dehydrogenative Coupling of Benzyl Alcohols and Ammonia Catalyzed by a Manganese Pincer Complex: Unexpected Crucial Role of Base. *J. Am. Chem. Soc.* **2019**, *141*, 12202–12206.
- (24) Kumar, A.; Espinosa-Jalapa, N. A.; Leitus, G.; Diskin-Posner, Y.; Avram, L.; Milstein, D. Direct Synthesis of Amides by Dehydrogenative Coupling of Amines with Either Alcohols or Esters: Manganese Pincer Complex as Catalyst. *Angew. Chem. Int. Ed.* **2017**, *56*, 14992–14996.
- (25) Hu, P.; Milstein, D. Conversion of Alcohols to Carboxylates Using Water and Base with H<sub>2</sub> Liberation BT - Organometallics for Green Catalysis; Dixneuf, P. H., Soulé, J.-F., Eds.; Springer International Publishing: Cham, 2019; pp 175–192.
- (26) Townsend, T. M.; Bernskoetter, W. H.; Hazari, N.; Mercado, B. Q. Dehydrogenative Synthesis of Carbamates from Formamides and Alcohols Using a Pincer-Supported Iron Catalyst. *ACS Catal.* **2021**, *11*, 10614–10624.
- (27) Kassie, A. A.; Castro De la Torre, I. Y.; Remy, M. S.; Mukhopadhyay, S.; Kampf, J.; Qu, F.; Sanford, M. S. Metal Identity Effects in the Pincer Complex-Catalyzed Dehydrogenative Coupling of Formamides with Alcohols to Form Carbamates. *Organometallics* **2023**.
- (28) Lane, E. M.; Hazari, N.; Bernskoetter, W. H. Iron-Catalyzed Urea Synthesis: Dehydrogenative Coupling of Methanol and Amines. *Chem. Sci.* **2018**, *9*, 4003–4008.
- (29) Bruffaerts, J.; Von Wolff, N.; Diskin-Posner, Y.; Ben-David, Y.; Milstein, D. Formamides as Isocyanate Surrogates: A Mechanistically Driven Approach to the Development of Atom-Efficient, Selective Catalytic Syntheses of Ureas, Carbamates, and Heterocycles. *J. Am. Chem. Soc.* **2019**, *141*, 16486–16493.
- (30) Kim, S. H.; Hong, S. H. Ruthenium-Catalyzed Urea Synthesis Using Methanol as the C1 Source. *Org. Lett.* **2016**, *18*, 212–215.

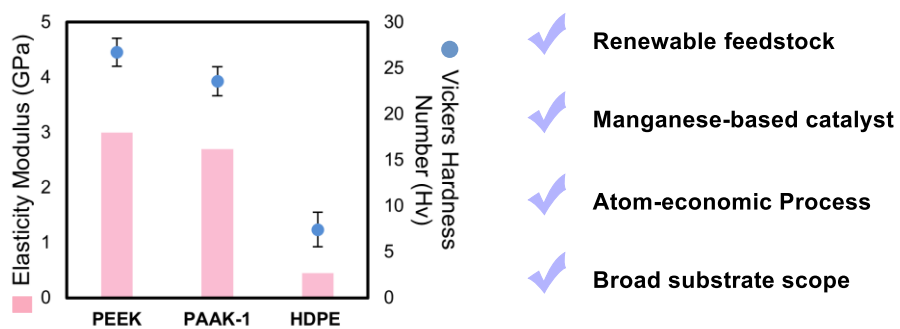
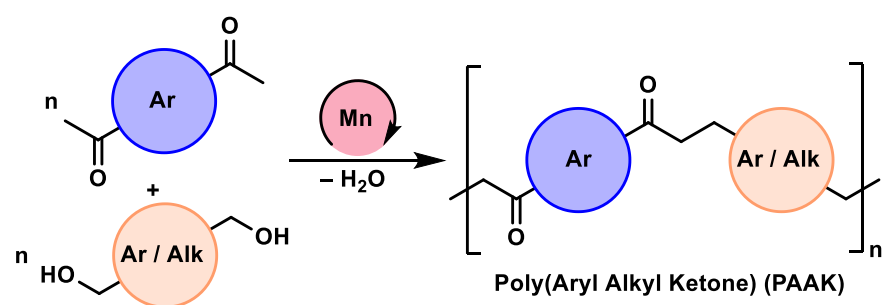
- (31) Gunanathan, C.; Milstein, D. Selective Synthesis of Primary Amines Directly from Alcohols and Ammonia. *Angew. Chem. Int. Ed.* **2008**, *47*, 8661–8664.
- (32) Ye, X.; Plessow, P. N.; Brinks, M. K.; Schelwies, M.; Schaub, T.; Rominger, F.; Paciello, R.; Limbach, M.; Hofmann, P. Alcohol Amination with Ammonia Catalyzed by an Acridine-Based Ruthenium Pincer Complex: A Mechanistic Study. *J. Am. Chem. Soc.* **2014**, *136*, 5923–5929.
- (33) Gunanathan, C.; Shimon, L. J. W.; Milstein, D. Direct Conversion of Alcohols to Acetals and H<sub>2</sub> Catalyzed by an Acridine-Based Ruthenium Pincer Complex. *J. Am. Chem. Soc.* **2009**, *131*, 3146–3147.
- (34) Gnanaprakasam, B.; Zhang, J.; Milstein, D. Direct Synthesis of Imines from Alcohols and Amines with Liberation of H<sub>2</sub>. *Angew. Chem. Int. Ed.* **2010**, *49*, 1468–1471.
- (35) Maggi, A.; Madsen, R. Dehydrogenative Synthesis of Imines from Alcohols and Amines Catalyzed by a Ruthenium N-Heterocyclic Carbene Complex. *Organometallics* **2012**, *31*, 451–455.
- (36) Mondal, A.; Sharma, R.; Pal, D.; Srimani, D. Recent Progress in the Synthesis of Heterocycles through Base Metal-Catalyzed Acceptorless Dehydrogenative and Borrowing Hydrogen Approach. *European J. Org. Chem.* **2021**, *2021*, 3690–3720.
- (37) Hunsicker, D. M.; Dauphinais, B. C.; Mc Ilrath, S. P.; Robertson, N. J. Synthesis of High Molecular Weight Polyesters via In Vacuo Dehydrogenation Polymerization of Diols. *Macromol. Rapid Commun.* **2012**, *33*, 232–236.
- (38) Malineni, J.; Keul, H.; Möller, M. An Efficient N-Heterocyclic Carbene-Ruthenium Complex: Application towards the Synthesis of Polyesters and Polyamides. *Macromol. Rapid Commun.* **2015**, *36*, 547–552.
- (39) Zeng, H.; Guan, Z. Direct Synthesis of Polyamides via Catalytic Dehydrogenation of Diols and Diamines. *J. Am. Chem. Soc.* **2011**, *133*, 1159–1161.
- (40) Gnanaprakasam, B.; Balaraman, E.; Gunanathan, C.; Milstein, D. Synthesis of Polyamides from Diols and Diamines with Liberation of H<sub>2</sub>. *J. Polym. Sci. Part A Polym. Chem.* **2012**, *50*, 1755–1765.

- (41) Guo, J.; Tang, J.; Xi, H.; Zhao, S.-Y.; Liu, W. Manganese Catalyzed Urea and Polyurea Synthesis Using Methanol as C1 Source. *Chinese Chem. Lett.* **2023**, *34*, 107731.
- (42) Langsted, C. R.; Paulson, S. W.; Bomann, B. H.; Suhail, S.; Aguirre, J. A.; Saumer, E. J.; Baclasky, A. R.; Salmon, K. H.; Law, A. C.; Farmer, R. J.; Furchtenicht, C. J.; Stankowski, D. S.; Johnson, M. L.; Corcoran, L. G.; Dolan, C. C.; Carney, M. J.; Robertson, N. J. Isocyanate-Free Synthesis of Ureas and Polyureas via Ruthenium Catalyzed Dehydrogenation of Amines and Formamides. *J. Appl. Polym. Sci.* **2021**, *n/a*, 52088.
- (43) Owen, A. E.; Preiss, A.; McLuskie, A.; Gao, C.; Peters, G.; Bühl, M.; Kumar, A. Manganese-Catalyzed Dehydrogenative Synthesis of Urea Derivatives and Polyureas. *ACS Catal.* **2022**, *12*, 6923–6933.
- (44) Langsted, C. R.; Paulson, S. W.; Bomann, B. H.; Suhail, S.; Aguirre, J. A.; Saumer, E. J.; Baclasky, A. R.; Salmon, K. H.; Law, A. C.; Farmer, R. J.; Furchtenicht, C. J.; Stankowski, D. S.; Johnson, M. L.; Corcoran, L. G.; Dolan, C. C.; Carney, M. J.; Robertson, N. J. Isocyanate-Free Synthesis of Ureas and Polyureas via Ruthenium Catalyzed Dehydrogenation of Amines and Formamides. *J. Appl. Polym. Sci.* **2022**, *139*, 52088.
- (45) Brodie, C. N.; Owen, A. E.; Kolb, J. S.; Bühl, M.; Kumar, A. Synthesis of Polyethyleneimines from the Manganese-Catalysed Coupling of Ethylene Glycol and Ethylenediamine. *Angew. Chem. Int. Ed.* **2023**, e202306655.
- (46) Huang, F.; Liu, Z.; Yu, Z. C-Alkylation of Ketones and Related Compounds by Alcohols: Transition-Metal-Catalyzed Dehydrogenation. *Angew. Chem. Int. Ed.* **2016**, *55*, 862–875.
- (47) Sharma, R.; Samanta, A.; Sardar, B.; Roy, M.; Srimani, D. Progressive Study on Ruthenium Catalysis for de(Hydrogenative) Alkylation and Alkenylation Using Alcohols as a Sustainable Source. *Org. Biomol. Chem.* **2022**, *20*, 7998–8030.
- (48) Reed-Berendt, B. G.; Latham, D. E.; Dambatta, M. B.; Morrill, L. C. Borrowing Hydrogen for Organic Synthesis. *ACS Cent. Sci.* **2021**, *7*, 570–585.
- (49) Reed-Berendt, B. G.; Polidano, K.; Morrill, L. C. Recent Advances in Homogeneous Borrowing Hydrogen Catalysis Using Earth-Abundant First Row Transition Metals. *Org. Biomol. Chem.* **2019**, *17*, 1595–1607.

- (50) Irrgang, T.; Kempe, R. 3d-Metal Catalyzed N- and C-Alkylation Reactions via Borrowing Hydrogen or Hydrogen Autotransfer. *Chem. Rev.* **2019**, *119*, 2524–2549.
- (51) Deibl, N.; Kempe, R. General and Mild Cobalt-Catalyzed C-Alkylation of Unactivated Amides and Esters with Alcohols. *J. Am. Chem. Soc.* **2016**, *138*, 10786–10789.
- (52) Obora, Y. Recent Advances in  $\alpha$ -Alkylation Reactions Using Alcohols with Hydrogen Borrowing Methodologies. *ACS Catal.* **2014**, *4*, 3972–3981.
- (53) Peña-López, M.; Piehl, P.; Elangovan, S.; Neumann, H.; Beller, M. Manganese-Catalyzed Hydrogen-Autotransfer C–C Bond Formation:  $\alpha$ -Alkylation of Ketones with Primary Alcohols. *Angew. Chem. Int. Ed.* **2016**, *55*, 14967–14971.
- (54) Guo, J.; Ye, Y.; Gao, S.; Feng, Y. Synthesis of Polyketone Catalyzed by Pd/C Catalyst. *J. Mol. Catal. A Chem.* **2009**, *307*, 121–127.
- (55) Thiyagarajan, S.; Vijaya Sankar, R.; Gunanathan, C. Ruthenium-Catalyzed  $\alpha$ -Alkylation of Ketones Using Secondary Alcohols to  $\beta$ -Disubstituted Ketones. *Org. Lett.* **2020**, *22*, 7879–7884.
- (56) Baratta, W.; Bossi, G.; Putignano, E.; Rigo, P. Pincer and Diamine Ru and Os Diphosphane Complexes as Efficient Catalysts for the Dehydrogenation of Alcohols to Ketones. *Chem. – Eur. J.* **2011**, *17*, 3474–3481.
- (57) Araya-Hermosilla, E.; Giannetti, A.; Lima, G. M. R.; Orozco, F.; Picchioni, F.; Mattoli, V.; Bose, R. K.; Pucci, A. Thermally Switchable Electrically Conductive Thermoset RGO/PK Self-Healing Composites. *Polymers*. 2021.
- (58) Tebeta, R. T.; Fattahi, A. M.; Ahmed, N. A. Experimental and Numerical Study on HDPE/SWCNT Nanocomposite Elastic Properties Considering the Processing Techniques Effect. *Microsyst. Technol.* **2020**, *26*, 2423–2441.
- (59) Yan, Y.; Jiang, C.; Huo, Y.; Li, C. Preparation and Tribological Behaviors of Lubrication-Enhanced PEEK Composites. *Applied Sciences*. 2020.
- (60) Liao, C.; Li, Y.; Tjong, S. C. Polyetheretherketone and Its Composites for Bone Replacement and Regeneration. *Polymers*. 2020.
- (61) Hejmady, P.; van Breemen, L. C. A.; Anderson, P. D.; Cardinaels, R. A Processing Route to

- Spherical Polymer Particles via Controlled Droplet Retraction. *Powder Technol.* **2021**, *388*, 401–411.
- (62) <https://www.jabil.com/services/additive-manufacturing/additive-materials/compare-powders/pk-5000.html>. No Title.
- (63) Andreas Pfister, Frank Müller, Martin Leuterer, 2010, E. No Title.
- (64) Saxon, D. J.; Luke, A. M.; Sajjad, H.; Tolman, W. B.; Reineke, T. M. Next-Generation Polymers: Isosorbide as a Renewable Alternative. *Prog. Polym. Sci.* **2020**, *101*, 101196.
- (65) Alberico, E.; Lennox, A. J. J.; Vogt, L. K.; Jiao, H.; Baumann, W.; Drexler, H. J.; Nielsen, M.; Spannenberg, A.; Checinski, M. P.; Beller, M.; et. al. Unravelling the Mechanism of Basic Aqueous Methanol Dehydrogenation Catalyzed by Ru-PNP Pincer Complexes. *J. Am. Chem. Soc.* **2016**, *138*, 14890–14904.
- (66) Ribeiro Gouveia, L.; Ison, E. A. Well-Defined ENENES Re and Mn Complexes and Their Application in Catalysis: The Role of Potassium Tert-Butoxide. *Organometallics* **2022**, *41*, 2678–2687.
- (67) Krall, E. M.; Klein, T. W.; Andersen, R. J.; Nett, A. J.; Glasgow, R. W.; Reader, D. S.; Dauphinais, B. C.; Mc Ilrath, S. P.; Fischer, A. A.; Carney, M. J.; Hudson, D. J.; Robertson, N. J. Controlled Hydrogenative Depolymerization of Polyesters and Polycarbonates Catalyzed by Ruthenium(II) PNN Pincer Complexes. *Chem. Commun.* **2014**, *50*, 4884–4887.
- (68) Westhues, S.; Idel, J.; Klankermayer, J. Molecular Catalyst Systems as Key Enablers for Tailored Polyesters and Polycarbonate Recycling Concepts. *Sci. Adv.* **2018**, *4*, eaat9669.
- (69) Jana, A.; Das, K.; Kundu, A.; Thorve, P. R.; Adhikari, D.; Maji, B. A Phosphine-Free Manganese Catalyst Enables Stereoselective Synthesis of (1 + n)-Membered Cycloalkanes from Methyl Ketones and 1,n-Diols. *ACS Catal.* **2020**, *10*, 2615–2626.
- (70) Chakraborty, S.; Daw, P.; Ben David, Y.; Milstein, D. Manganese-Catalyzed  $\alpha$ -Alkylation of Ketones, Esters, and Amides Using Alcohols. *ACS Catal.* **2018**, *8*, 10300–10305.

TOC-Graphics:



# Manganese Catalysed Synthesis of Polyketones using Hydrogen Borrowing Approach

Pavel Kulyabin,<sup>†</sup> Oxana V Magdysyuk,<sup>†</sup> Aaron B Naden,<sup>†</sup> Daniel M Dawson,<sup>†</sup> Ketan Pancholi,<sup>δ</sup> Matthew Walker,<sup>γ</sup> Massimo Vassalli,<sup>ζ</sup> and Amit Kumar<sup>†\*</sup>

<sup>†</sup>EaStCHEM, School of Chemistry, University of St Andrews, North Haugh, St Andrews, KY16 9ST, UK.

<sup>δ</sup> The Sir Ian Wood Building, Robert Gordon University, Garthdee Rd, Garthdee, Aberdeen, AB10 7GE, UK.

<sup>γ</sup>Centre for the Cellular Microenvironment, Advanced Research Centre, University of Glasgow, Glasgow, G116EW, UK.

<sup>ζ</sup> James Watt School of Engineering, University of Glasgow, Glasgow G12 8QQ, UK.

E-mail: [ak336@st-andrews.ac.uk](mailto:ak336@st-andrews.ac.uk)

## Contents

1. Experimental Details .....	S2
1.1 General Considerations .....	S2
1.2 Synthesis of 3,3'-(1,4-phenylene)bis(1-phenylpropan-1-one) as a model substrate.....	S3
1.3 Coupling of 1,4-diacetylbenzene and 1,4-benzenedimethanol. ....	S5
1.4 NMR spectra of mother liquor from coupling reaction of 1,4-diacetylbenzene and 1,4-benzenedimethanol as described in Table S1. ....	S27
1.5 Synthesis of polyketones from diketones and diols. ....	S28
1.6 Syntheses of polychalcones from diketones and dialdehydes.....	S62
1.7 Reaction 4-acetylphenyl ether and potassium tert-butoxide. ....	S65
1.8 Syntheses of polyketones in the presence of hydrogen atmosphere.....	S67
1.9 Catalyst reuse experiments. ....	S72
1.10 Headspace gas analysis from the synthesis of polyketone PAAK-7. ....	S73
1.11 Hydrogenative depolymerization of polyethyleneterephthalate (PET). ....	S74
1.12 Hydrogenation of trans-Chalcone by transfer hydrogenation. ....	S75
1.13 Infrared spectra of starting materials and commercially available compounds. ....	S76
1.14 TGA of commercial PEEK. ....	S80
1.15 Powder XRD patterns of starting materials. ....	S81
1.16 Scanning Electron Microscopy .....	S83
1.17 Powder XRD and Scanning Electron Microscopy analysis .....	S88
2. Mechanical properties.....	S89
3. References .....	S92

## 1. Experimental Details

### 1.1 General Considerations

All manipulations, unless otherwise stated, were performed under an argon atmosphere using standard Schlenk line and glove-box techniques. Glassware was oven-dried and flamed under vacuum prior to use. THF and toluene were dried using a Grubbs-type solvent purification system (Innovative Technologies SPS) equipped with a degasser. Pre-catalyst **1**<sup>[1]</sup> was prepared in accordance with the literature procedure. Cs<sub>2</sub>CO<sub>3</sub> (anhydrous) were stored at 80 °C and dried before use. Precatalysts **2–4**, Mn(CO)<sub>5</sub>Br, triphenylphosphine, NMR solvents and iPr-PN<sup>H</sup>P (10 wt% solution in THF) were purchased from Strem Chemicals and used as received.

Solution state NMR spectra were recorded on a Bruker AVIII-HD 400 MHz NMR spectrometer at 298 K unless otherwise specified. Residual protons of solvent were used as a reference for <sup>1</sup>H NMR spectra in deuterated solvent samples. All chemical shifts ( $\delta$ ) are quoted in ppm and coupling constants ( $J$ ) in Hz.

Solid-state NMR spectra were recorded using a Bruker Avance III spectrometer, equipped with a 9.4 T wide-bore superconducting magnet (<sup>1</sup>H and <sup>13</sup>C Larmor frequencies of 400.1 and 100.6 MHz, respectively). Some samples were submerged in liquid nitrogen and then ground to a powder. The remaining nitrogen and any condensed water were allowed to evaporate. Samples were packed into 4 mm zirconia magic angle spinning (MAS) rotors and rotated at a MAS rate of 12.5 kHz. <sup>13</sup>C NMR spectra were recorded with cross polarisation (CP) from <sup>1</sup>H using a contact pulse (ramped for <sup>1</sup>H) of between 0.5 and 2 ms. Signal averaging was carried out for 2048 transients (NM118(II)) with a recycle interval of 2 s. High power ( $\nu 1 \approx 100$  kHz) TPPM-15 decoupling of <sup>1</sup>H was applied during acquisition. Chemical shift is reported in ppm relative to (CH<sub>3</sub>)<sub>4</sub>Si using the CH<sub>3</sub> signal of L-alanine ( $\delta = 20.5$  ppm) as a secondary solid reference.

Infrared spectra (ATR-FTIR) were collected using a Shimadzu IRAffinity-1. Thermogravimetric Analysis (TGA) was performed using Stanton Redcroft STA-780 Series Thermal Analyser between 30–900 °C at a heating rate of 10 °C/min under a flow of nitrogen gas (25 mL/min). Decomposition temperature ( $T_d$ , °C) was estimated as the temperature of 10% weight loss.

Differential Scanning Calorimetry (DSC) analyses were performed using a Netzsch DSC204 or Queens STA449 DSC217C between 25–300 or 600 °C at a heating rate of 10 °C/min under a flow of nitrogen gas (20 mL/min) after an initial heat/cool cycle (25–120 °C at 10 °C/min with a 20-minute isothermal at 120 °C) to remove the thermal history of the sample.

Scanning electron microscopy (SEM) was performed on an FEI Scios dual-beam instrument operated at 3 kV, samples were prepared by dispersion onto adhesive carbon tape (Labtech International Ltd.) and sputter coated with a thin layer of gold to dissipate the charge.

Powder X-ray diffraction data was collected using Bruker AXS D8 Advance diffractometer with a Vantec detector, using Cu K $\alpha$  radiation. The data from powder samples were collected in the range of  $2^\circ < 2\theta < 70$  or  $90^\circ$ . Some samples were measured on a PTFE pad which led to the appearance of additional peaks (originated from PTFE) at high  $2\theta$ . The broad peak at  $2\theta = 26^\circ$  in several samples originates from the polyester film that was used to cover the powder.

GC-MS data were collected as solutions in HPLC grade DCM using an Agilent 8860 GC system coupled to an Agilent 5977B EI instrument. EI spectra were collected as solutions in acetonitrile using a Micromass LCT spectrometer.

Headspace analysis was performed using an Agilent GC8860 with TCD. Gas separation is performed using dual columns (Agilent porous Polymer and Agilent Mol sieve). A gas sample (2.5 mL) is introduced to the columns using a gas-tight syringe through a sample loop (0.25 mL).

## 1.2 Synthesis of 3,3'-(1,4-phenylene)bis(1-phenylpropan-1-one) as a model substrate.

A 15 mL pressure vessel was charged with pre-catalyst **1** (10 mg, 0.02 mmol, 2 mol%), 1,4-benzenedimethanol (138 mg, 1.0 mmol), acetophenone (240 mg, 2.0 mmol) and  $\text{Cs}_2\text{CO}_3$  (33 mg, 0.10 mmol, 10 mol%). *Tert*-amyl alcohol (5 mL) was added, and the flask was sealed under a nitrogen atmosphere in a glove box before heating to 140 °C for 18 hours with stirring. After this period, the reaction vessel was allowed to cool to room temperature. Next, the crude was directly purified by flash chromatography on silica gel to afford, after concentration and high-vacuum drying, 284 mg (83%) of the product as a white solid.  $^1\text{H}$  NMR (400 MHz,  $\text{CDCl}_3$ ):  $\delta$  7.96 (m, 4H), 7.56 (m, 2H), 7.47 (m, 4H), 7.20 (s, 4H), 3.30 (m, 4H), 3.05 (m, 4H).  $^{13}\text{C}$  NMR (100 MHz,  $\text{CDCl}_3$ ):  $\delta$  199.2, 139.0, 136.8, 133.0, 128.6, 128.0, 40.4, 29.9. IR (ATR-FTIR,  $\text{cm}^{-1}$ ):  $\nu$  2920w (C-H), 1680s (C=O), 1593w, 1516w, 1447m, 1204m, 972m, 745s, 691s, 548m.  $[\text{M}+\text{Na}]^+$  Calcd for  $\text{C}_{24}\text{H}_{22}\text{NaO}_2^+$ , 365.1512; found: 365.1507.

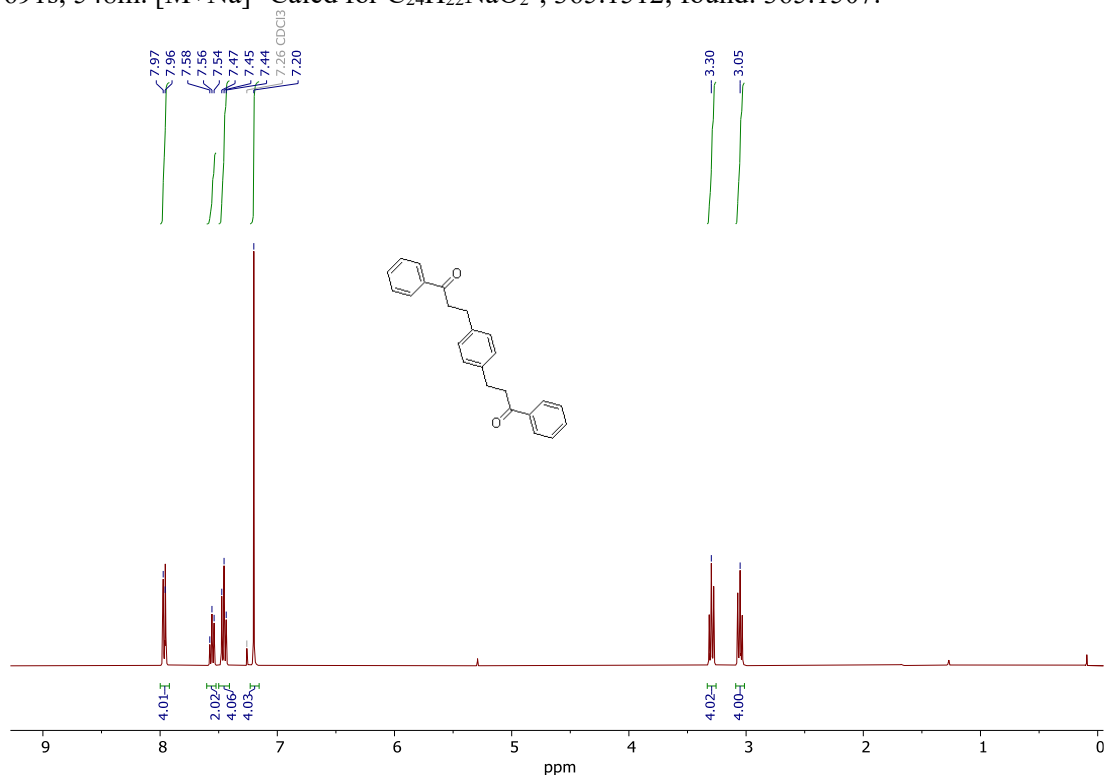
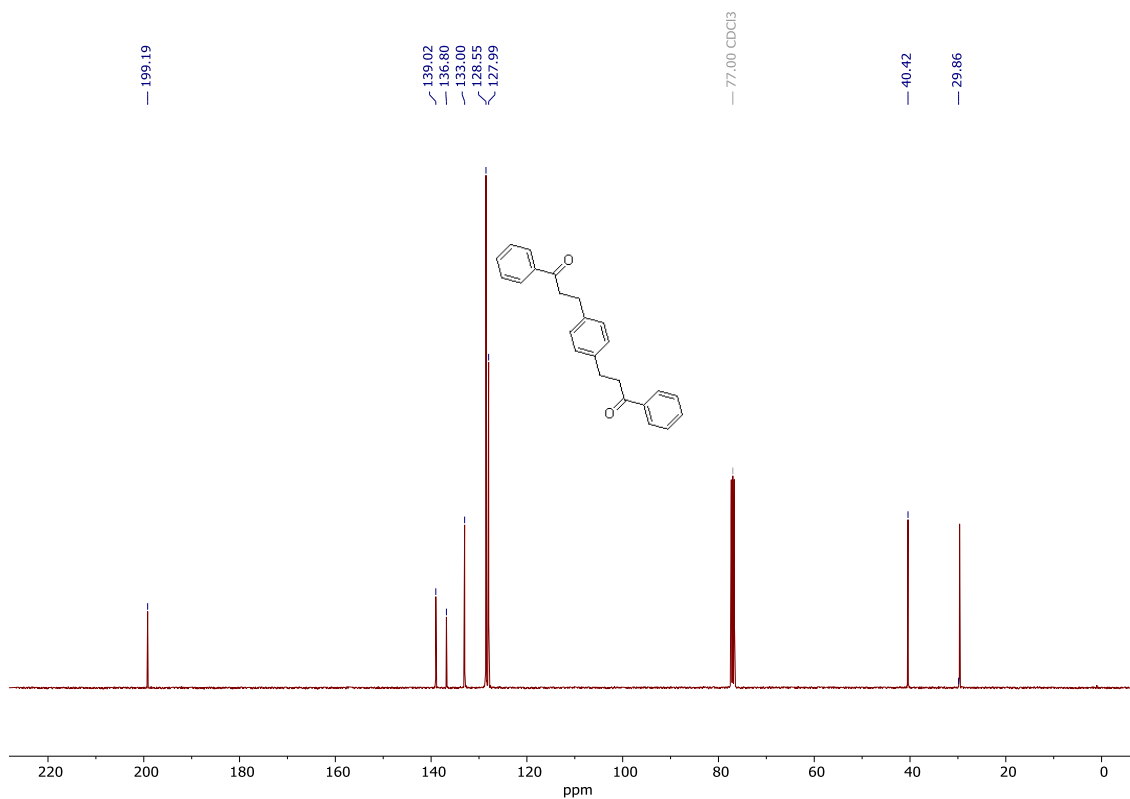
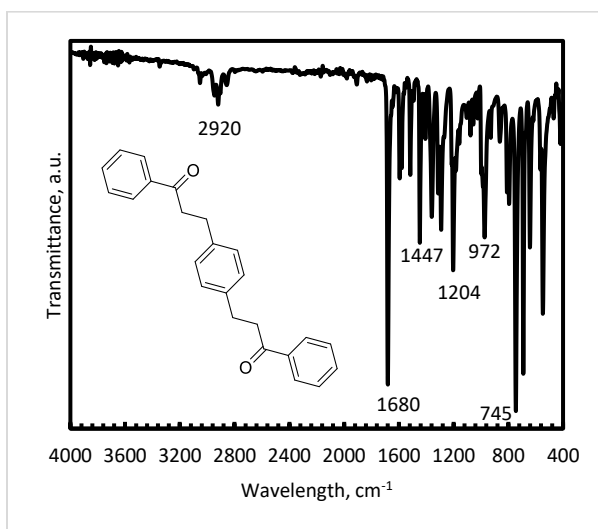


Figure S1.  $^1\text{H}$  NMR ( $\text{CDCl}_3$ , 298 K) spectrum of 3,3'-(1,4-phenylene)bis(1-phenylpropan-1-one).



**Figure S2.**  $^{13}\text{C}\{^1\text{H}\}$  NMR ( $\text{CDCl}_3$ , 298 K) spectrum of 3,3'-(1,4-phenylene)bis(1-phenylpropan-1-one).



**Figure S3.** Infrared spectrum (ATR-FTIR) of 3,3'-(1,4-phenylene)bis(1-phenylpropan-1-one).

### 1.3 Coupling of 1,4-diacetylbenzene and 1,4-benzenedimethanol.

A 100 mL ampoule equipped with a J-Young's valve or a 15 mL pressure vessel was charged with pre-catalyst (e.g. **1**; 10 mg, 0.02 mmol, 2 mol%), 1,4-benzenedimethanol (138 mg, 1.0 mmol), 1,4-diacetylketone (162 mg, 1.0 mmol) and Cs<sub>2</sub>CO<sub>3</sub> (e.g. 33 mg, 0.10 mmol, 10 mol%). *Tert*-amyl alcohol or toluene (e.g. 5 mL) was added and the flask was sealed under an argon atmosphere before heating to the desired temperature (e.g. 140 °C) for the desired length of time (e.g. 18 hours) with stirring. After this period, the reaction vessel was allowed to cool to room temperature, and any gas evolved (presumably H<sub>2</sub>) during the reaction was measured using the inverted cylinder in water method. To the resulting mixture, 5 mL of 1 M HCl was added and the flask had been heated at 90 °C for 1 h. The yellow precipitate was filtered and dried under reduced pressure at 120 °C.

**Table S1. Polyketone synthesis from 1,4-diacetylbenzene and 1,4-benzenedimethanol.<sup>a</sup>**

Entry	Complex	mol%	Conc.	Base (mol%)	Time (h)	Isolated Yield (%)	T <sub>d</sub> <sup>i</sup> (°C)
1 <sup>b,c</sup>	<b>1</b>	2	0.2 M	10%	18	61 <sup>d</sup>	325/266
2 <sup>b</sup>	<b>1</b>	2	0.2 M	10%	18	89	338
3 <sup>b</sup>	<b>2</b>	2	0.2 M	10%	18	< 5	n.d.
4 <sup>b</sup>	<b>3</b>	2	0.2 M	10%	18	51	353
5 <sup>b</sup>	<b>4</b>	2	0.2 M	10%	18	17	319
6 <sup>b</sup>	<b>1</b>	1	0.2 M	10%	18	87	356
7 <sup>b</sup>	<b>1</b>	0.5	0.2 M	10%	18	70	348
8	<b>1</b>	1	0.1 M	10%	18	85	373
9 <sup>c</sup>	<b>1</b>	1	0.1 M	10%	18	73	342
10	<b>1</b>	1	0.1 M	20%	18	90	369
11	<b>1</b>	1	0.1 M	3%	18	80	335
12 <sup>f</sup>	<b>1</b>	1	0.1M	10%	18	67	328
13 <sup>g</sup>	<b>1</b>	1	0.25 M	10%	18	94	352
14 <sup>h</sup>	<b>1</b>	1	0.05 M	10%	18	86	342
15	<b>1</b>	1	0.1 M	10%	2	89	363
16	<b>1</b>	1	0.1 M	10%	1	81	343
17	<b>1</b>	1	0.1 M	3%	2	81	344
18	<b>none</b>	none	0.1 M	10%	18	<10	396
19	<b>1</b>	1	0.1 M	none	18	none	—
20	<b>5</b>	1	0.1 M	10%	18	< 5	n.d.
21	<b>6</b>	1	0.1 M	10%	18	< 5	n.d.

**1**

**2**

**3**

**4**

**5**

**6**

<sup>a</sup>General reaction conditions: 1,4-diacetylbenzene (0.5 mmol), 1,4-benzenedimethanol (0.5 mmol), Cs<sub>2</sub>CO<sub>3</sub>, metal-complex, and 5 mL of tAmOH were placed into 100 mL ampoule with J-Young's valve under an argon atmosphere and heated at 140 °C for 18 h. <sup>b</sup>1 mmol of diol and diketone were used. <sup>c</sup>Toluene was used instead of tAmOH. <sup>d</sup>The reaction mixture consisted of two kinds of solid material: red chunk in the bottom (41%) and yellow brittle film on the edge of solution (20%) which were separated mechanically. <sup>e</sup>Reaction was carried out in 15 mL pressure vessel. <sup>f</sup>Reaction at 110°C. <sup>g</sup>2 mL of tAmOH were used. <sup>h</sup>10 mL of tAmOH were used. <sup>i</sup>Temperature of degradation. Calculated from TGA as a temperature of 10% weight loss.

Table S1, Entry 1

Yellow solid:

IR (ATR-FTIR,  $\text{cm}^{-1}$ ):  $\nu$  3470w (O-H), 3049w (C-H), 2922w (C-H), 1674s (C=O), 1601m (C=C), 1506w, 1406m, 1265s, 1213s, 982s, 818s, 731s, 544m.

TGA:  $T_d = 325\text{ }^\circ\text{C}$ .

Red solid:

3348m (O-H), 2924w (C-H), 1674s (C=O), 1605m (C-H), 1510w, 1373m, 1217m, 1213m, 1011m, 816s, 517s.

TGA:  $T_d = 266\text{ }^\circ\text{C}$ .

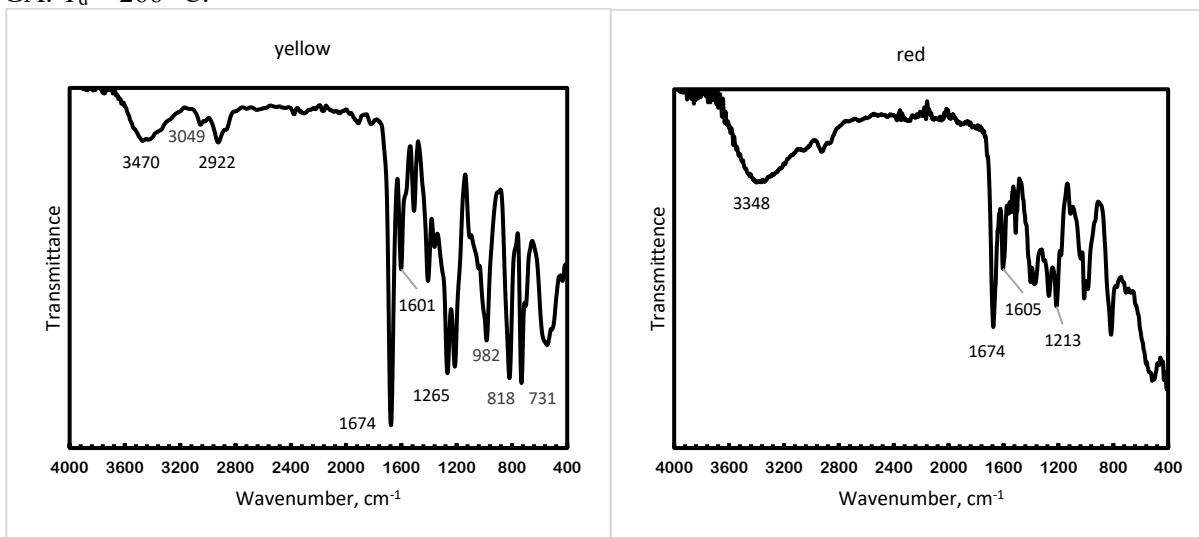


**Figure S4.** Infrared spectrum (ATR-FTIR) of the samples corresponding to Entry 1 in Table S1.

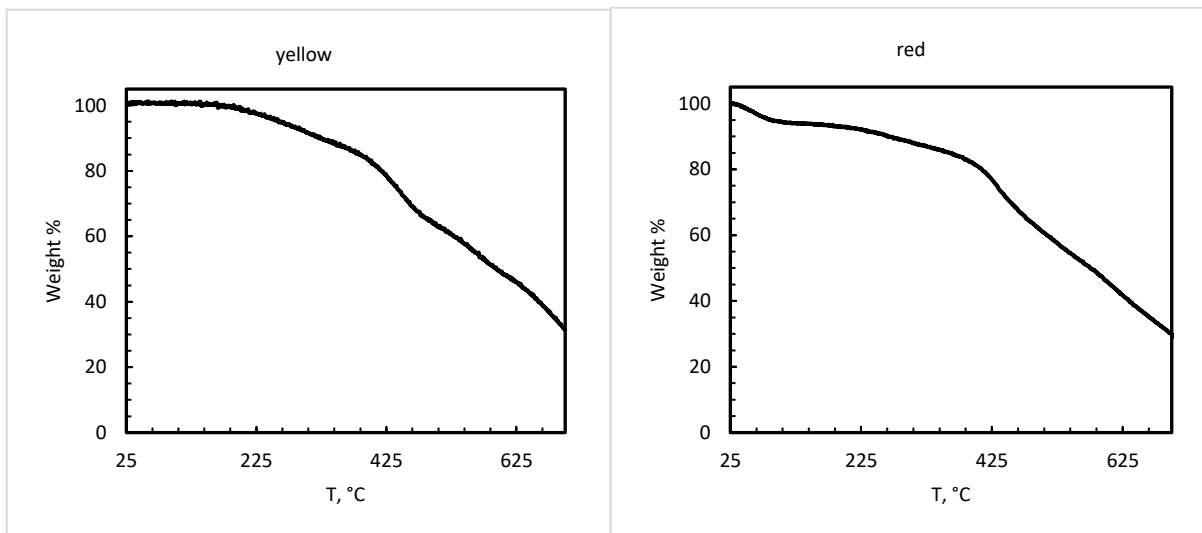


**Figure S5.** Mass loss as a function of temperature for samples corresponding to Entry 1 in Table S1.

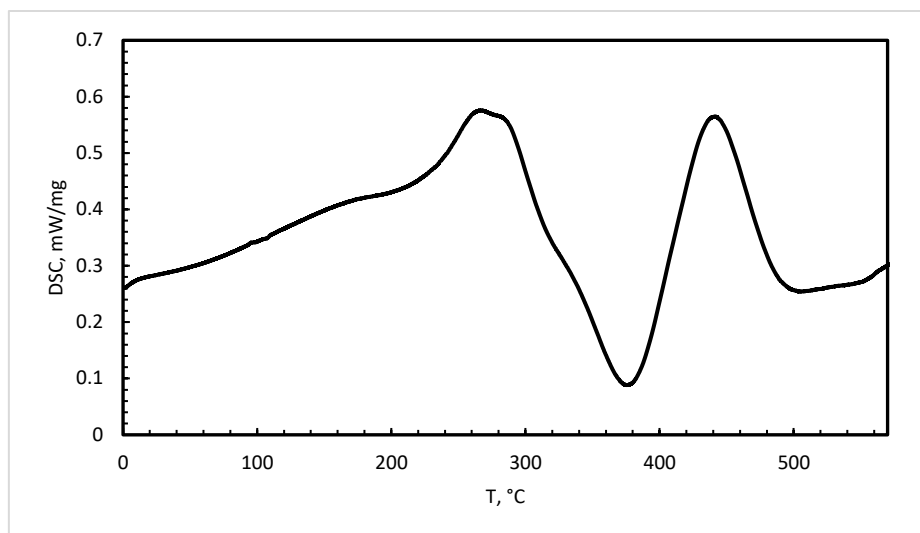


**Figure S6.** DSC trace corresponding to Entry 1 in Table S1, yellow solid.

**Table S1, Entry 2**

$^{13}\text{C}$  CP MAS NMR (100.6 MHz):  $\delta$  199.5, 151.6, 139.9, 128.4, 75.7, 70.2, 64.4, 42.2, 29.3.

IR (ATR-FTIR,  $\text{cm}^{-1}$ ):  $\nu$  3460w (O-H), 2926w (C-H), 1674s (C=O), 1603m (C=C), 1508w, 1406m, 1225s, 1211s, 982s, 818s, 546m.

TGA:  $T_d = 338\text{ }^\circ\text{C}$

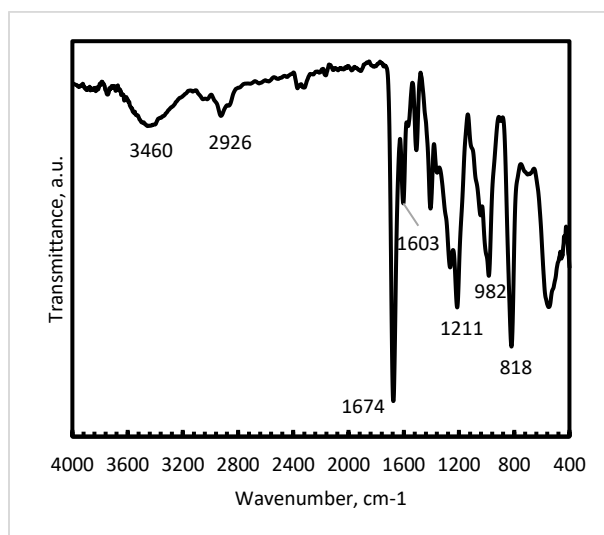


**Figure S7.** Infrared spectrum (ATR-FTIR) of the sample corresponding to Entry 2 in Table S1.

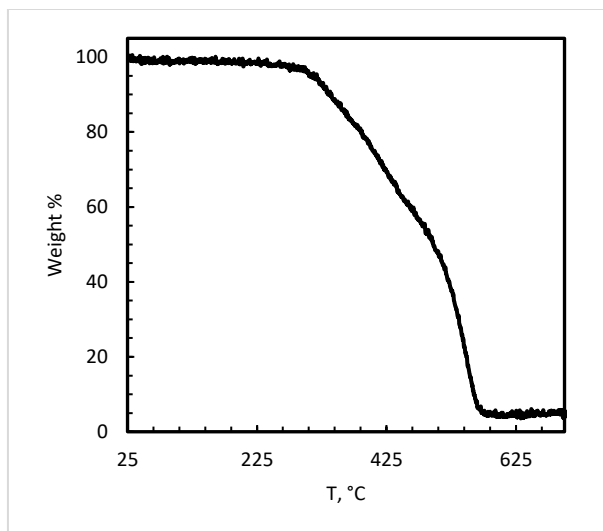


**Figure S8.** Mass loss as a function of temperature for sample corresponding to Entry 2 in Table S1.

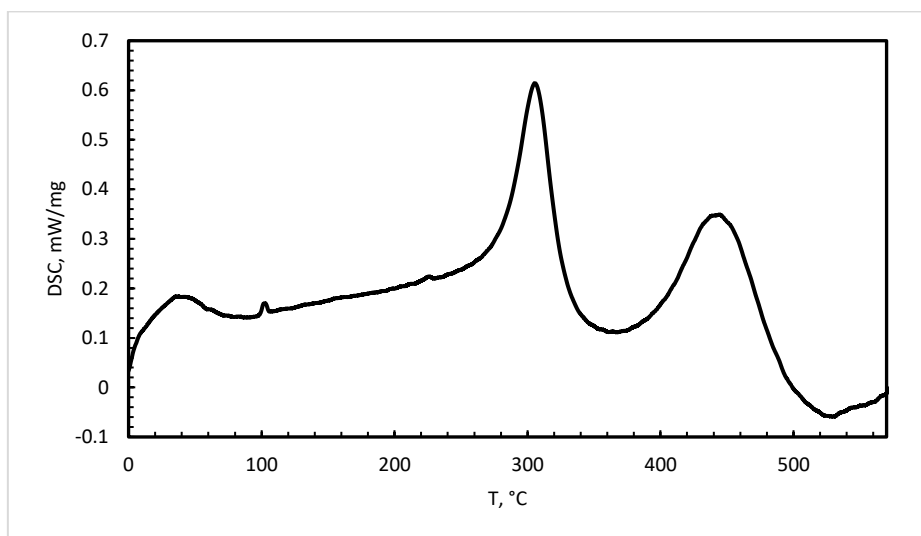


**Figure S9.** DSC trace corresponding to Entry 2 in Table S1.

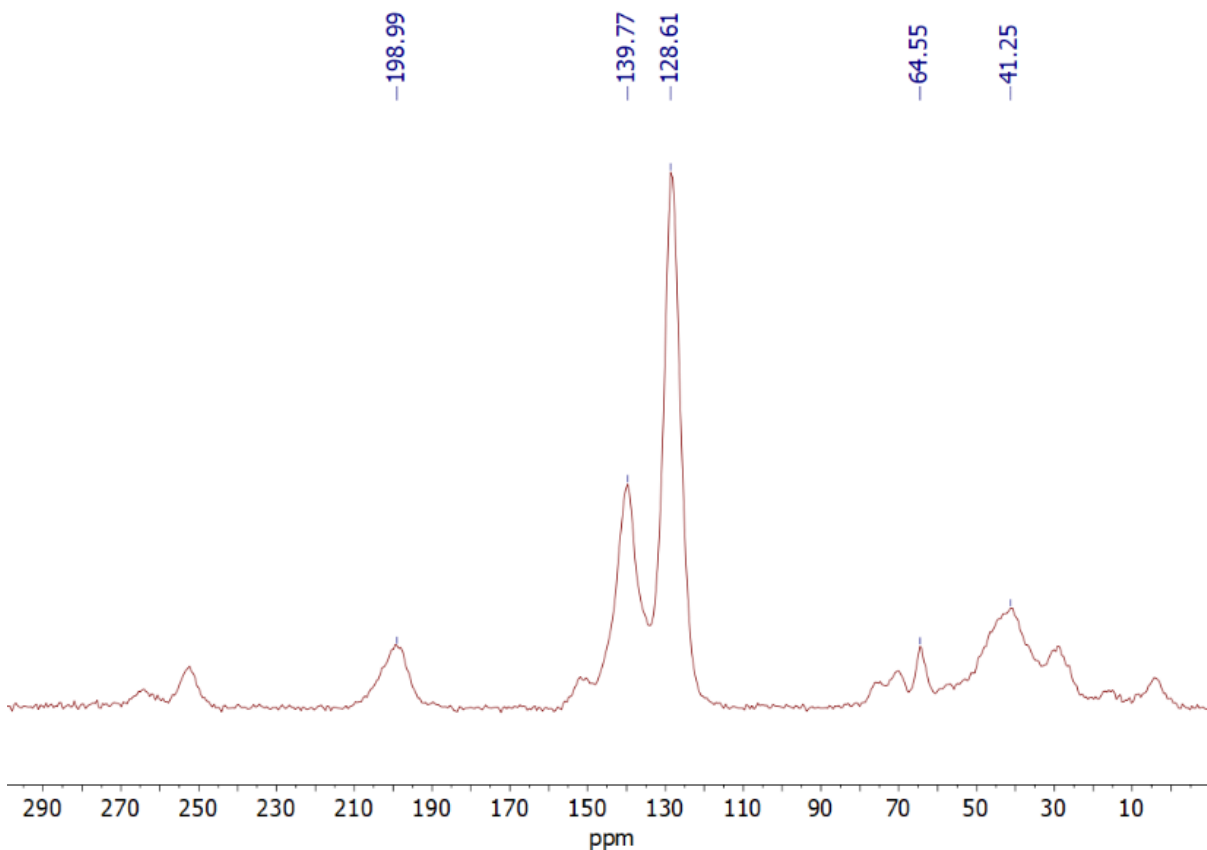


**Figure S10.**  $^{13}\text{C}$  CP MAS NMR spectrum of the polymer corresponding to Entry 2 in Table S1.

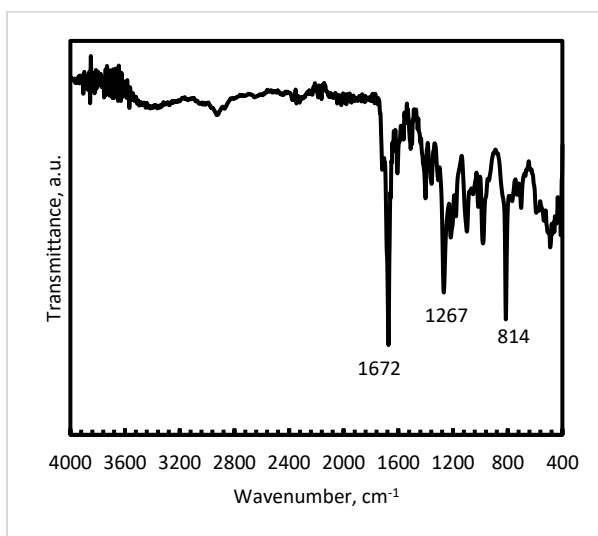
**Table S1, Entry 3**

The isolated amount was not enough to perform analysis.

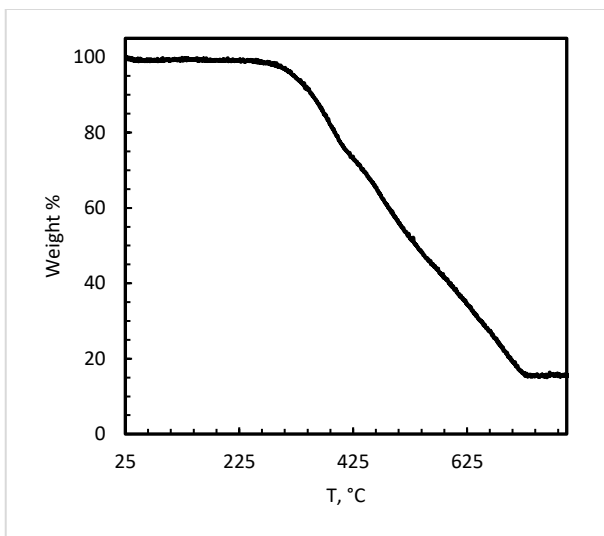
**Table S1, Entry 4**

IR (ATR-FTIR,  $\text{cm}^{-1}$ ):  $\nu$  3368w (O-H), 2920w (C-H), 1690w, 1672s (C=O), 1607w (C=C), 1510w, 1400m, 1267s, 978m, 814s.

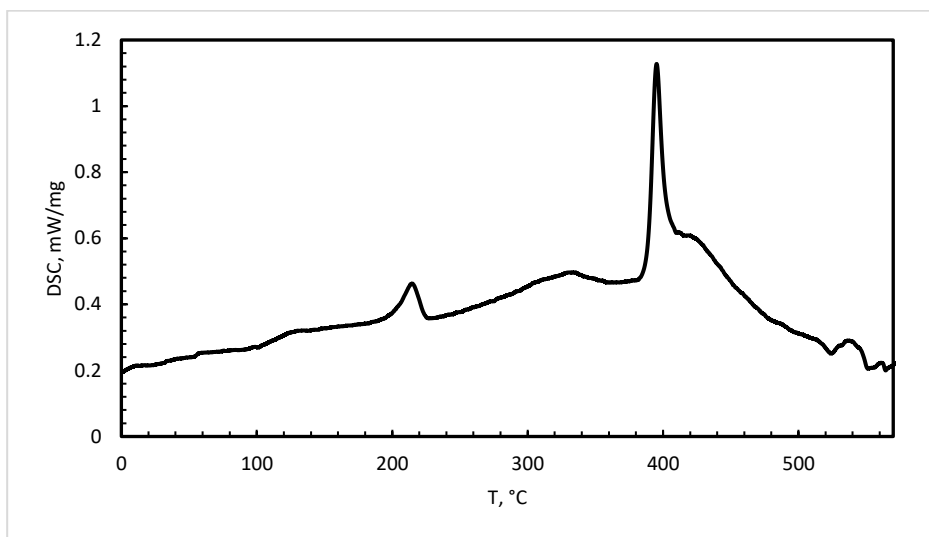
TGA:  $T_d = 353\text{ }^\circ\text{C}$



**Figure S11.** Infrared spectrum (ATR-FTIR) of the sample corresponding to Entry 4 in Table S1.



**Figure S12.** Mass loss as a function of temperature for sample corresponding to Entry 4 in Table S1.



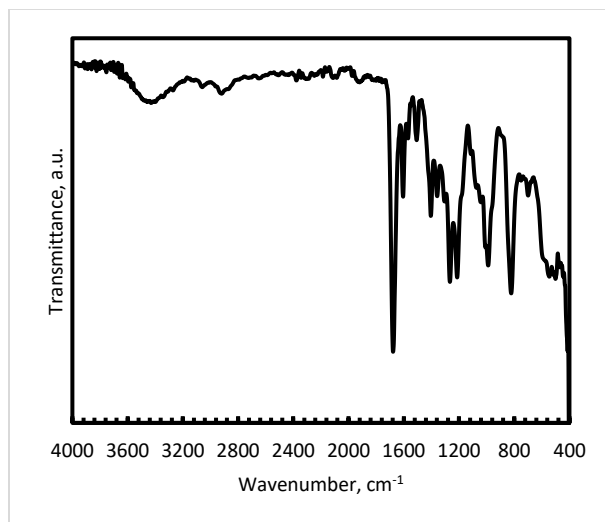
**Figure S13.** DSC trace corresponding to Entry 4 in Table S1.

Table S1, Entry 5

IR (ATR-FTIR,  $\text{cm}^{-1}$ ):  $\nu$  3416w (O-H), 2911w (C-H), 1676s (C=O), 1605m (C=C), 1506s, 1402m, 1265s,

1213s, 988s, 820s.

TGA:  $T_d = 319\text{ }^\circ\text{C}$



**Figure S14.** Infrared spectrum (ATR-FTIR) of the sample corresponding to Entry 5 in Table S1.

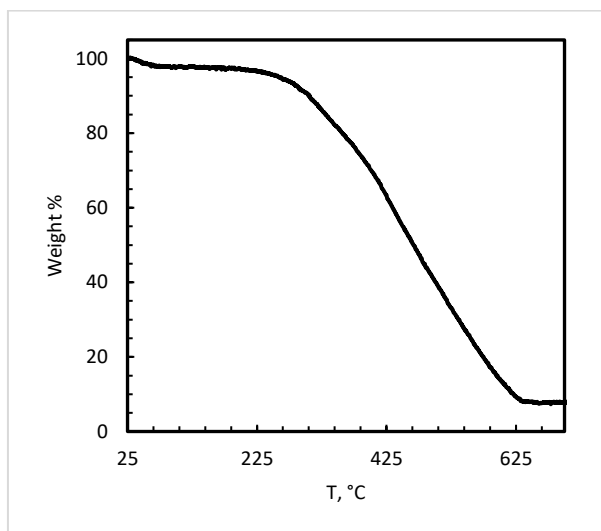


**Figure S15.** Mass loss as a function of temperature for sample corresponding to Entry 5 in Table S1.

Table S1, Entry 6

IR (ATR-FTIR,  $\text{cm}^{-1}$ ):  $\nu$  3424w (O-H), 2924w (C-H), 1676s (C=O), 1605m (C=C), 1510s, 1402m, 1225m, 1213s, 984m, 818s, 542m.

TGA:  $T_d = 356\text{ }^\circ\text{C}$

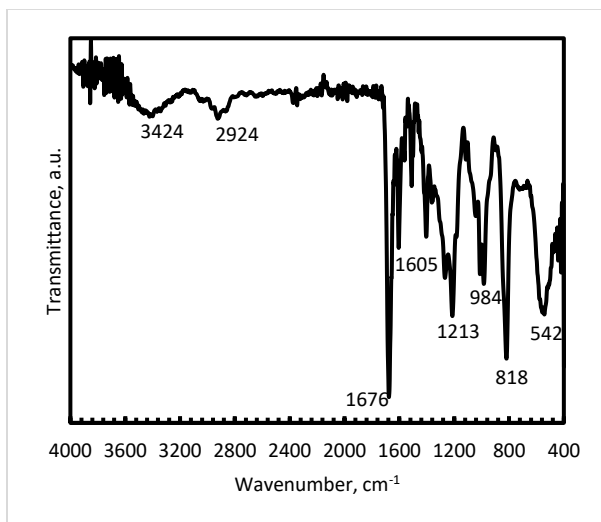


**Figure S16.** Infrared spectrum (ATR-FTIR) of the sample corresponding to Entry 6 in Table S1.

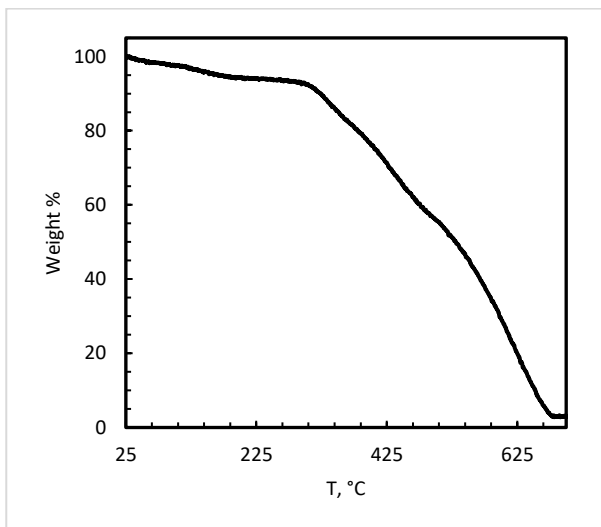


**Figure S17.** Mass loss as a function of temperature for sample corresponding to Entry 6 in Table S1.

Table S1, Entry 7

IR (ATR-FTIR,  $\text{cm}^{-1}$ ):  $\nu$  3420w (O-H), 2918w (C-H), 1674s (C=O), 1603m (C=C), 1422w, 1402m, 1265m, 1211s, 982s, 818s, 550m.

TGA:  $T_d = 348\text{ }^\circ\text{C}$

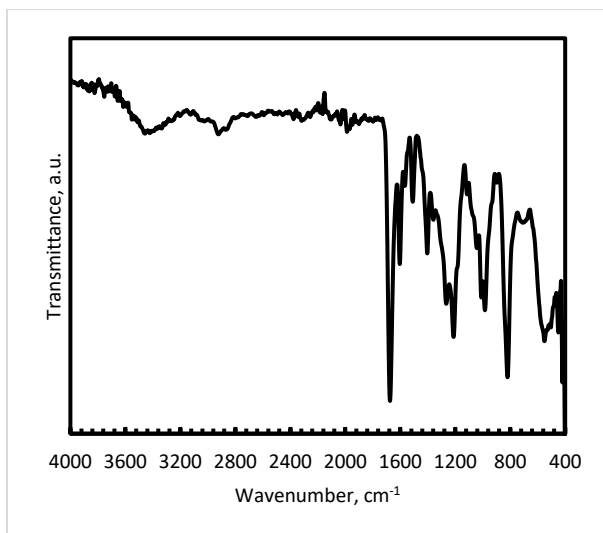


**Figure S18.** Infrared spectrum (ATR-FTIR) of the sample corresponding to Entry 7 in Table S1.

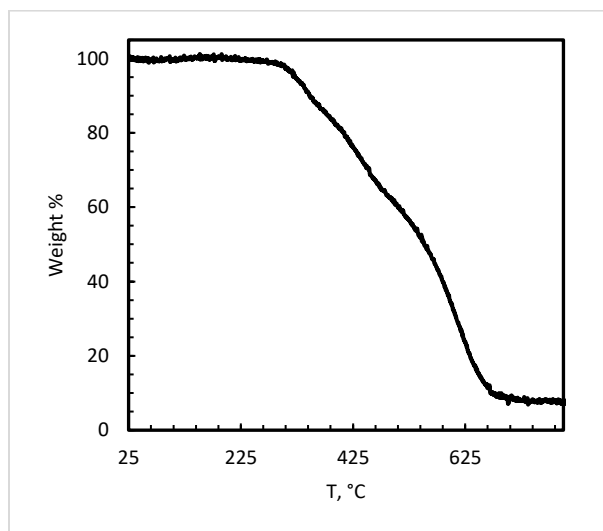


**Figure S19.** Mass loss as a function of temperature for sample corresponding to Entry 7 in Table S1.

Table S1, Entry 8

IR (ATR-FTIR,  $\text{cm}^{-1}$ ):  $\nu$  3402w (O-H), 2914w (C-H), 1674s (C=O), 1603m (C=C), 1510w, 1402m, 1225m, 1211s, 982m, 818s, 550m.

TGA:  $T_d = 373$  °C

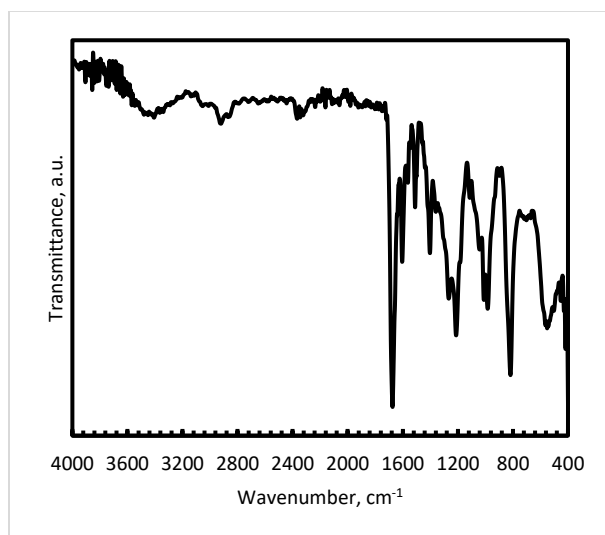


**Figure S20.** Infrared spectrum (ATR-FTIR) of the sample corresponding to Entry 8 in Table S1.

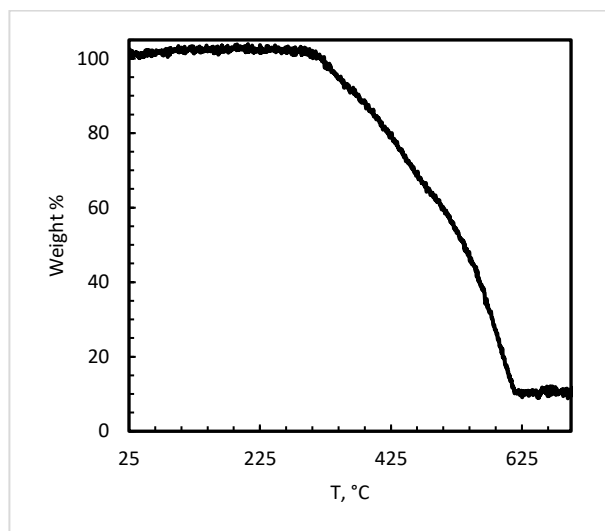


**Figure S21.** Mass loss as a function of temperature for sample corresponding to Entry 8 in Table S1.

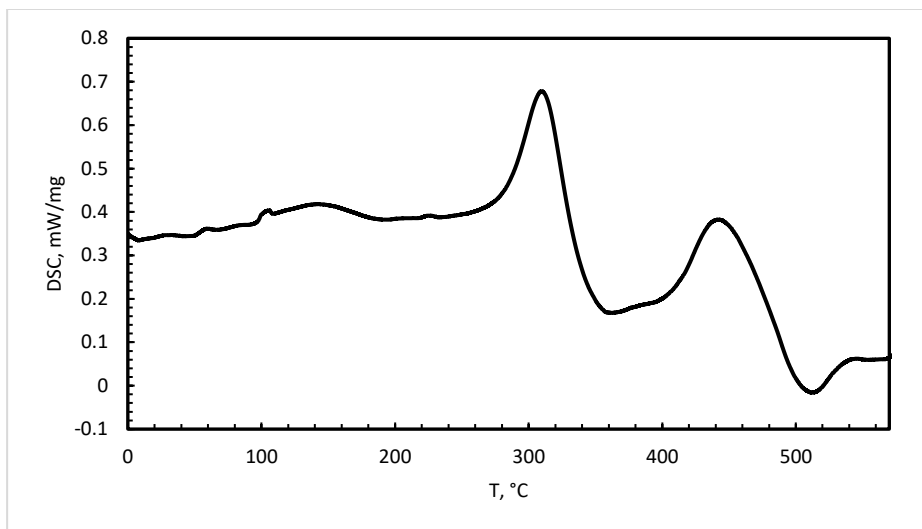


**Figure S22.** DSC trace corresponding to Entry 8 in Table S1.

Table S1, Entry 9

IR (ATR-FTIR,  $\text{cm}^{-1}$ ):  $\nu$  3449w (O-H), 2911w (C-H), 1676s (C=O), 1605m (C=C), 1510w, 1402m, 1221m, 1211s, 982s, 818s.

TGA:  $T_d = 342\text{ }^\circ\text{C}$

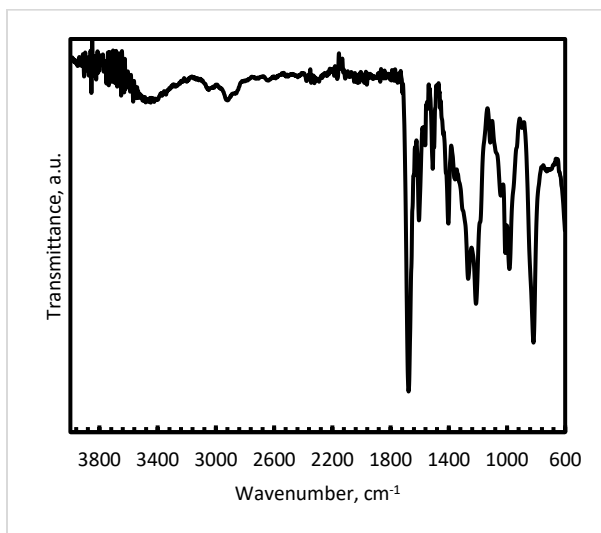


**Figure S23.** Infrared spectrum (ATR-FTIR) of the sample corresponding to Entry 9 in Table S1.

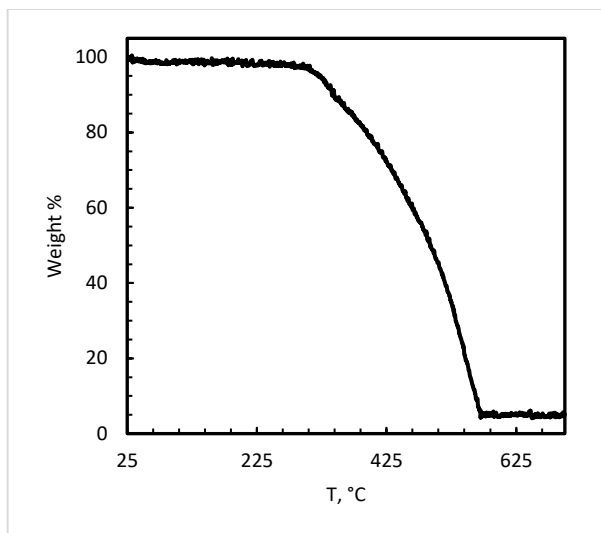


**Figure S24.** Mass loss as a function of temperature for sample corresponding to Entry 9 in Table S1.

Table S1, Entry 10

IR (ATR-FTIR,  $\text{cm}^{-1}$ ):  $\nu$  3464w (O-H), 2922w (C-H), 1676s (C=O), 1605m (C=C), 1418w, 1404m, 1220m, 1213s, 984m, 818s.

TGA:  $T_d = 369^\circ\text{C}$

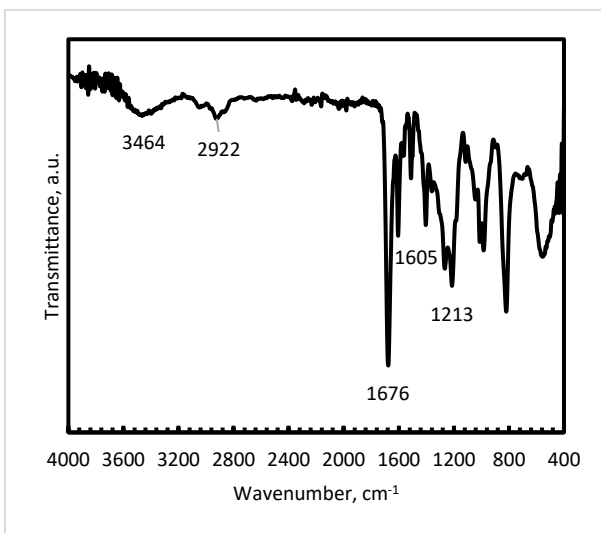


**Figure S25.** Infrared spectrum (ATR-FTIR) of the sample corresponding to Entry 10 in Table S1.

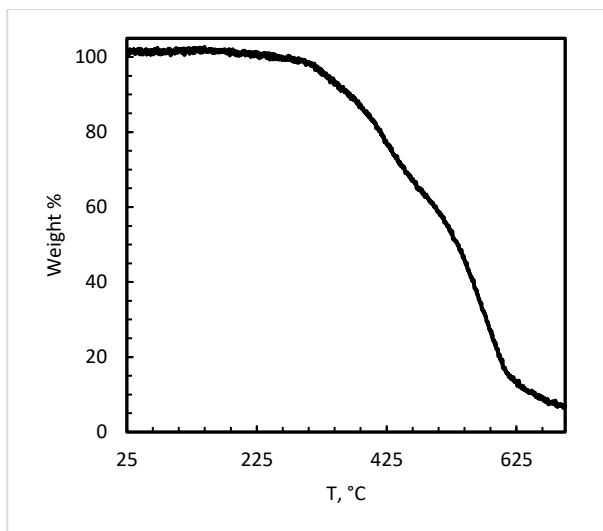


**Figure S26.** Mass loss as a function of temperature for sample corresponding to Entry 10 in Table S1.

Table S1, Entry 11

IR (ATR-FTIR,  $\text{cm}^{-1}$ ):  $\nu$  3400w (O-H), 2924w (C-H), 1676s (C=O), 1604m (C=C), 1510w, 1402m, 1222m, 1213s, 983m, 818s.

TGA:  $T_d = 335$  °C

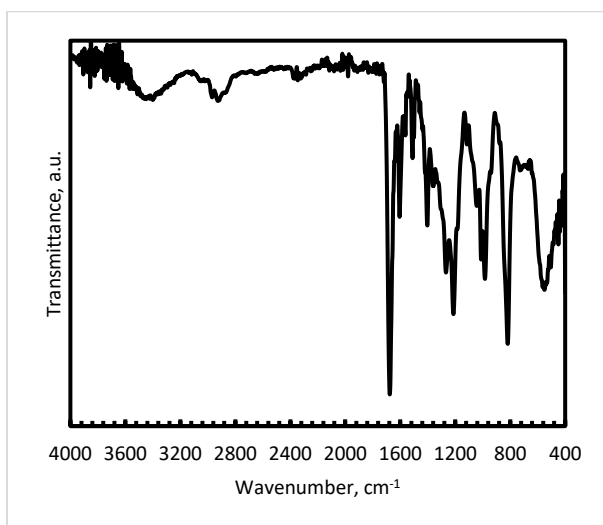


**Figure S27.** Infrared spectrum (ATR-FTIR) of the sample corresponding to Entry 11 in Table S1.

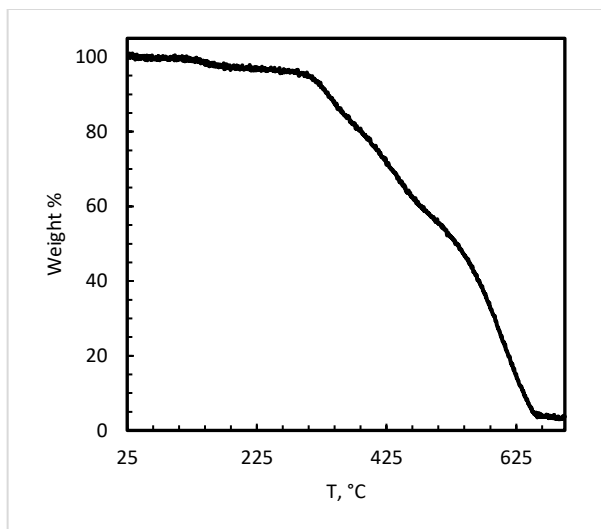


**Figure S 28.** Mass loss as a function of temperature for sample corresponding to Entry 11 in Table S1.

Table S1, Entry 12

IR (ATR-FTIR,  $\text{cm}^{-1}$ ):  $\nu$  3389w (O-H), 2907w (C-H), 1676s (C=O), 1604m (C=C), 1508w, 1402m, 1225m, 1211s, 983m, 818s.

TGA:  $T_d = 328$  °C

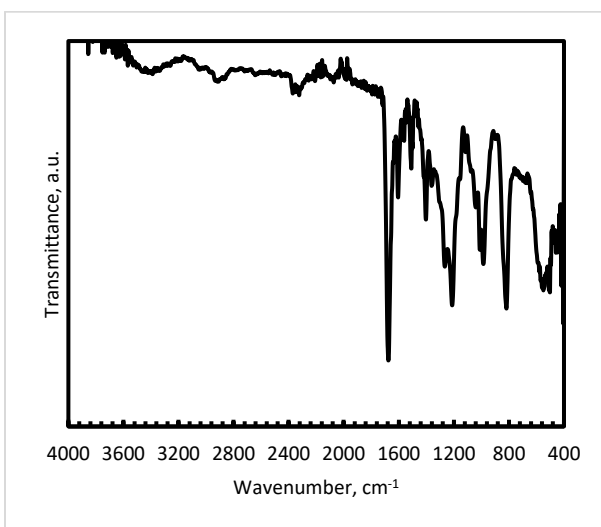


**Figure S29.** Infrared spectrum (ATR-FTIR) of the sample corresponding to Entry 12 in Table S1.

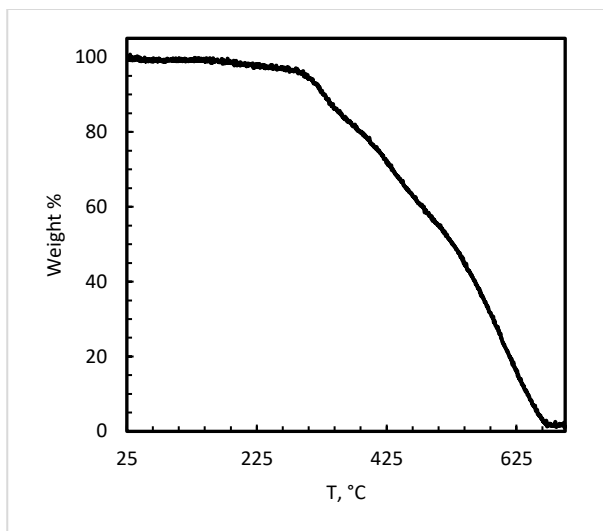


**Figure S30.** Mass loss as a function of temperature for sample corresponding to Entry 12 in Table S1.

Table S1, Entry 13

IR (ATR-FTIR,  $\text{cm}^{-1}$ ):  $\nu$  3401w (O-H), 2926w (C-H), 1676s (C=O), 1605m (C=C), 1510w, 1404m, 1225m, 1213s, 982s, 818s, 555w.

TGA:  $T_d = 352$  °C

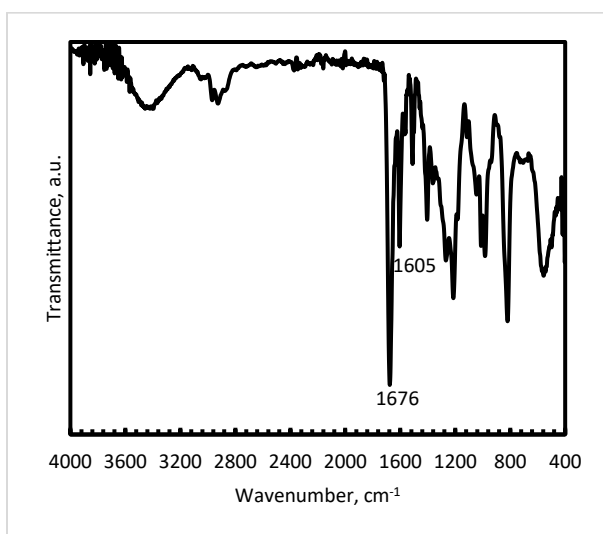


**Figure S31.** Infrared spectrum (ATR-FTIR) of the sample corresponding to Entry 13 in Table S1.

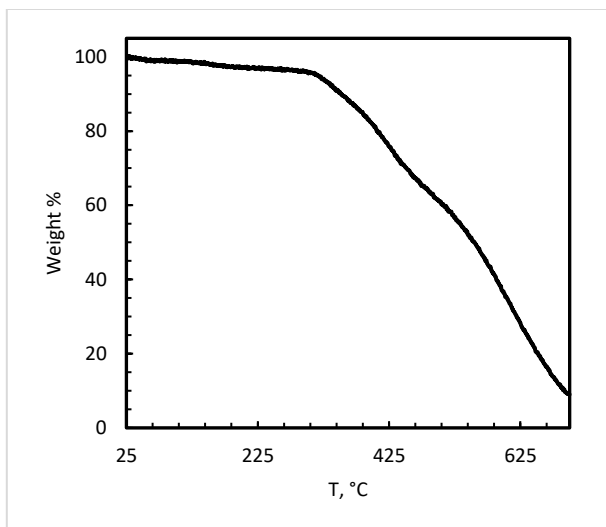


**Figure S32.** Mass loss as a function of temperature for sample corresponding to Entry 13 in Table S1.

Table S1, Entry 14

IR (ATR-FTIR,  $\text{cm}^{-1}$ ):  $\nu$  3427w (O-H), 2918w (C-H), 1676s (C=O), 1601m (C=C), 1506w, 1404m, 1228s, 1211s, 982m, 820s, 542m.

TGA:  $T_d = 342\text{ }^\circ\text{C}$

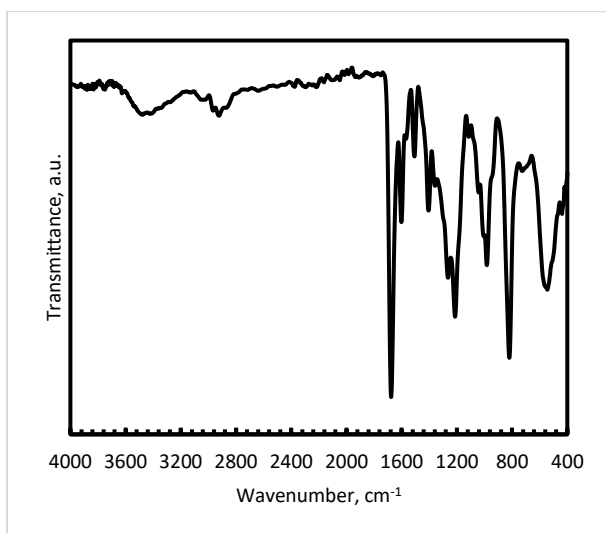


**Figure S33.** Infrared spectrum (ATR-FTIR) of the sample corresponding to Entry 14 in Table S1.

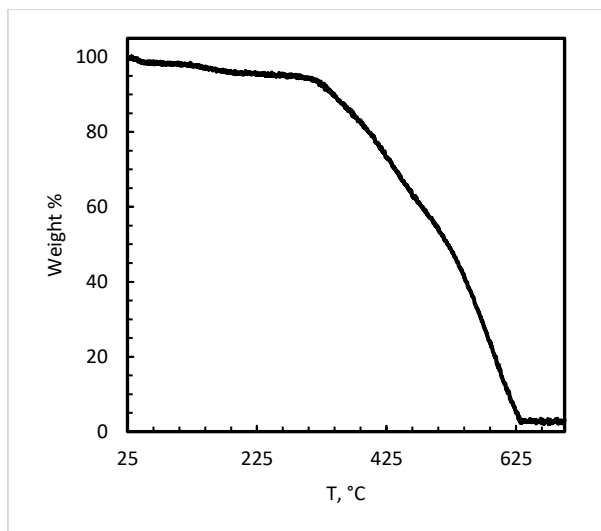


**Figure S34.** Mass loss as a function of temperature for sample corresponding to Entry 14 in Table S1.

Table S1, Entry 15

IR (ATR-FTIR,  $\text{cm}^{-1}$ ):  $\nu$  3445w (O-H), 2918w (C-H), 1678s (C=O), 1605m (C=C), 1510w, 1402m, 1263m, 1213s, 981s, 818s, 550m.

TGA:  $T_d = 363$  °C

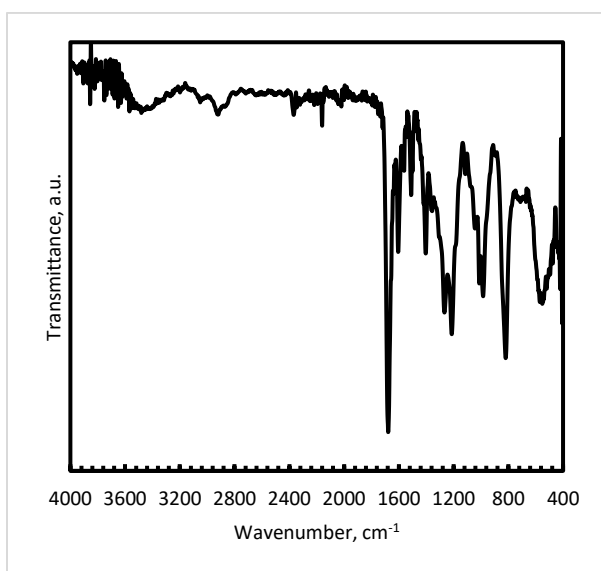


**Figure S35.** Infrared spectrum (ATR-FTIR) of the sample corresponding to Entry 15 in Table S1.

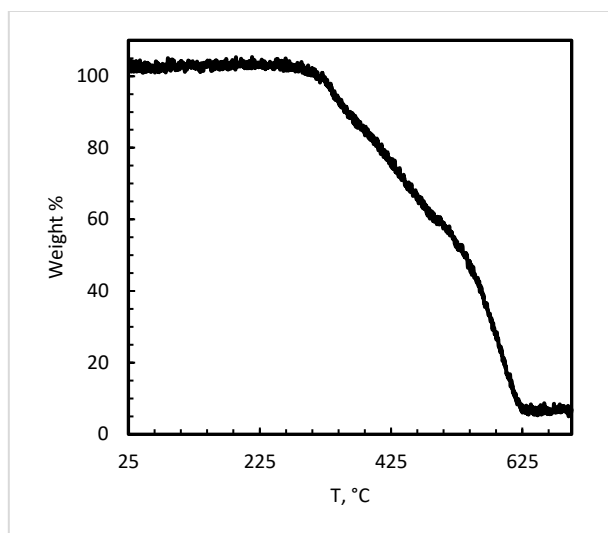


**Figure S36.** Mass loss as a function of temperature for sample corresponding to Entry 15 in Table S1.

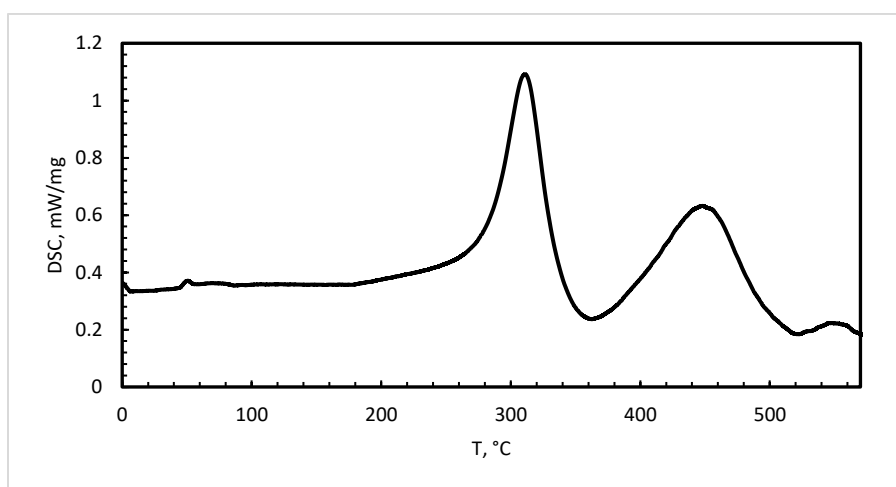


**Figure S37.** DSC trace corresponding to Table S1; Entry 15.

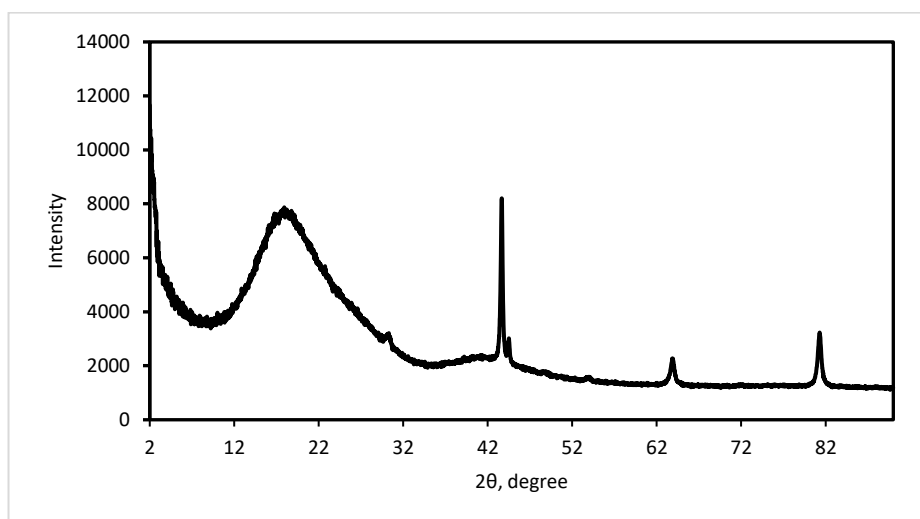


**Figure S38.** Experimental powder XRD patterns of the sample corresponding to Entry 15 in Table S1. Crystalline peaks are from Teflon substrate.

Table S1, Entry 16

IR (ATR-FTIR,  $\text{cm}^{-1}$ ):  $\nu$  3404w (O-H), 2911w (C-H), 1676s (C=O), 1603m (C=C), 1508w, 1402m, 1267s, 1211s, 984m, 818s, 555m.

TGA:  $T_d = 343$  °C

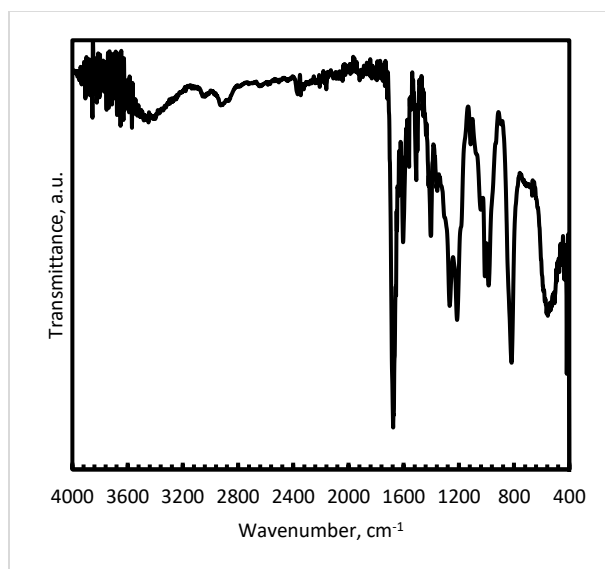


**Figure S39.** Infrared spectrum (ATR-FTIR) of the sample corresponding to Entry 16 in Table S1.

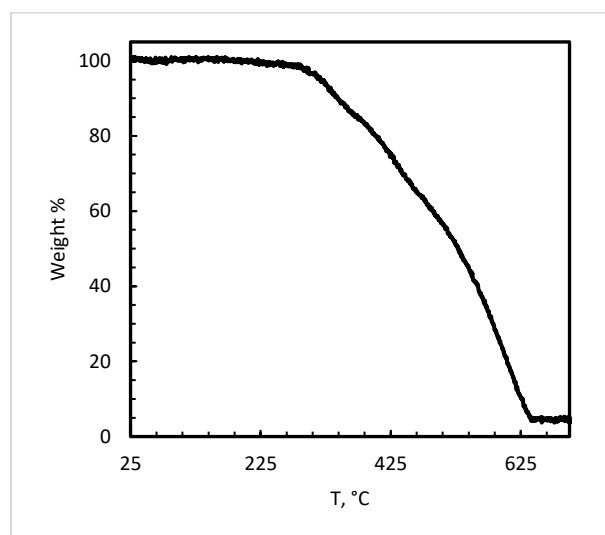


**Figure S40.** Mass loss as a function of temperature for sample corresponding to Entry 16 in Table S1.

Table S1, Entry 17

IR (ATR-FTIR,  $\text{cm}^{-1}$ ):  $\nu$  3449w (O-H), 2914w (C-H), 1676s (C=O), 1604m (C=C), 1510w, 1402m, 1267s, 1213s, 983m, 818s, 548m.

TGA:  $T_d = 344\text{ }^\circ\text{C}$

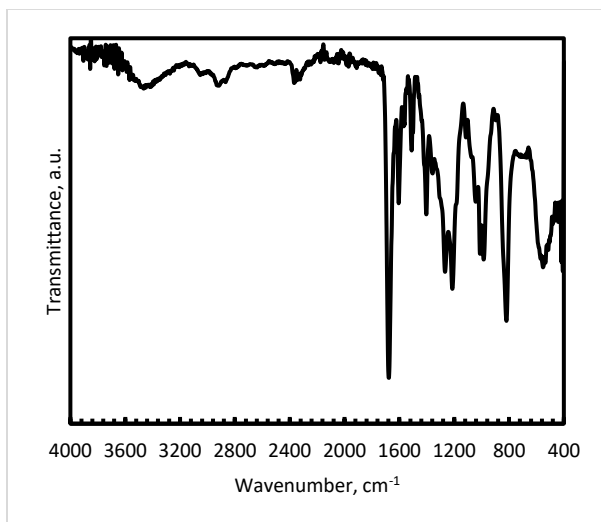


**Figure S41.** Infrared spectrum (ATR-FTIR) of the sample corresponding to Entry 17 in Table S1.

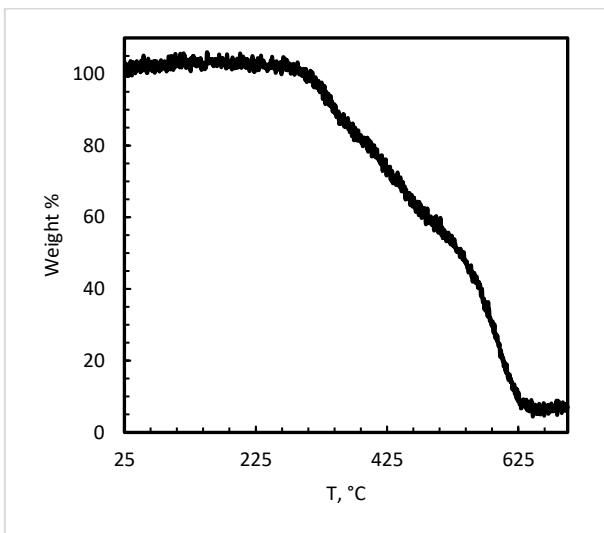


**Figure S42.** Mass loss as a function of temperature for sample corresponding to Entry 17 in Table S1.

Table S1, Entry 18

IR (ATR-FTIR,  $\text{cm}^{-1}$ ):  $\nu$  3424w (O-H), 2924w (C-H), 1672s (C=O), 1599s (C=C), 1287m, 1267s, 1015m, 824s.

TGA:  $T_d = 396\text{ }^\circ\text{C}$

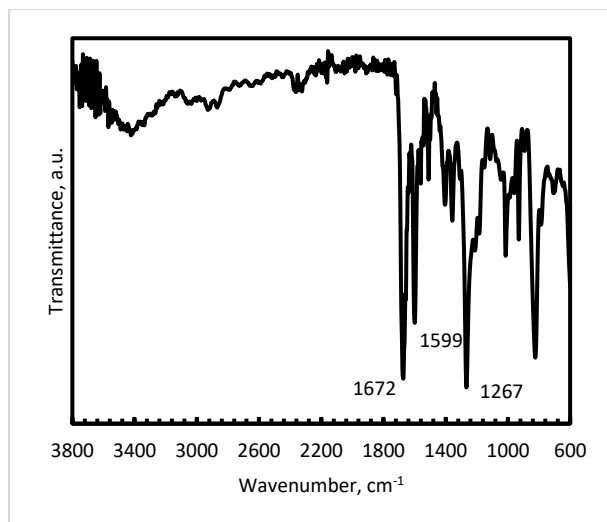


**Figure S43.** Infrared spectrum (ATR-FTIR) of the sample corresponding to Entry 18 in Table S1.

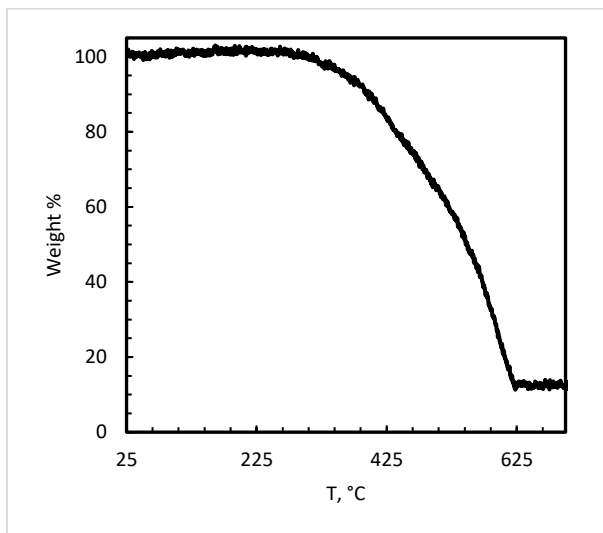


**Figure S44.** Mass loss as a function of temperature for sample corresponding to Entry 18 in Table S1.

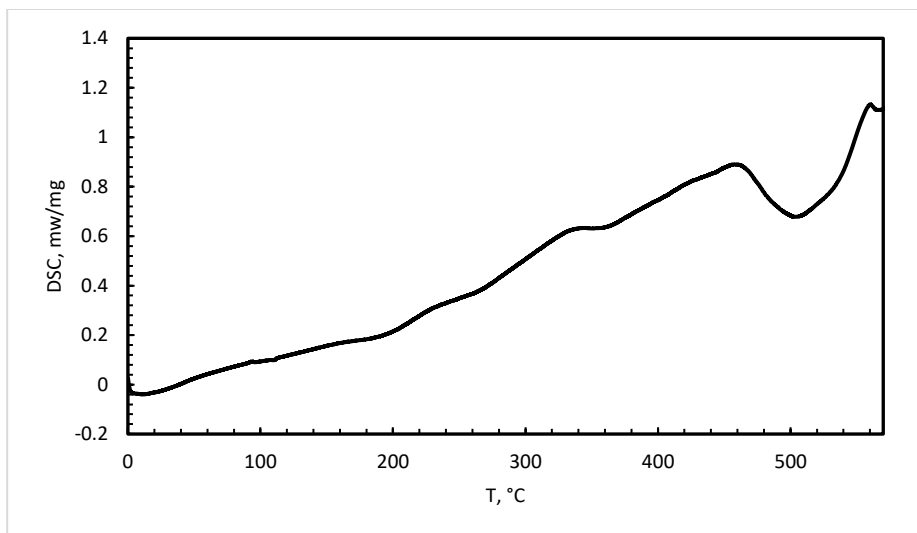


**Figure S45.** DSC trace corresponding to Entry 18 in Table S1.

Table S1, Entry 19

The isolated amount was not enough to perform analysis.

Table S1, Entry 20

The isolated amount was not enough to perform analysis.

**1.4 NMR spectra of mother liquor from coupling reaction of 1,4-diacetylbenzene and 1,4-benzenedimethanol as described in Table S1.**

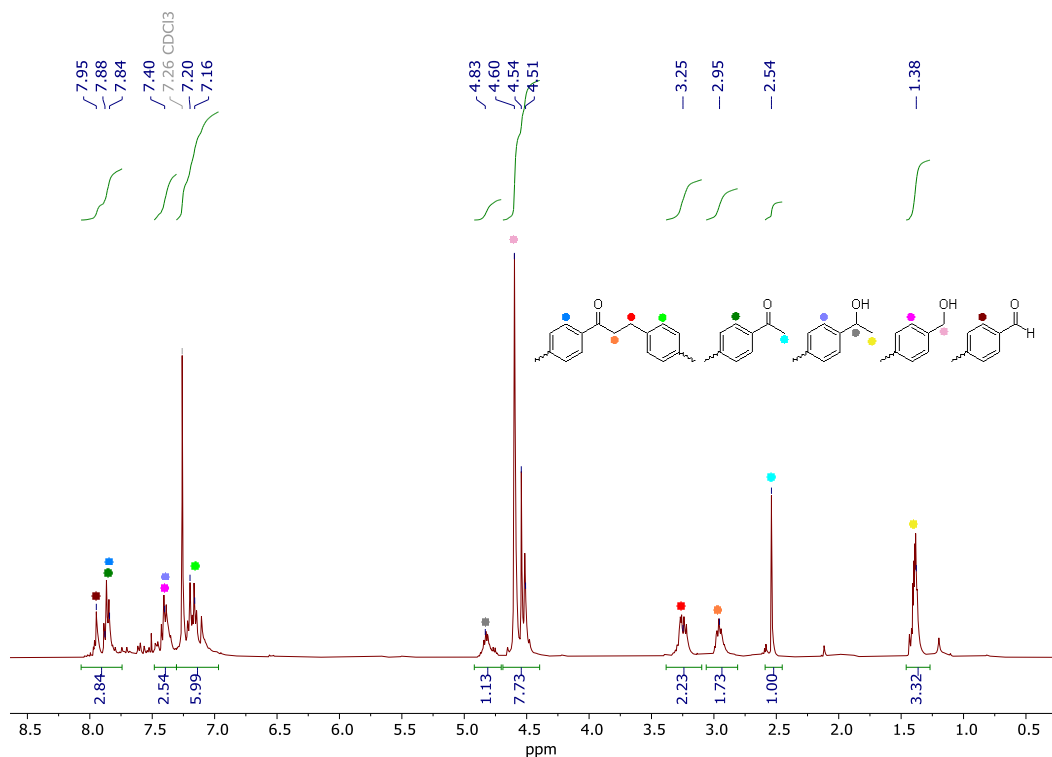


**Figure S46.**  $^1\text{H}$  NMR spectrum of mother liquor after polymer precipitation from the reaction Table S1; Entry 7 in  $\text{CDCl}_3/\text{CD}_3\text{OD} = 3/1$  at room temperature.

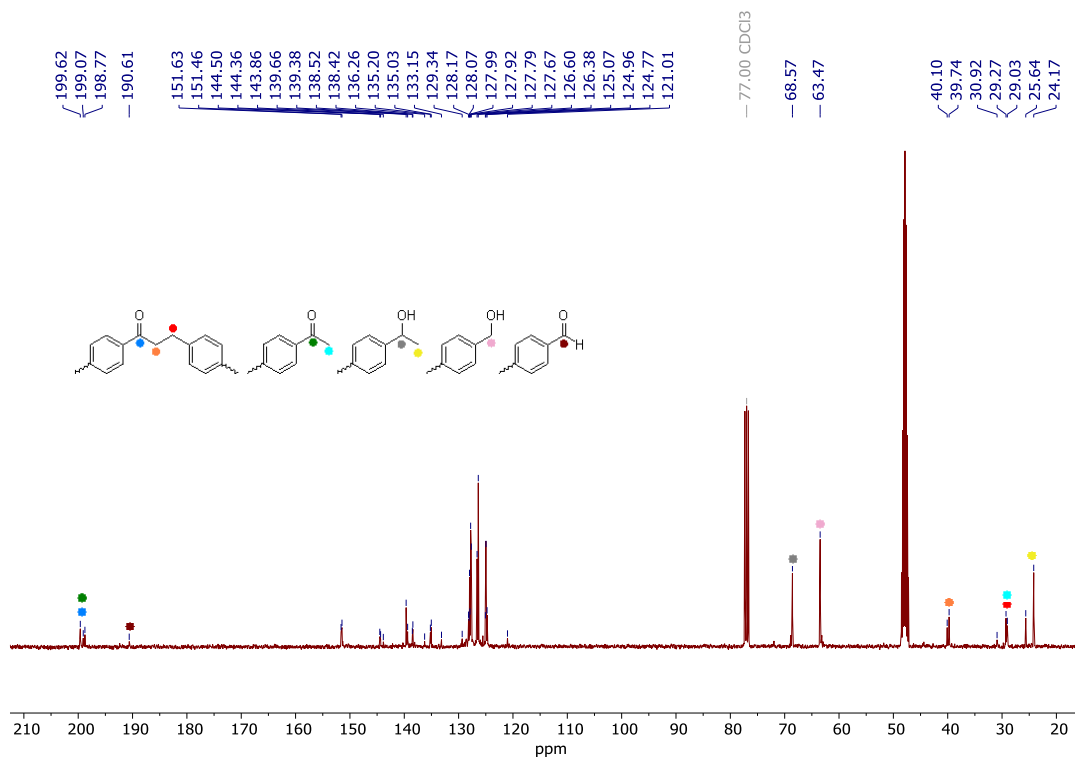


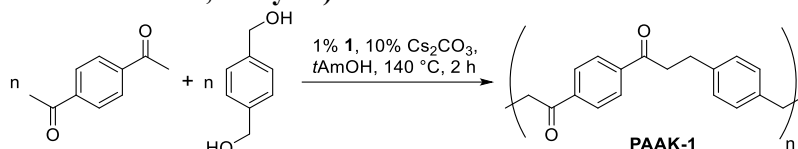
**Figure S47.**  $^{13}\text{C}\{^1\text{H}\}$  NMR spectrum of mother liquor after polymer precipitation from the reaction Entry 7 in Table S1 in  $\text{CDCl}_3/\text{CD}_3\text{OD} = 3/1$  at room temperature.

## 1.5 Synthesis of polyketones from diketones and diols.

General method for the coupling of diketones and 1,4-benzenedimethanol, 1,3-benzenedimethanol and 1,4-cyclohexanedimethanol:

A 100 mL ampoule equipped with a J-Young's valve was charged with pre-catalyst **1** (2.5 mg, 0.005 mmol, 1 mol%) and Cs<sub>2</sub>CO<sub>3</sub> (16.5 mg, 0.05 mmol, 10 mol%), diol (0.5 mmol) and diketone (0.5 mmol). The flask was sealed under an argon atmosphere and *tert*-amyl alcohol (5 mL) was added before heating to 140 °C for 2 or 18 h with stirring. After this period, the reaction vessel was allowed to cool to room temperature and any gas evolved (presumably H<sub>2</sub>) during the reaction was measured when possible. To the resulting mixture 5 mL of 1 M HCl were added and the flask had been heated at 90 °C for 1 h. The precipitate was filtered and dried under reduced pressure at 120 °C.

### PAAK-1 (corresponds to Table S1, entry 15)



1,4-Dimethanolbenzene (69 mg, 0.5 mmol) and 1,4-diacetylbenzene (81 mg, 0.5 mmol) were used. The polymer was obtained in 89% yield (117 mg) as a yellow solid.

IR (ATR-FTIR, cm<sup>-1</sup>):  $\nu$  3445w (O-H), 2918w (C-H), 1678s (C=O), 1605m (C=C), 1510w, 1402m, 1263m, 1213s, 981s, 818s, 550m.

TGA: T<sub>d</sub> = 363 °C

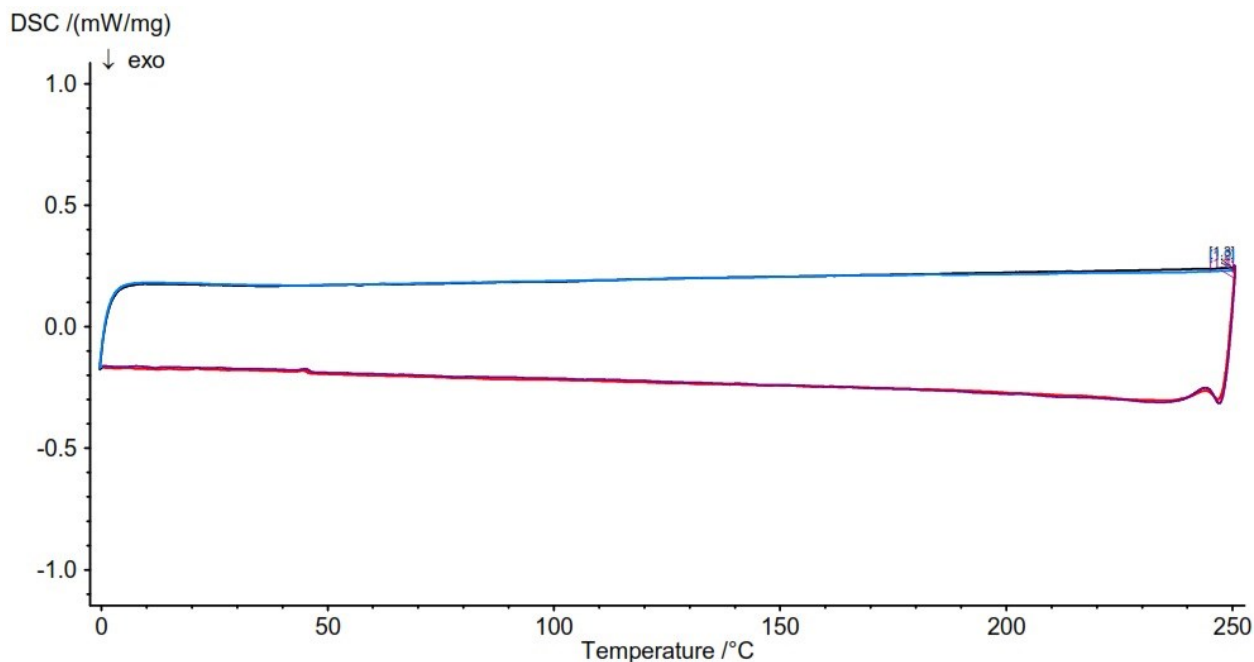
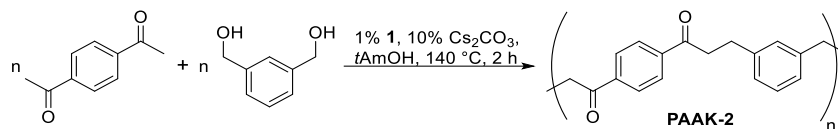


Figure S48. DSC trace corresponding to PAAK-1 (two cycles at 0–250 °C).

## PAAK-2



1,3-benzenedimethanol (69 mg, 0.5 mmol) and 1,4-diacetylbenzene (81 mg, 0.5 mmol) were used. The polymer was obtained with 77% yield (101 mg) as a yellow solid.

<sup>13</sup>C CP MAS NMR (100.6 MHz): δ 199.4, 151.3, 141.1, 128.2, 70.8, 64.5, 41.1, 36.2, 28.8.

IR (ATR-FTIR, cm<sup>-1</sup>): ν 3422w (O-H), 2918w (C-H), 1678s (C=O), 1605m (C=C), 1449w, 1402m, 1265m, 1211s, 984s, 793m, 704s.

TGA: T<sub>d</sub> = 351 °C

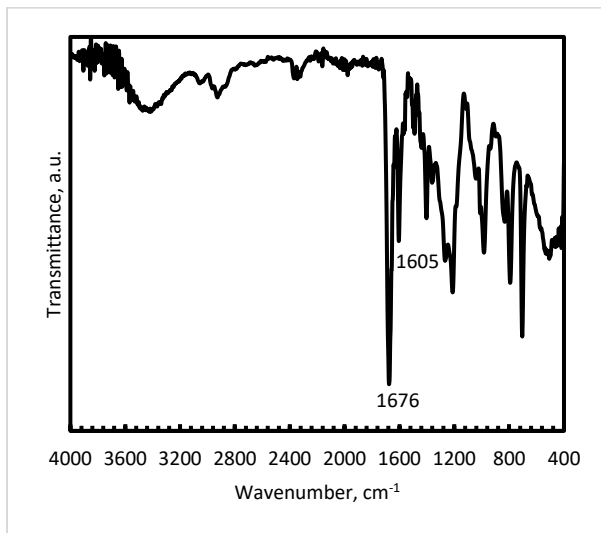


Figure S49. Infrared spectrum (ATR-FTIR) of polyketone PAAK-2.

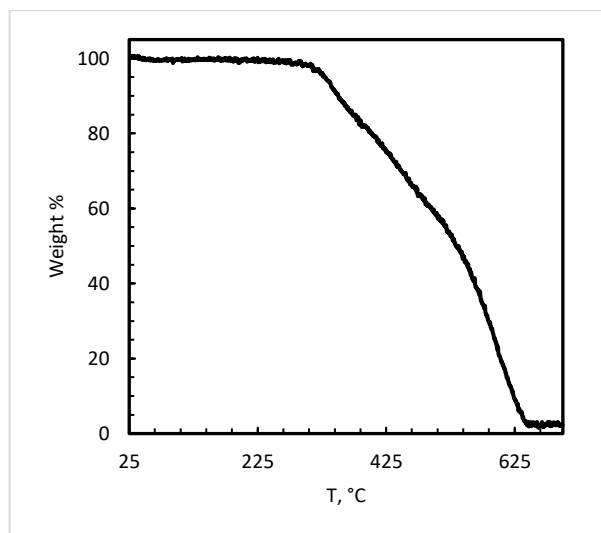
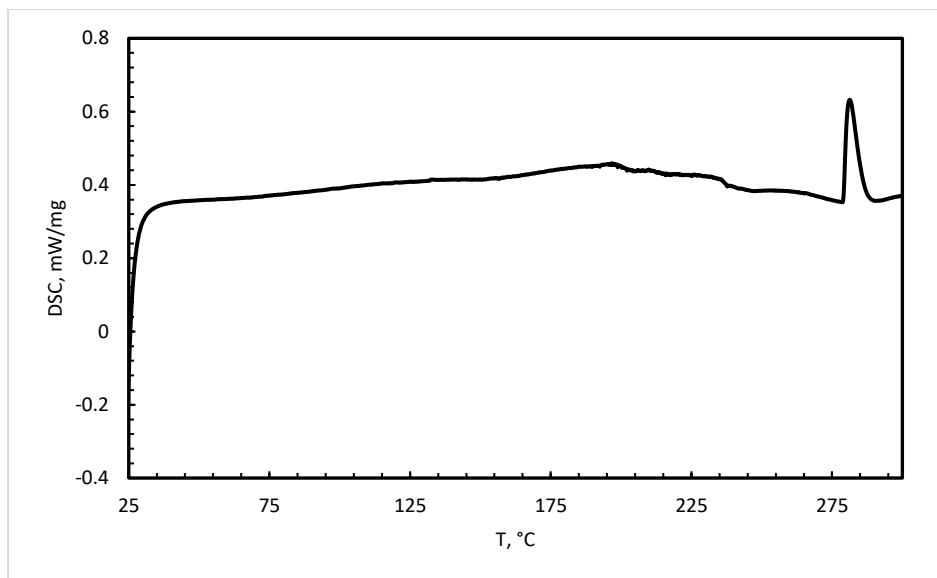
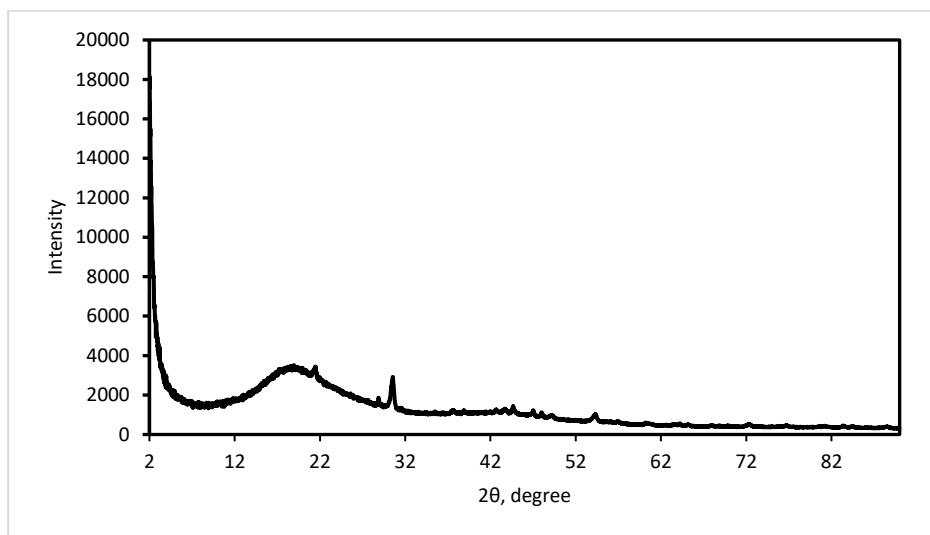


Figure S50. Mass loss as a function of temperature for polyketone PAAK-2.



**Figure S51.** DSC trace corresponding to **PAAK-2**.



**Figure S52.** Experimental powder XRD patterns of **PAAK-2**. Crystalline peaks were indexed in the small-volume unit cell which remains unidentified.

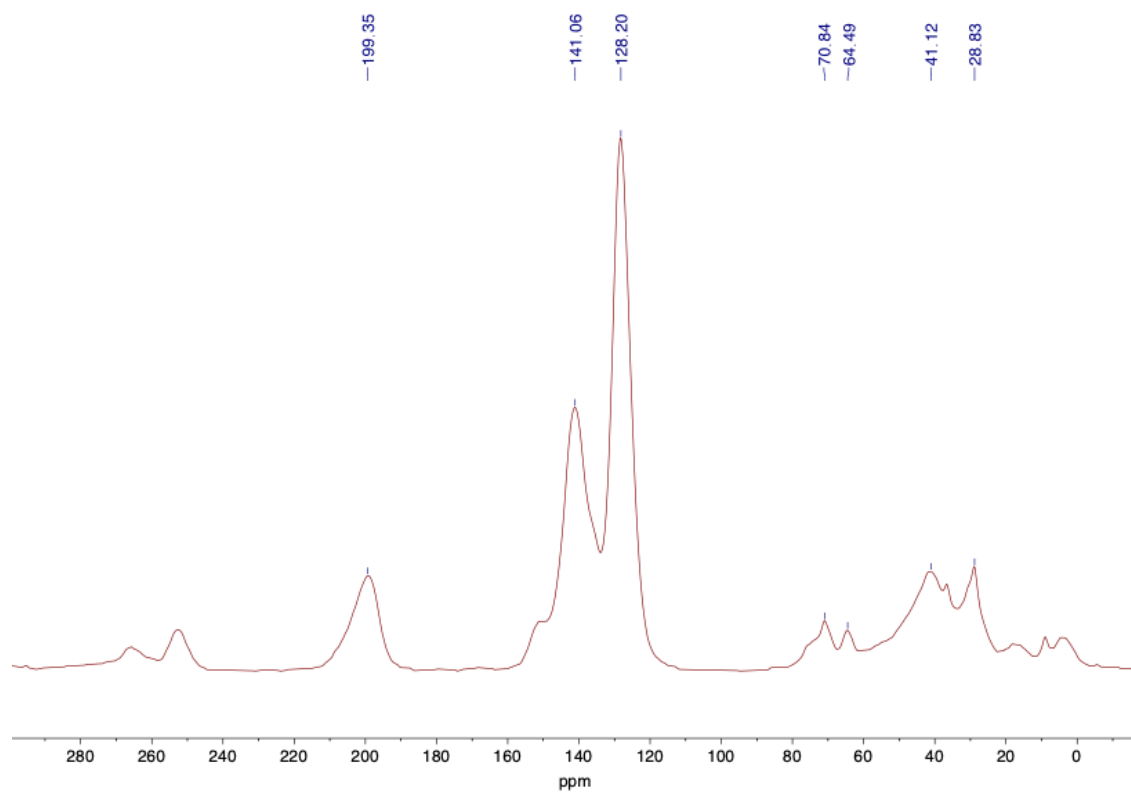
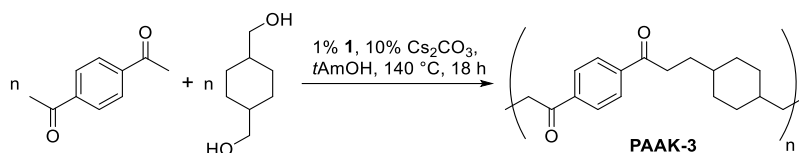


**Figure S53.**  $^{13}\text{C}$  CP MAS NMR spectrum of **PAAK-2**.

### PAAK-3



1,4-Cyclohexanedimethanol (72 mg, 0.5 mmol) and 1,4-diacetylbenzene (81 mg, 0.5 mmol) were used. The polymer was obtained in 41% yield (55 mg) as a yellow solid.

<sup>13</sup>C CP MAS NMR (100.6 MHz): δ 199.9, 148.1, 140.2, 128.4, 75.8, 68.4, 48.5, 36.7, 41.1, 30.7.

IR (ATR-FTIR, cm<sup>-1</sup>): ν 3482w (O-H), 2918m (C-H), 2853m (C-H), 1676s (C=O), 1605m (C=C), 1402m, 1269m, 1217m, 1011m, 829m, 503m.

TGA: T<sub>d</sub> = 369 °C

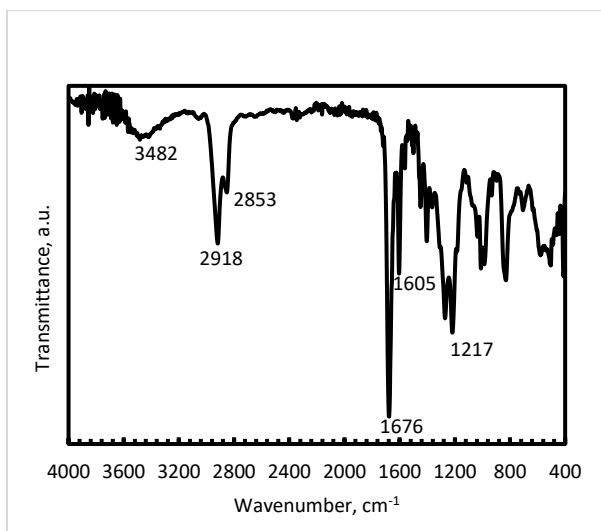


Figure S54. Infrared spectrum (ATR-FTIR) of polyketone PAAK-3.

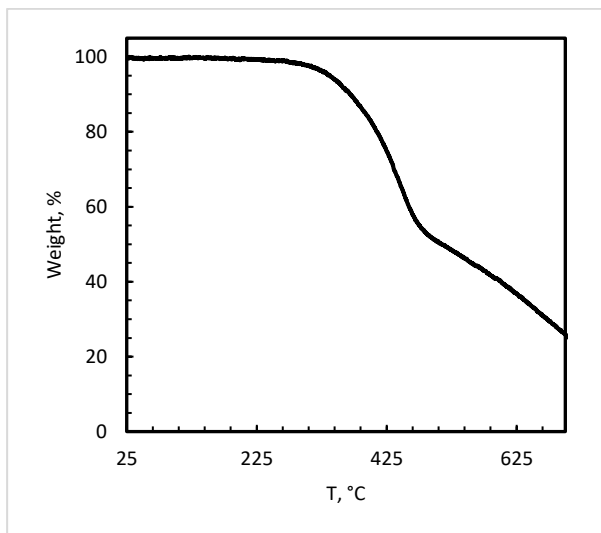


Figure S55. Mass loss as a function of temperature for polyketone PAAK-3.

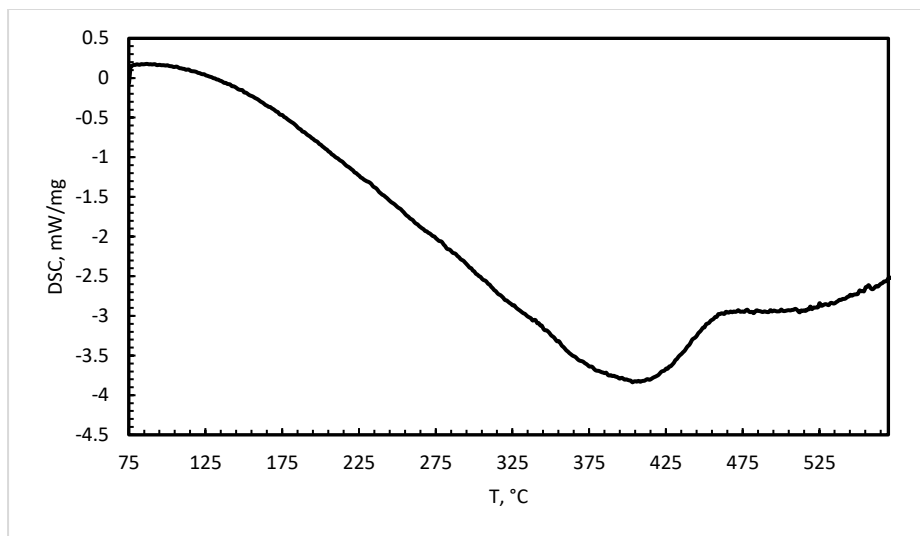


Figure S56. DSC trace corresponding to PAAK-3.

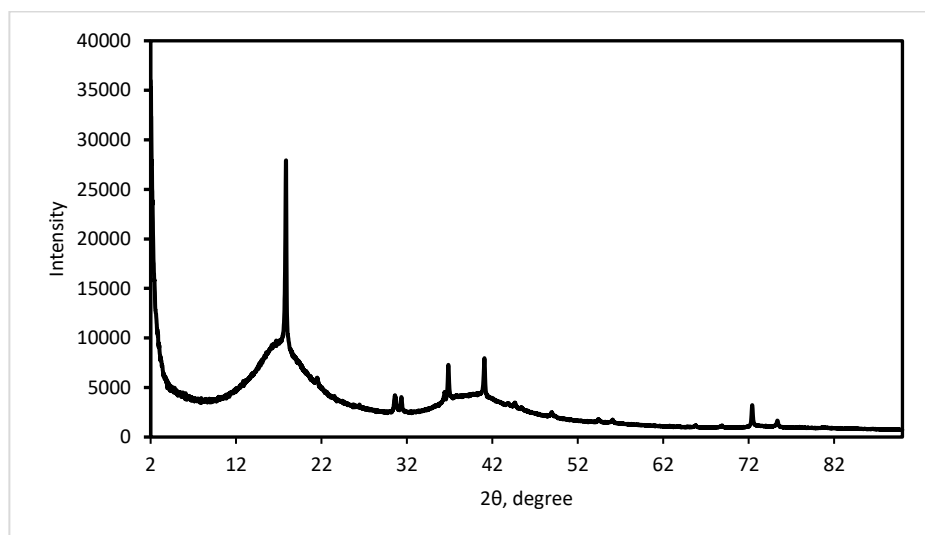
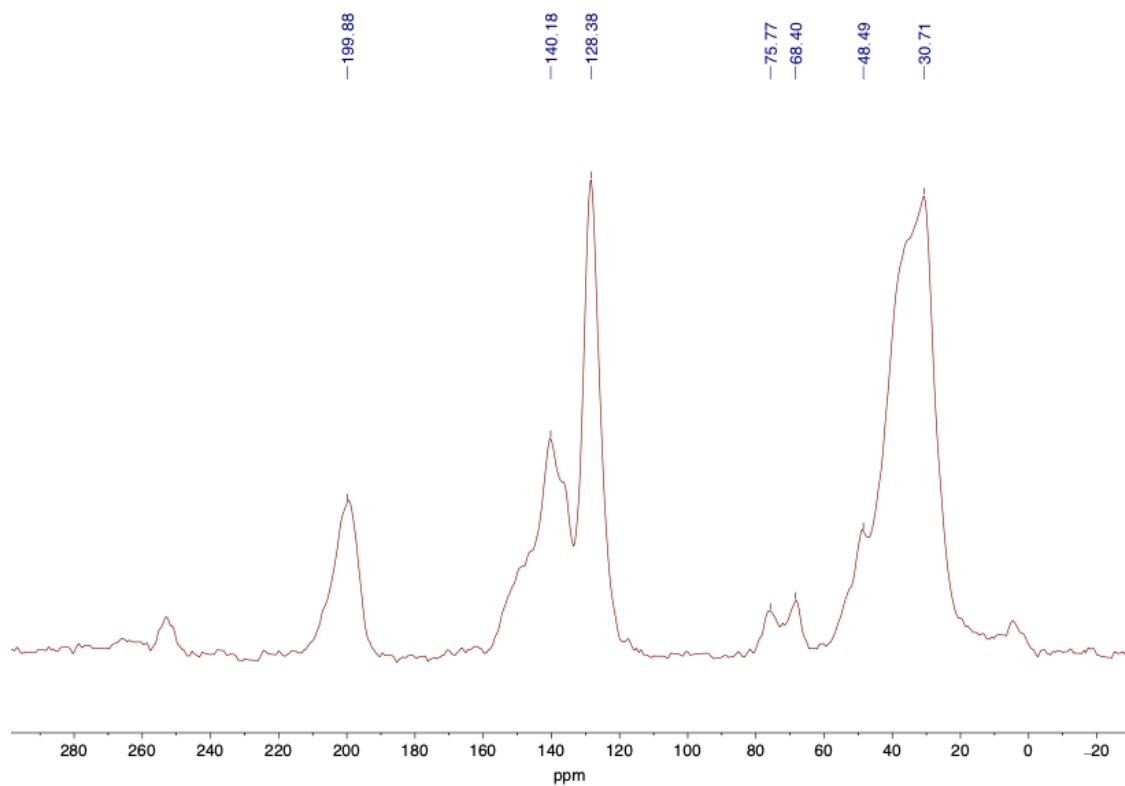
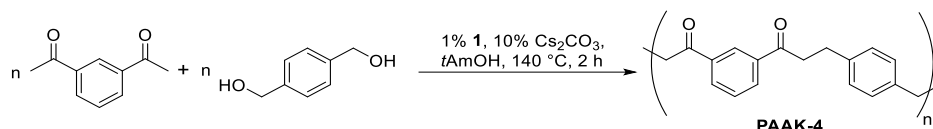


Figure S57. Experimental powder XRD patterns of PAAK-3. Unidentifiable crystalline phase presents.



**Figure S58.**  $^{13}\text{C}$  CP MAS NMR spectrum of PAAK-3.

## PAAK-4



1,4-Benzenedimethanol (69 mg, 0.5 mmol) and 1,3-diacetylbenzene (81 mg, 0.5 mmol) were used. The polymer was obtained in 98 % yield (129 mg) as a yellow solid.

$^{13}\text{C}$  CP MAS NMR (100.6 MHz):  $\delta$  199.5, 141.0, 137.9, 128.6, 75.1, 71.0, 64.5, 41.2, 37.2, 29.1.

IR (ATR-FTIR,  $\text{cm}^{-1}$ ):  $\nu$  3472w (O-H), 3059w, 2920w (C-H), 1680s (C=O), 1597m, 1171m, 999w, 795m, 704m.

TGA:  $T_d = 321\text{ }^\circ\text{C}$

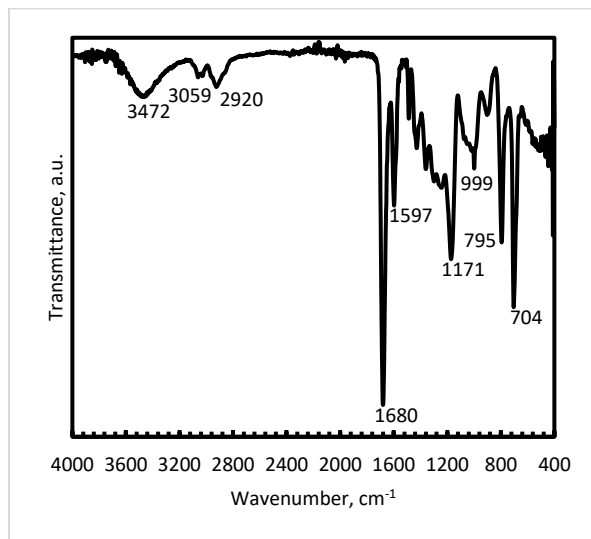


Figure S59. Infrared spectrum (ATR-FTIR) of polyketone PAAK-4.

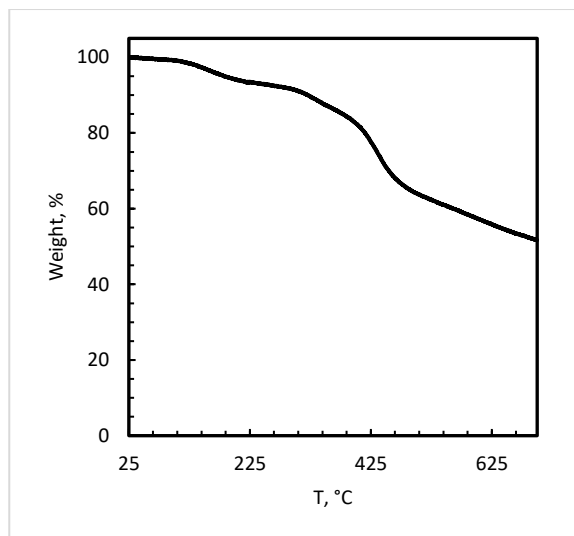


Figure S60. Mass loss as a function of temperature for polyketone PAAK-4.

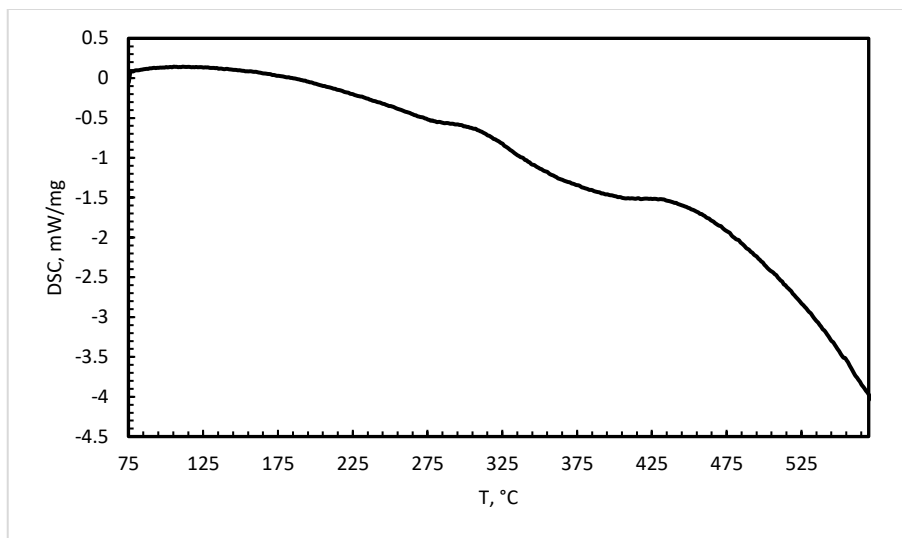


Figure S61. DSC trace corresponding to PAAK-4.

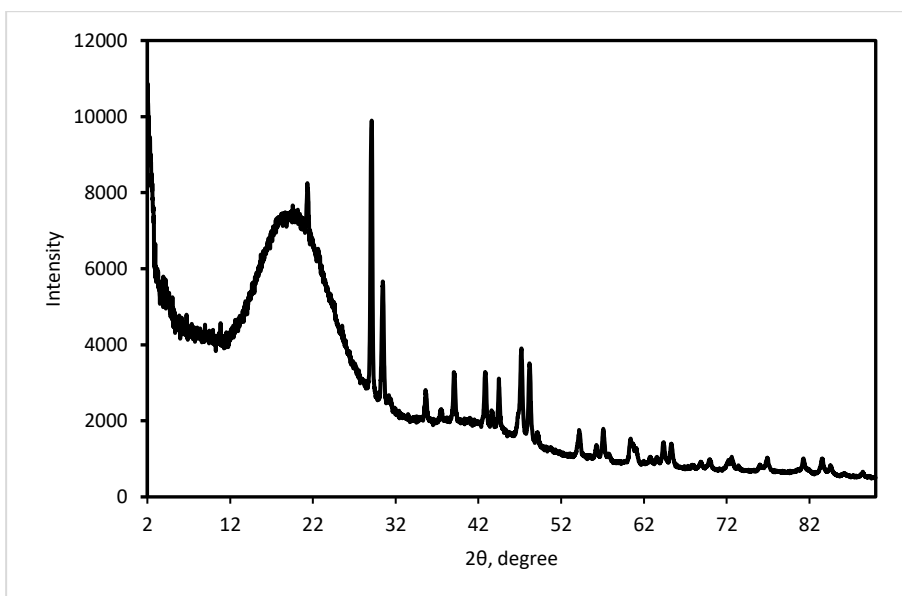
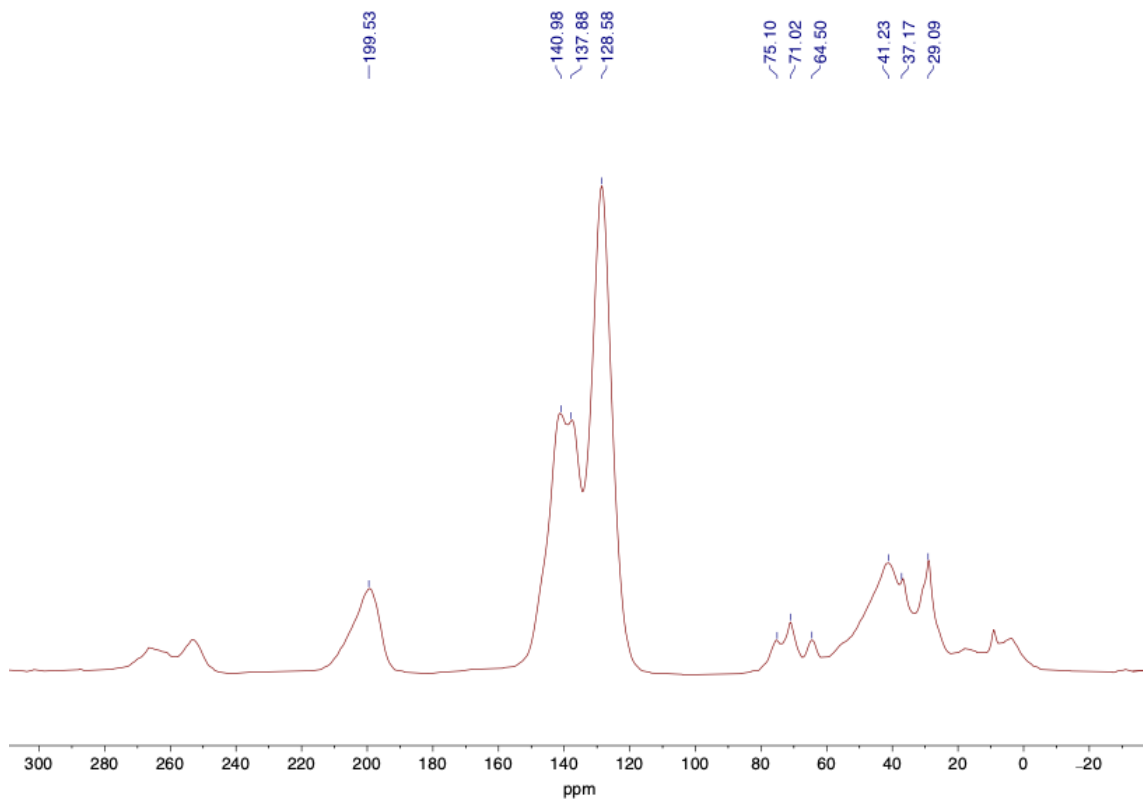
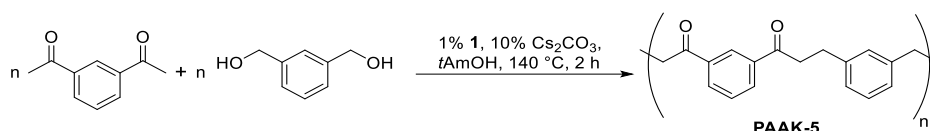


Figure S62. Experimental powder XRD patterns of PAAK-4. Unidentifiable crystalline phase presents.



**Figure S63.**  $^{13}\text{C}$  CP MAS NMR spectrum of PAAK-4.

## PAAK-5



1,3-Benzenedimethanol (69 mg, 0.5 mmol) and 1,3-diacetylbenzene (81 mg, 0.5 mmol) were used. The polymer was obtained in 97 % yield (128 mg) as a yellow solid.

$^{13}\text{C}$  CP MAS NMR (100.6 MHz):  $\delta$  199.5, 138.3, 128.9, 75.1, 70.9, 64.2, 41.4, 29.0.

IR (ATR-FTIR,  $\text{cm}^{-1}$ ):  $\nu$  3422w (O-H), 3049w, 2914w (C-H), 1678s (C=O), 1597m, 1171m, 1016w, 804m, 696w, 554m.

TGA:  $T_d = 338\text{ }^\circ\text{C}$

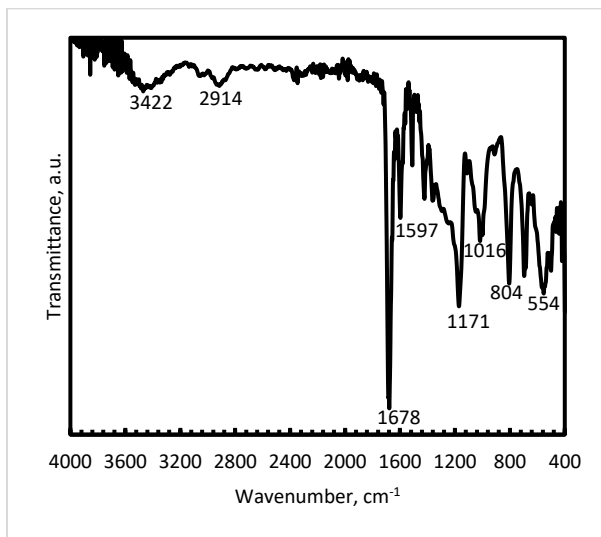


Figure S64. Infrared spectrum (ATR-FTIR) of polyketone PAAK-5.

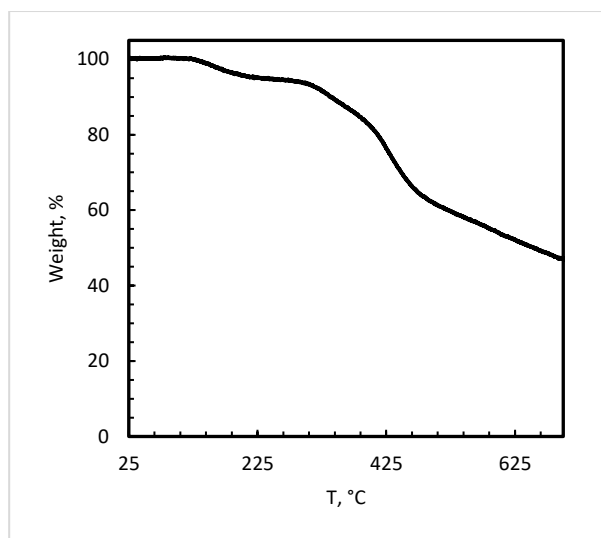
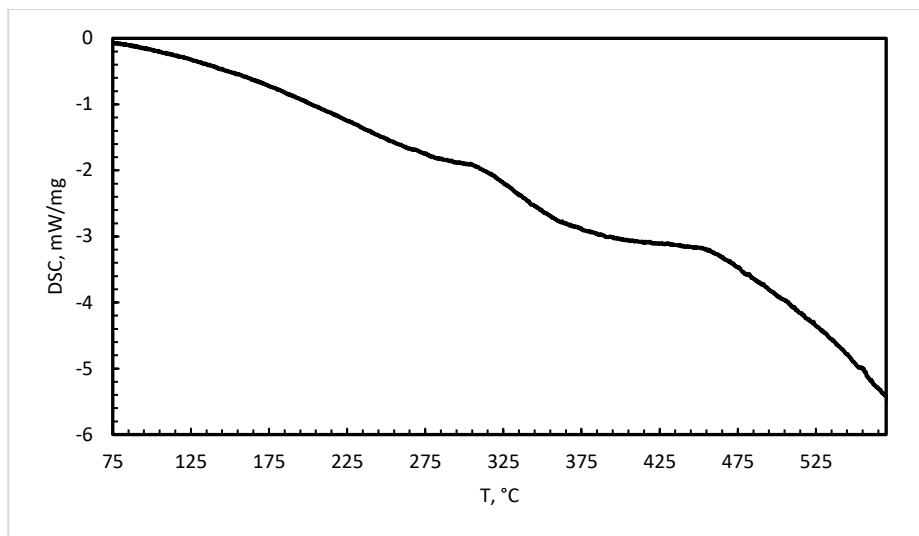
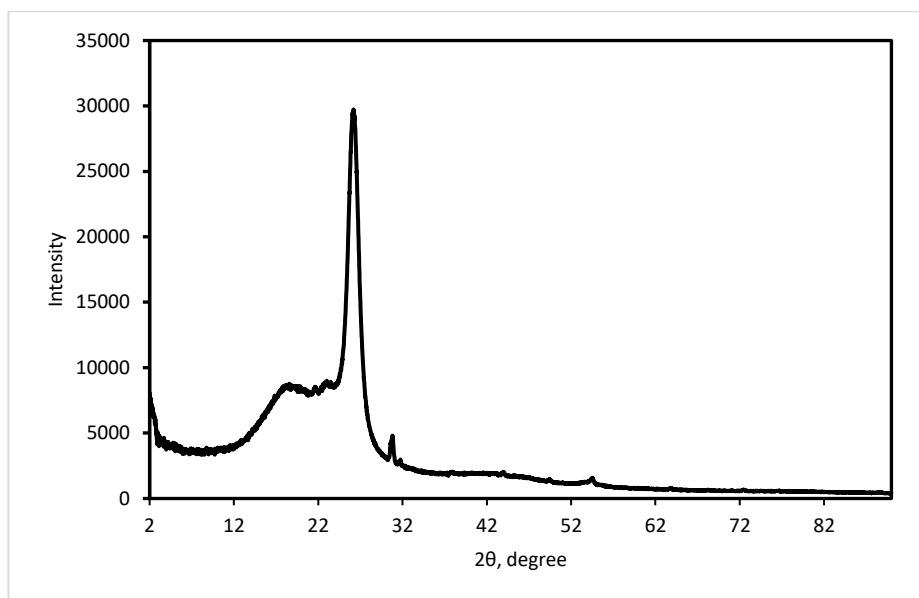


Figure S65. Mass loss as a function of temperature for polyketone PAAK-5.



**Figure S66.** DSC trace corresponding to **PAAK-5**.



**Figure S67.** Experimental powder XRD patterns of **PAAK-5**. Crystalline peaks were indexed in the small-volume unit cell which remains unidentified. Tall thin amorphous halo is from polyester films used for measurements of small amount of sample.

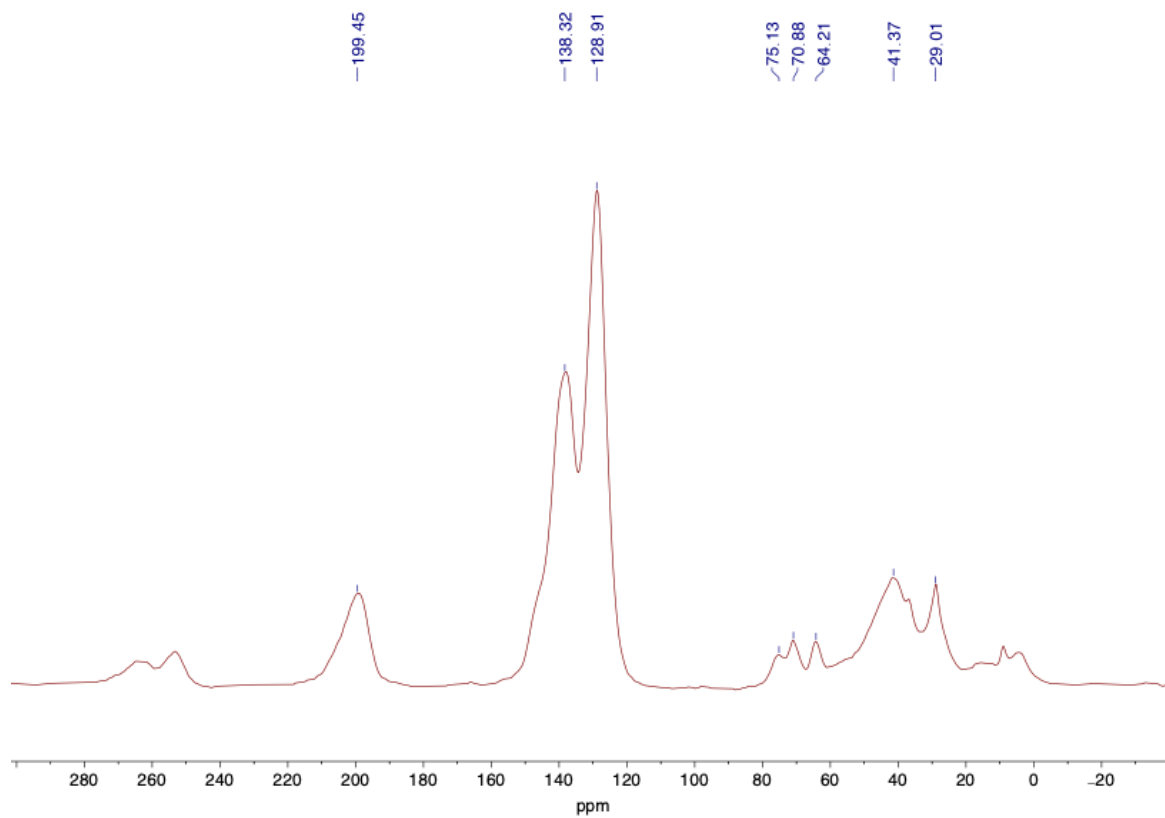
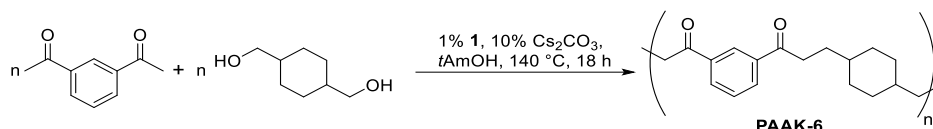


**Figure S68.**  $^{13}\text{C}$  CP MAS NMR spectrum of PAAK-5.

## PAAK-6



1,4-Cyclohexanedimethanol (72 mg, 0.5 mmol) and 1,3-diacetylbenzene (81 mg, 0.5 mmol) were used. The polymer was obtained in 99 % yield (134 mg) as a yellowish solid.

$^{13}\text{C}$  CP MAS NMR (100.6 MHz):  $\delta$  199.9, 146.9, 137.5, 128.8, 74.4, 71.0, 47.9, 36.4, 34.0, 29.3.

IR (ATR-FTIR,  $\text{cm}^{-1}$ ):  $\nu$  3485w (O-H), 2926s (C-H), 2851m (C-H), 1678s (C=O), 1597m, 1449m, 1269m, 1167s, 799m, 696s.

TGA:  $T_d = 357\text{ }^\circ\text{C}$

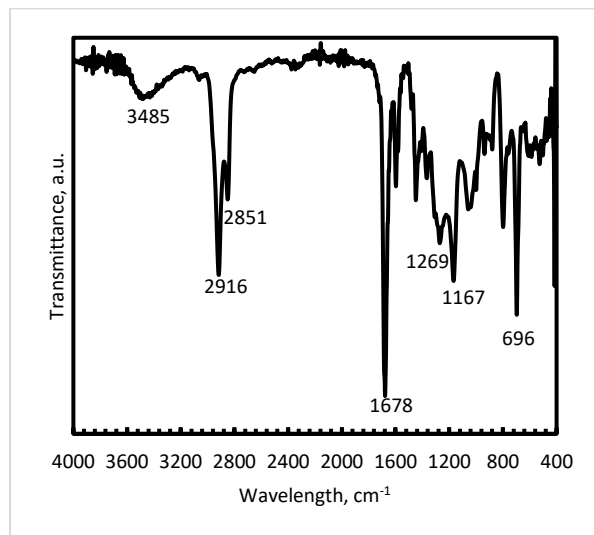


Figure S69. Infrared spectrum (ATR-FTIR) of polyketone PAAK-6.

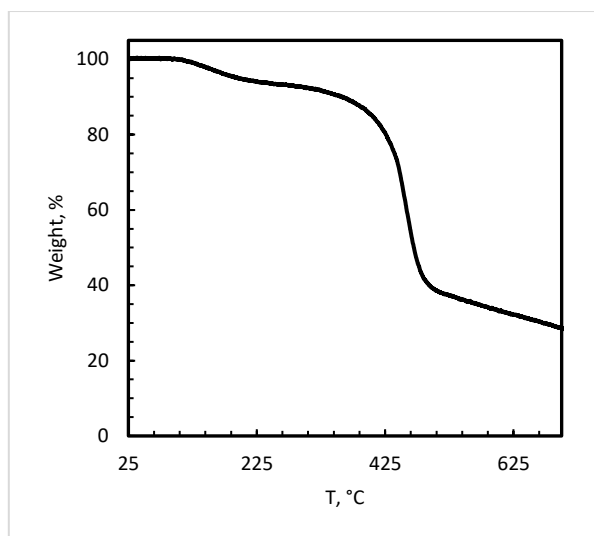
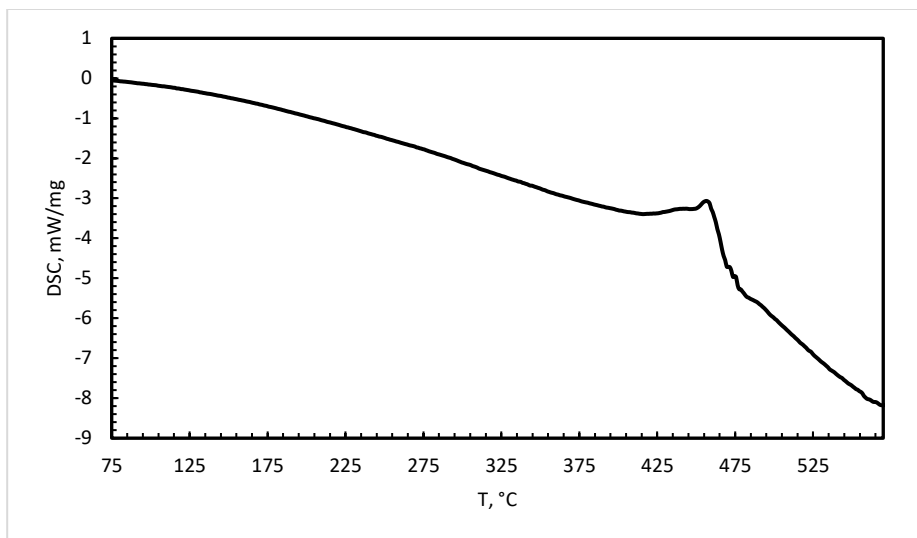
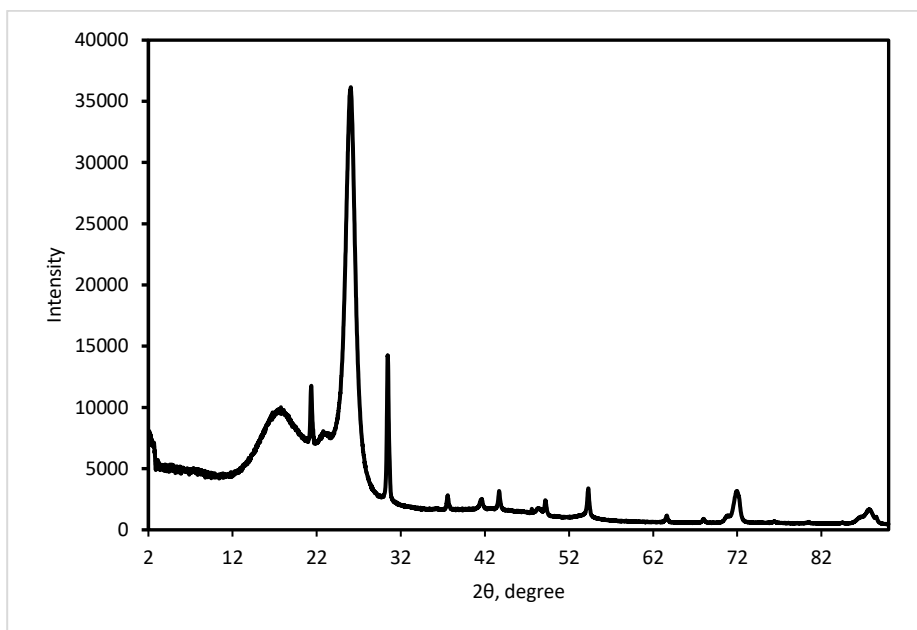


Figure S70. Mass loss as a function of temperature for polyketone PAAK-6.



**Figure S71.** DSC trace corresponding to **PAAK-6**.



**Figure S72.** Experimental powder XRD patterns of **PAAK-6**. Crystalline peaks were indexed in the small-volume unit cell which remains unidentified. Tall thin amorphous halo is from polyester film used for measurements of small amount of samples.

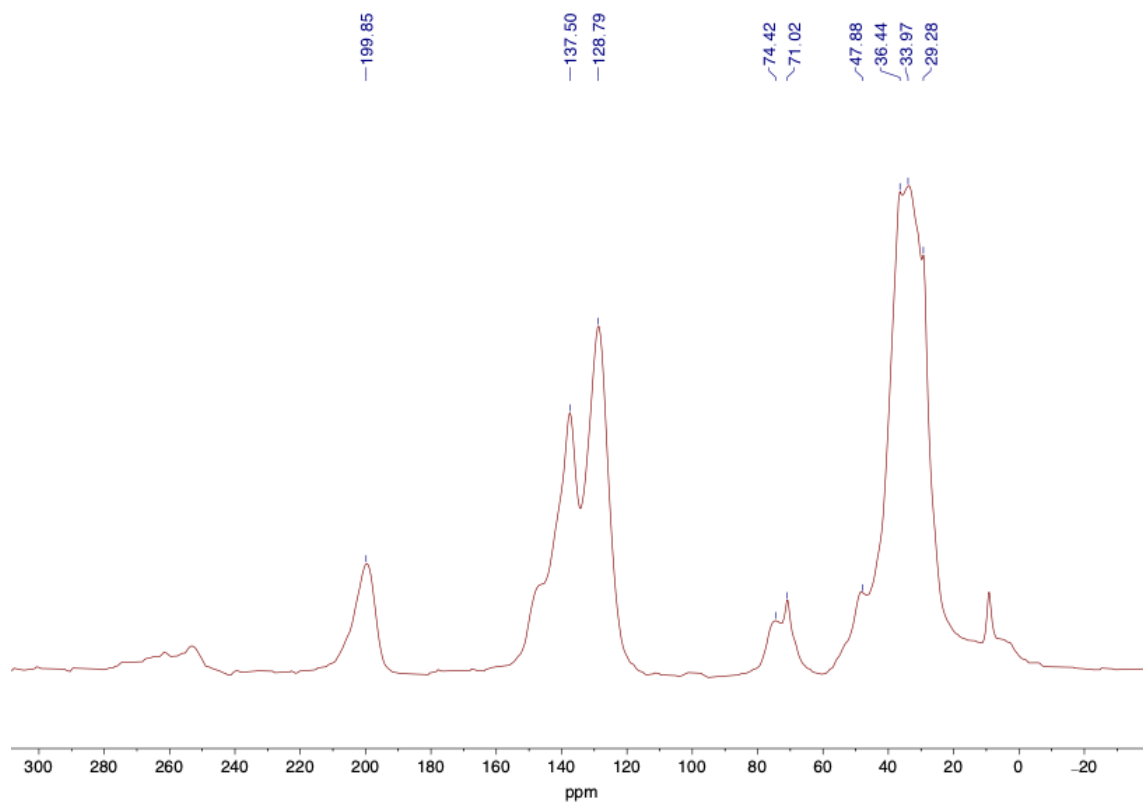
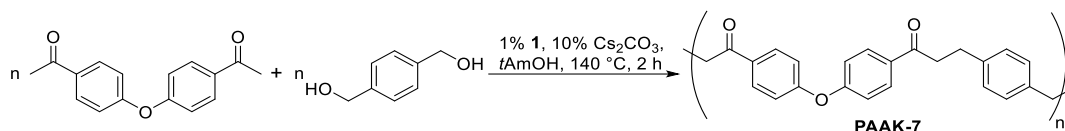


**Figure S73.**  $^{13}\text{C}$  CP MAS NMR spectrum of PAAK-6.

### PAAK-7



1,4-Dimethanolbenzene (69 mg, 0.5 mmol) and 4-acetylphenylether (127 mg, 0.5 mmol) were used. The polymer was obtained in 93% yield (165 mg) as a white solid.

$^{13}\text{C}$  CP MAS NMR (100.6 MHz):  $\delta$  198.1, 160.1, 140.3, 130.8, 121.0, 75.3, 64.4, 42.7.

IR (ATR-FTIR,  $\text{cm}^{-1}$ ):  $\nu$  3466w (O-H), 3055w, 2922w (C-H), 1672s (C=O), 1587s (C=C), 1497s, 1411w, 1233s (C-O), 1163s, 983m, 833s, 554m.

TGA:  $T_d = 362\text{ }^\circ\text{C}$

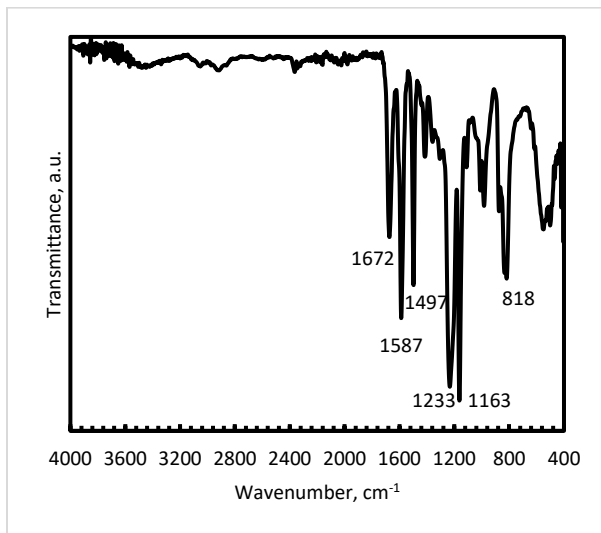


Figure S74. Infrared spectrum (ATR-FTIR) of polyketone PAAK-7.

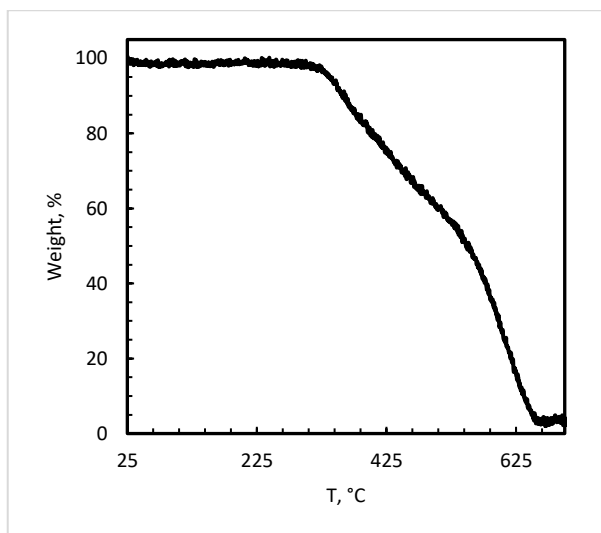
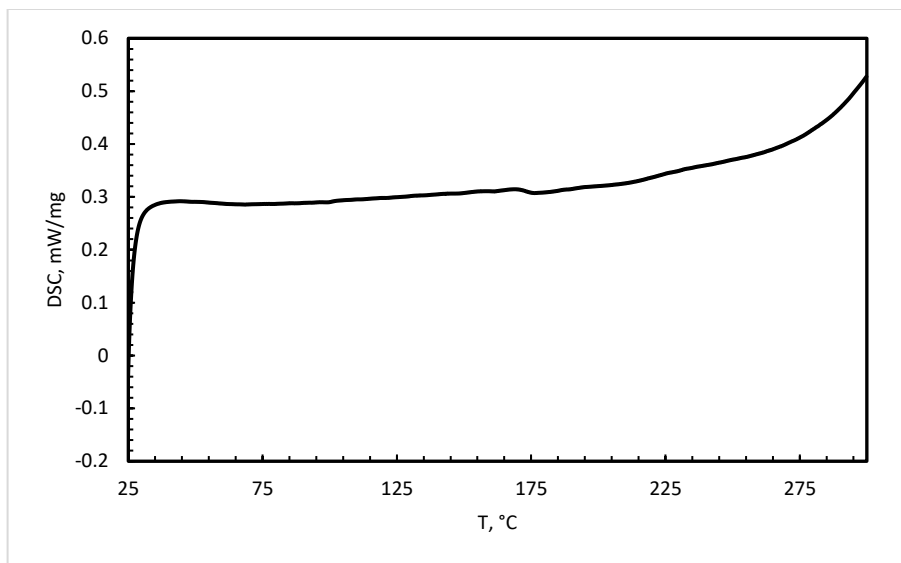
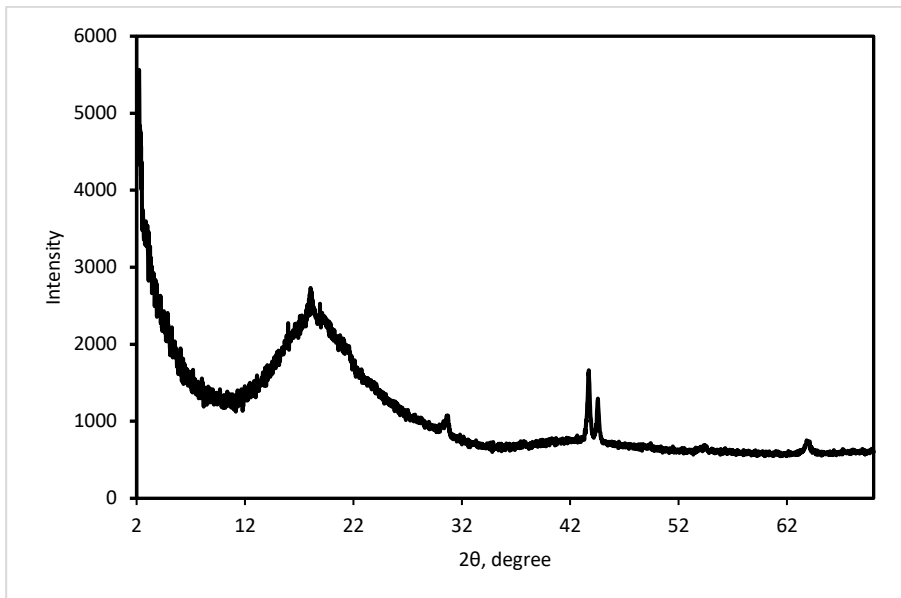


Figure S75. Mass loss as a function of temperature for polyketone PAAK-7.



**Figure S76.** DSC trace corresponding to PAAK-7.



**Figure S77.** Experimental powder XRD patterns of PAAK-7. Unidentifiable crystalline phase presents. Peaks at high angles are from crystalline Teflon substrate.

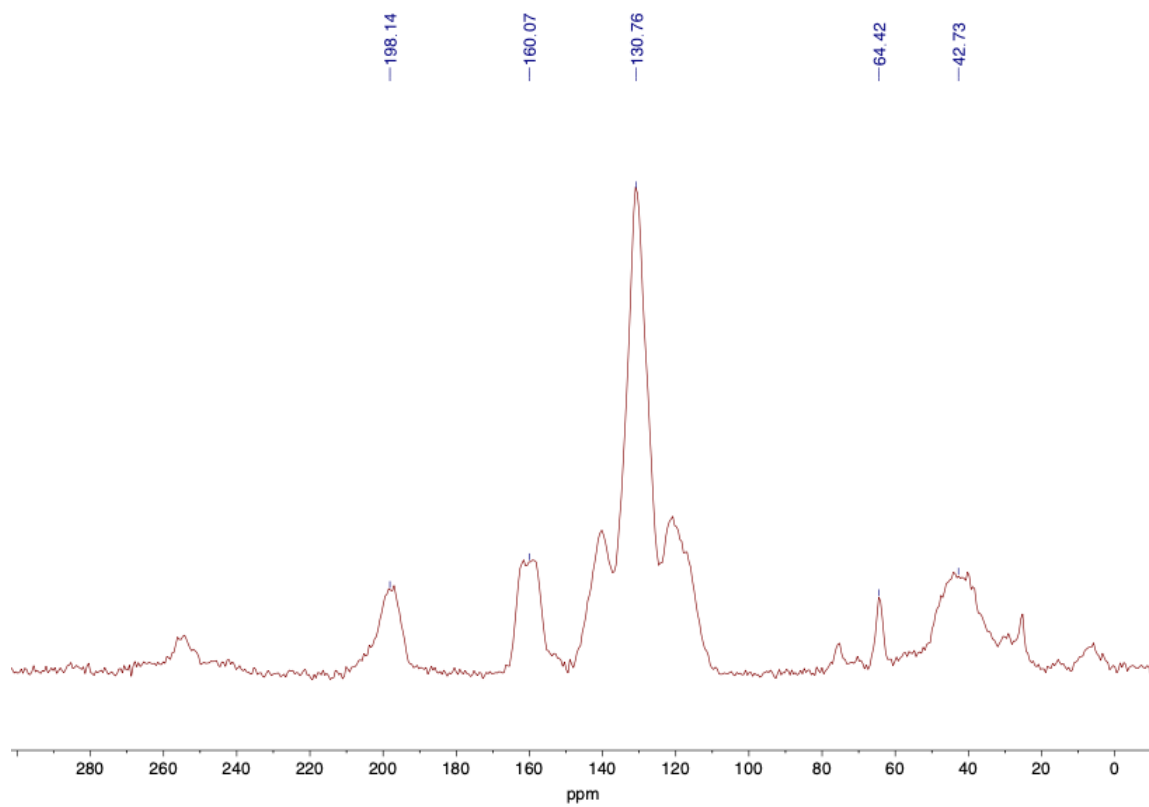
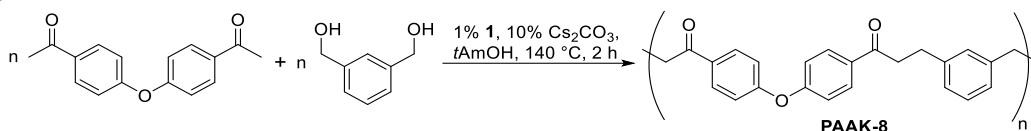


**Figure S78.**  $^{13}\text{C}$  CP MAS NMR spectrum of PAAK-7.

### PAAK-8



1,3-Dimethanolbenzene (69 mg, 0.5 mmol) and 4-acetylphenylether (127 mg, 0.5 mmol) were used. The polymer was obtained in 79% yield (140 mg) as a white solid.

$^{13}\text{C}$  CP MAS NMR (100.6 MHz):  $\delta$  198.0, 162.1, 158.9, 142.2, 131.0, 121.6, 75.3, 64.5, 41.7.

IR (ATR-FTIR,  $\text{cm}^{-1}$ ):  $\nu$  3066w (C-H), 2904w (C-H) 1674m (C=O), 1587s (C=C), 1499s, 1410w, 1234s, 1163s, 984w, 835m, 704w, 501w.

TGA:  $T_d = 365\text{ }^\circ\text{C}$

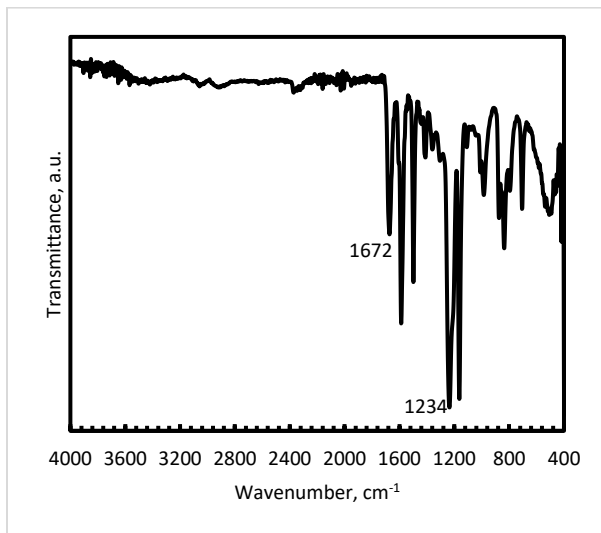


Figure S79. Infrared spectrum (ATR-FTIR) of polyketone PAAK-8.

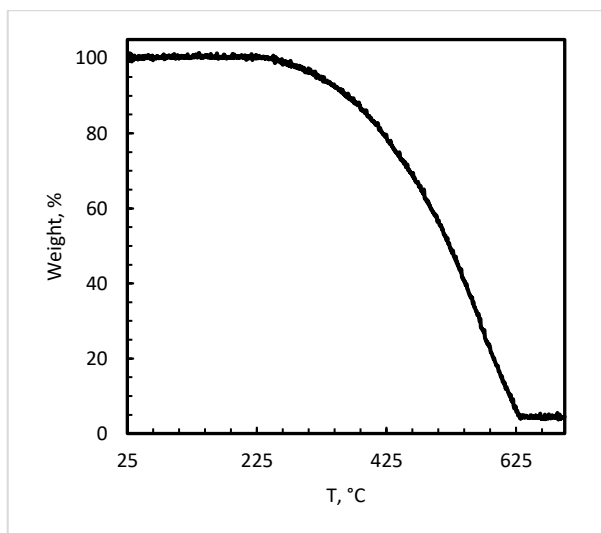
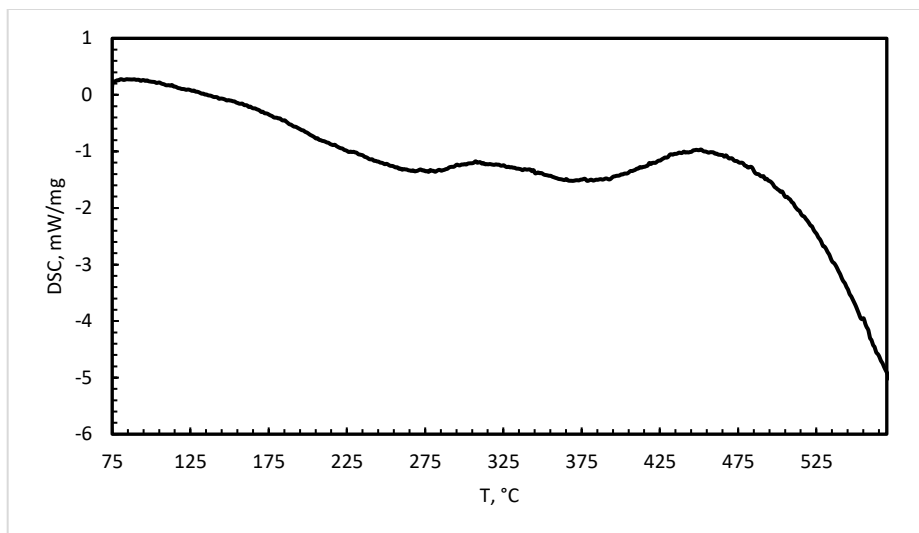
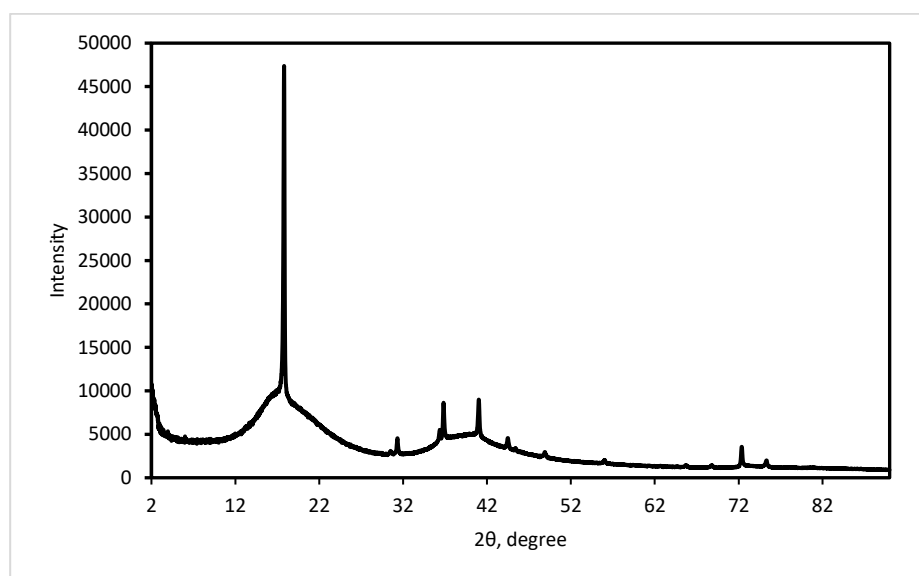


Figure S80. Mass loss as a function of temperature for polyketone PAAK-8.



**Figure S81.** DSC trace corresponding to **PAAK-8**.



**Figure S82.** Experimental powder XRD patterns of **PAAK-8**. Unidentifiable crystalline phase presents.

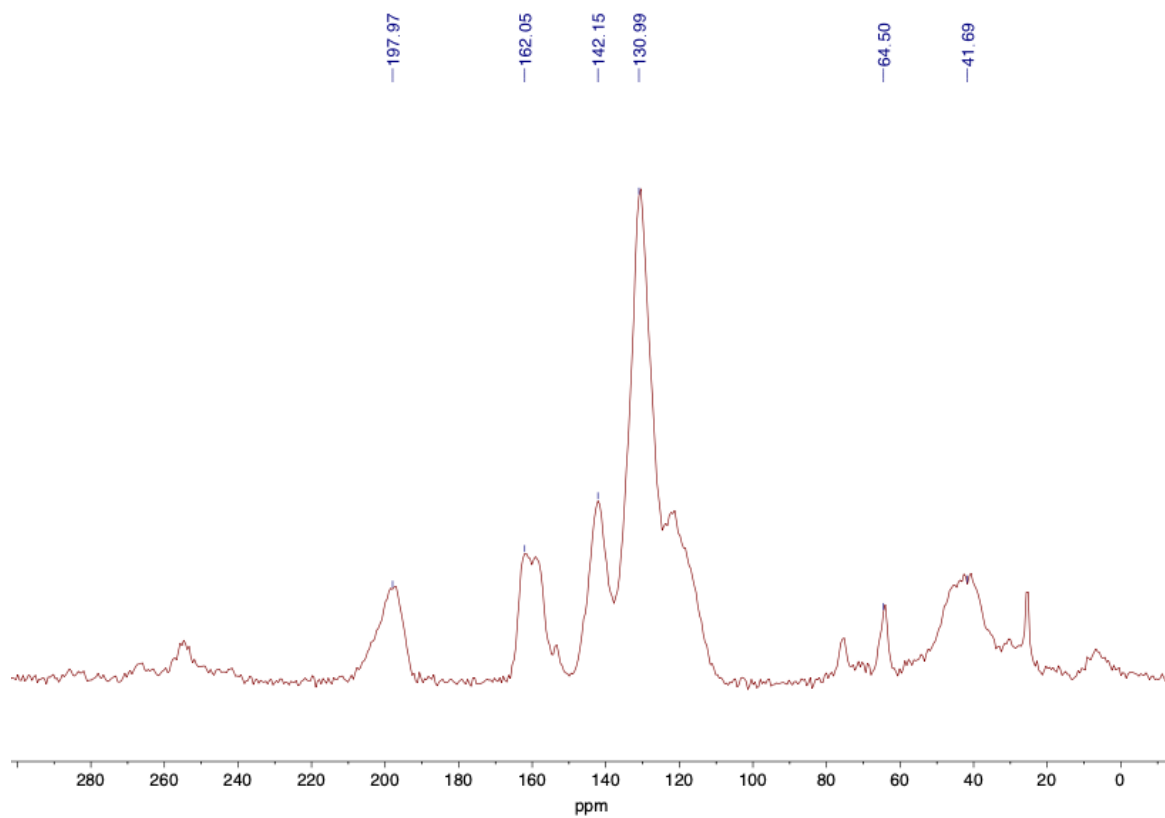
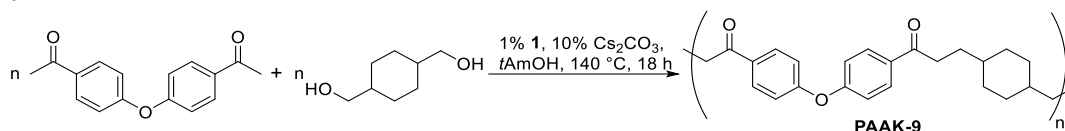


**Figure S83.**  $^{13}\text{C}$  CP MAS NMR spectrum of PAAK-8.

## PAAK-9



1,4-cyclohexanedimethanol (72 mg, 0.5 mmol) and 4-acetylphenylether (127 mg, 0.5 mmol) were used. The polymer was obtained in 71% yield (128 mg) as a white solid.

$^{13}\text{C}$  CP MAS NMR (100.6 MHz):  $\delta$  198.6, 161.7, 159.1, 153.9, 131.6, 120.5, 76.4, 68.4, 48.4, 36.5, 32.3, 30.8.

IR (ATR-FTIR,  $\text{cm}^{-1}$ ):  $\nu$  2916w (C-H), 2851w (C-H), 1674s (C=O), 1589s (C=C), 1499s, 1412w, 1236s (C-O), 1163s, 1011w, 835m, 567w.

TGA:  $T_d = 383\text{ }^\circ\text{C}$

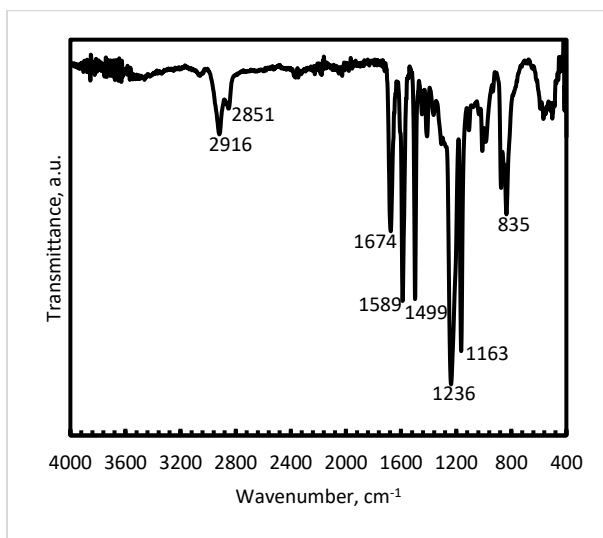


Figure S84. Infrared spectrum (ATR-FTIR) of polyketone PAAK-9.

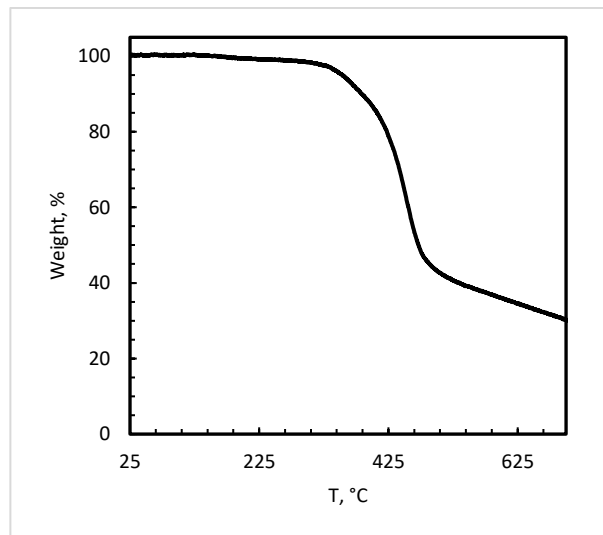


Figure S85. Mass loss as a function of temperature for polyketone PAAK-9.

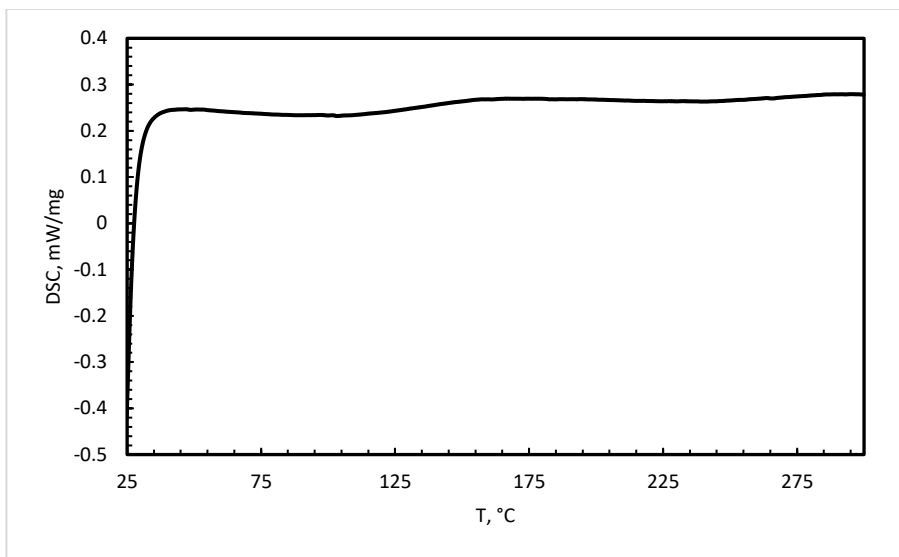


Figure S86. DSC trace corresponding to **PAAK-9**.

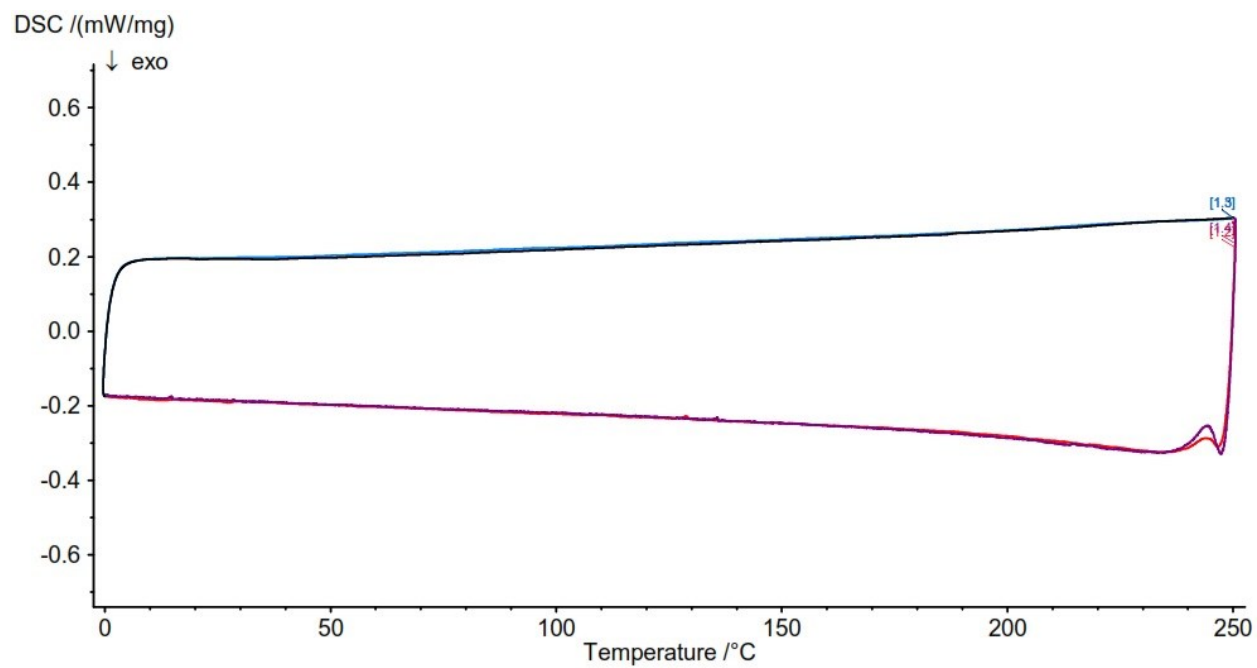
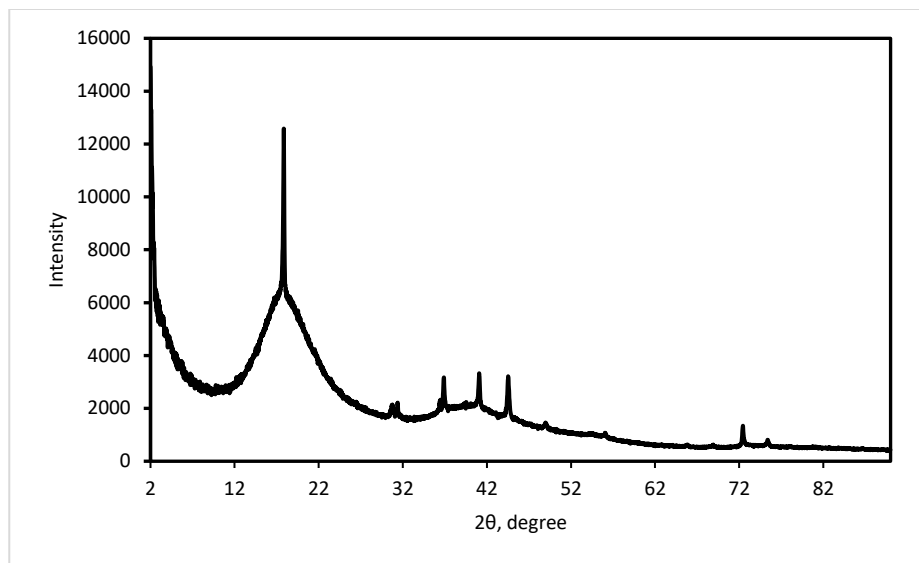
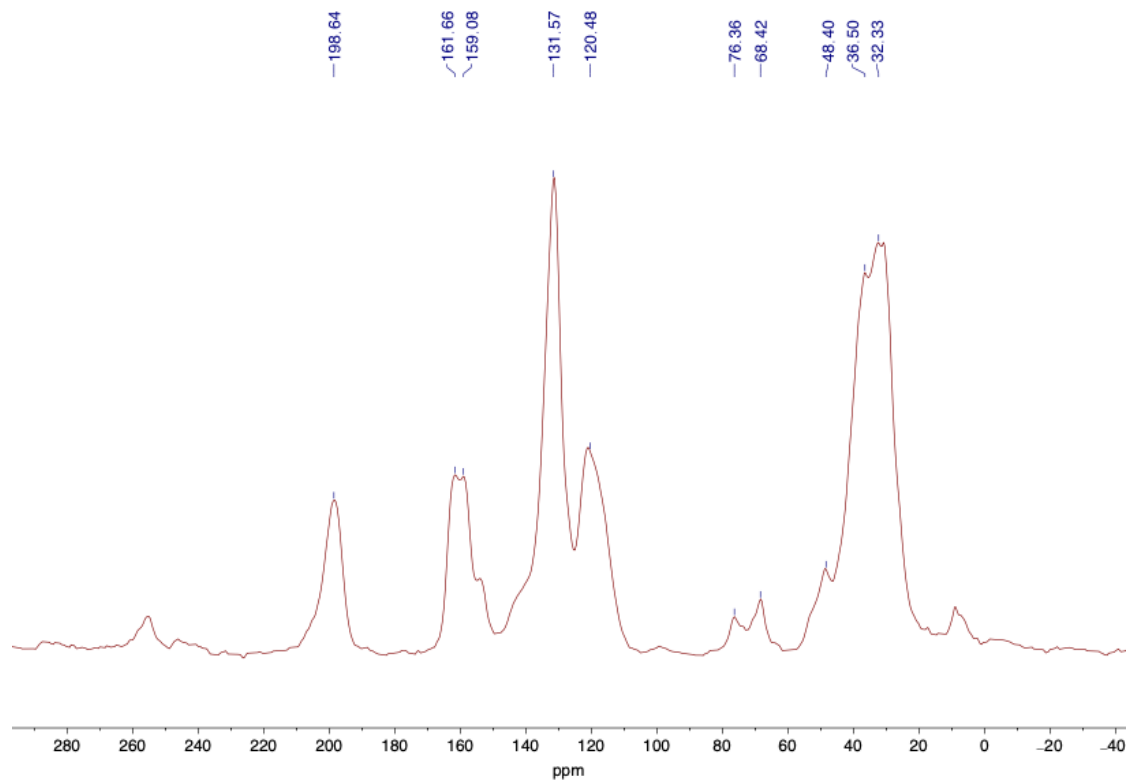


Figure S87. DSC trace corresponding to **PAAK-9** (two cycles 0–250 °C).

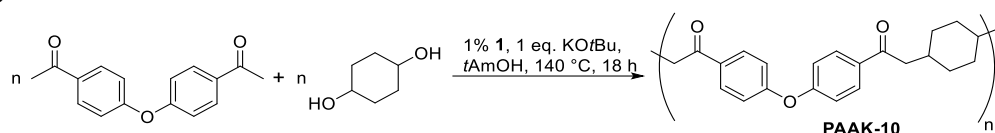


**Figure S88.** Experimental powder XRD patterns of **PAAK-9**. Unidentifiable crystalline phase presents.



**Figure S89.**  $^{13}\text{C}$  CP MAS NMR spectrum of **PAAK-9**.

## PAAK-10



Cyclohexane-1,4-diol (58 mg, 0.5 mmol) and 4-acetylphenylether (127 mg, 0.5 mmol) were used. The polymer was obtained in 57% yield (95 mg) as a yellow solid.

$^{13}\text{C}$  CP MAS NMR (100.6 MHz):  $\delta$  197.9, 157.6, 154.7, 129.8, 121.7, 71.5, 35.6, 28.7.

IR (ATR-FTIR,  $\text{cm}^{-1}$ ):  $\nu$  3346w (O-H), 2918w (C-H), 1676w (C=O), 1591m (C=C), 1497s, 1231s (C-O), 1161s, 1013m, 826m, 509m.

TGA:  $T_d = 363$  °C

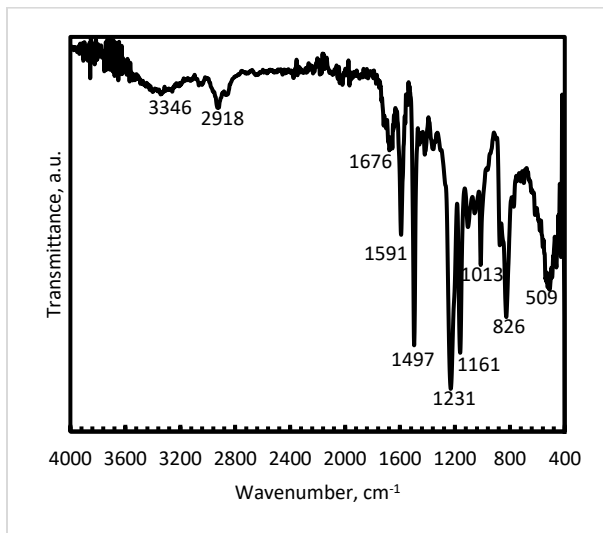


Figure S90. Infrared spectrum (ATR-FTIR) of polyketone PAAK-10.

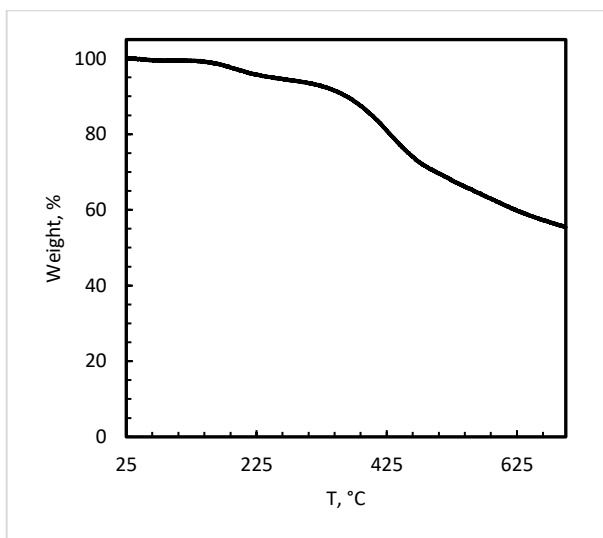
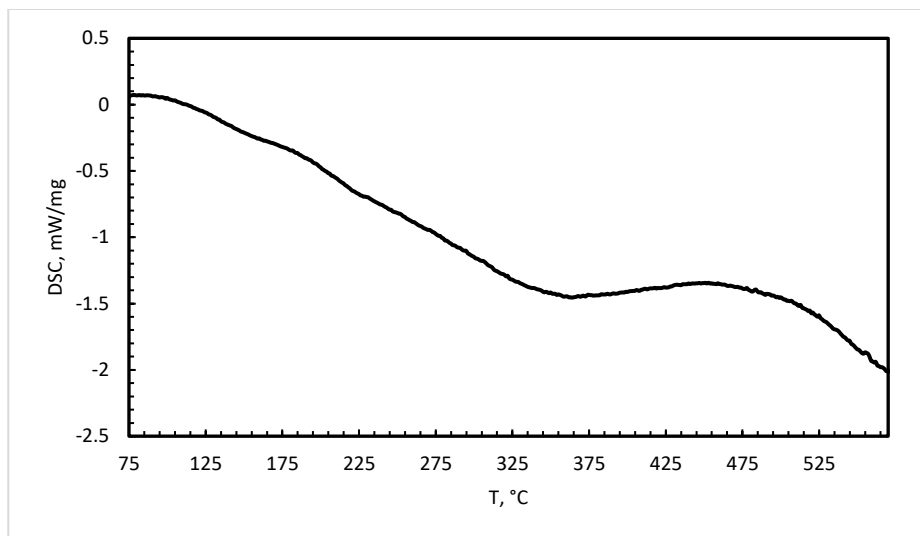
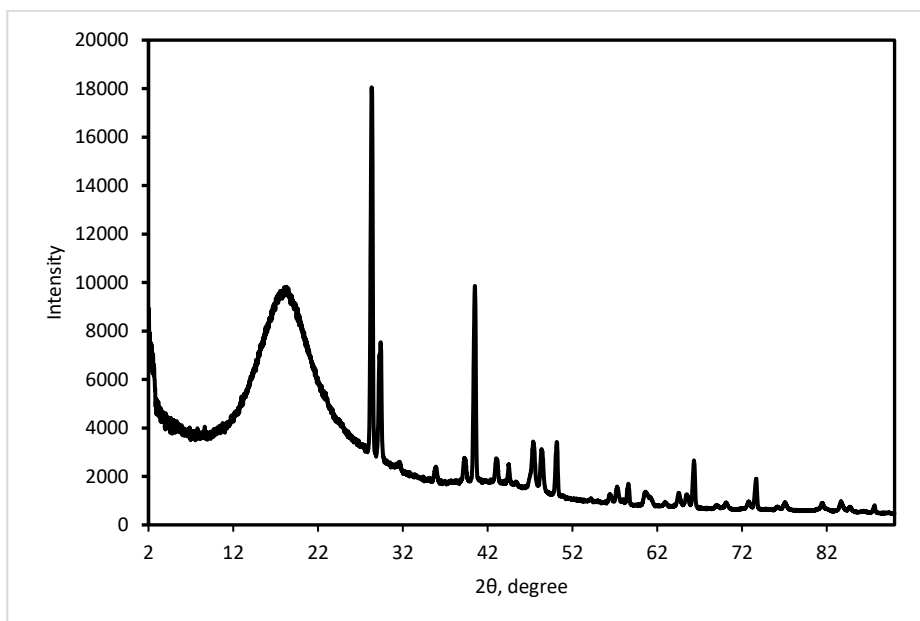


Figure S91. Mass loss as a function of temperature for polyketone PAAK-10.



**Figure S92.** DSC trace corresponding to **PAAK-10**.



**Figure S93.** Experimental powder XRD patterns of **PAAK-10**. Crystalline peaks were indexed in the small-volume unit cell which remains unidentified.

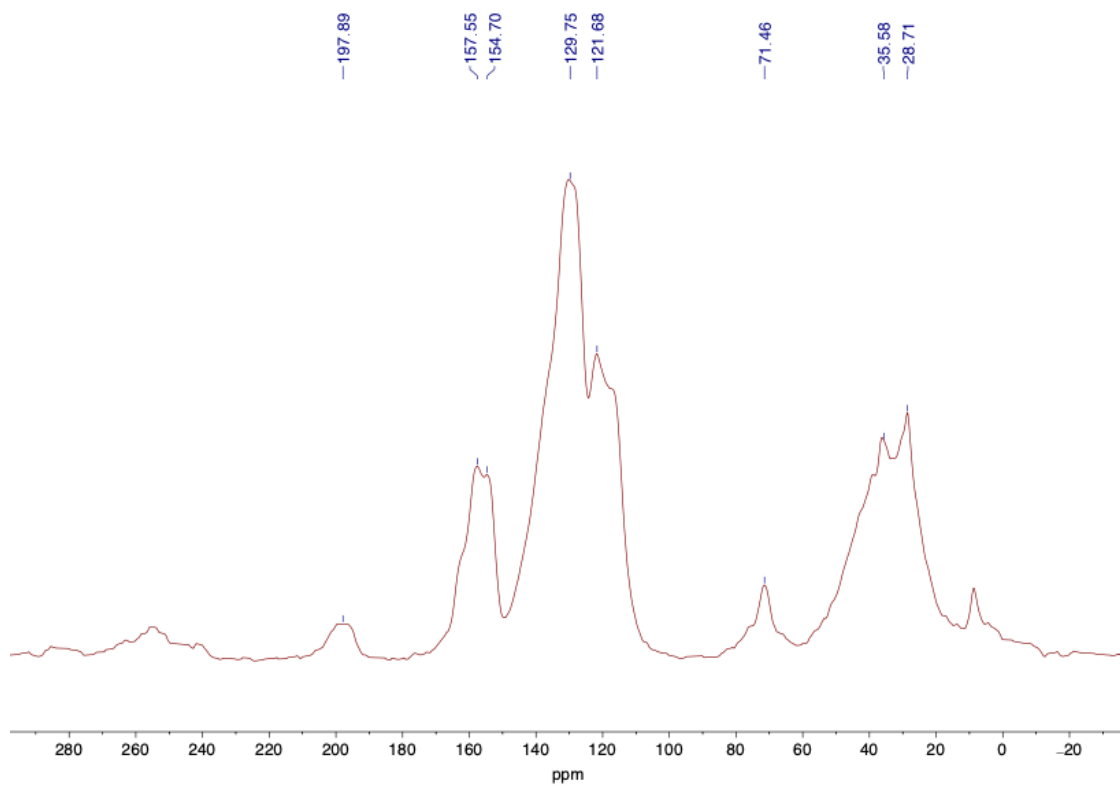


**Figure S94.**  $^{13}\text{C}$  CP MAS NMR spectrum of PAAK-10.



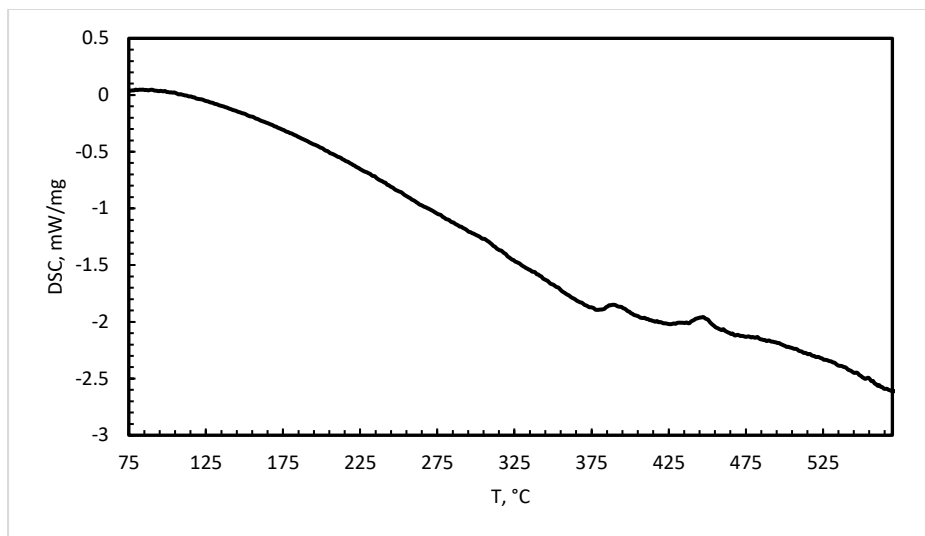


**Figure S97.** DSC trace corresponding to **PAAK-11**.

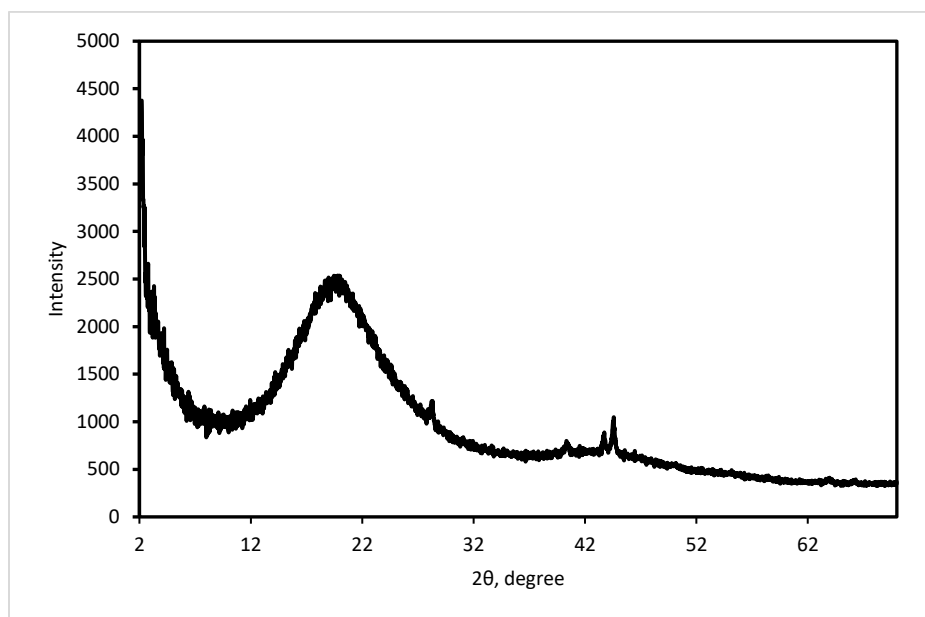


**Figure S98.** Experimental powder XRD patterns of **PAAK-11**. Some small crystalline peaks are from Teflon substrate, other were indexed in the small-volume unit cell which remains unidentified.

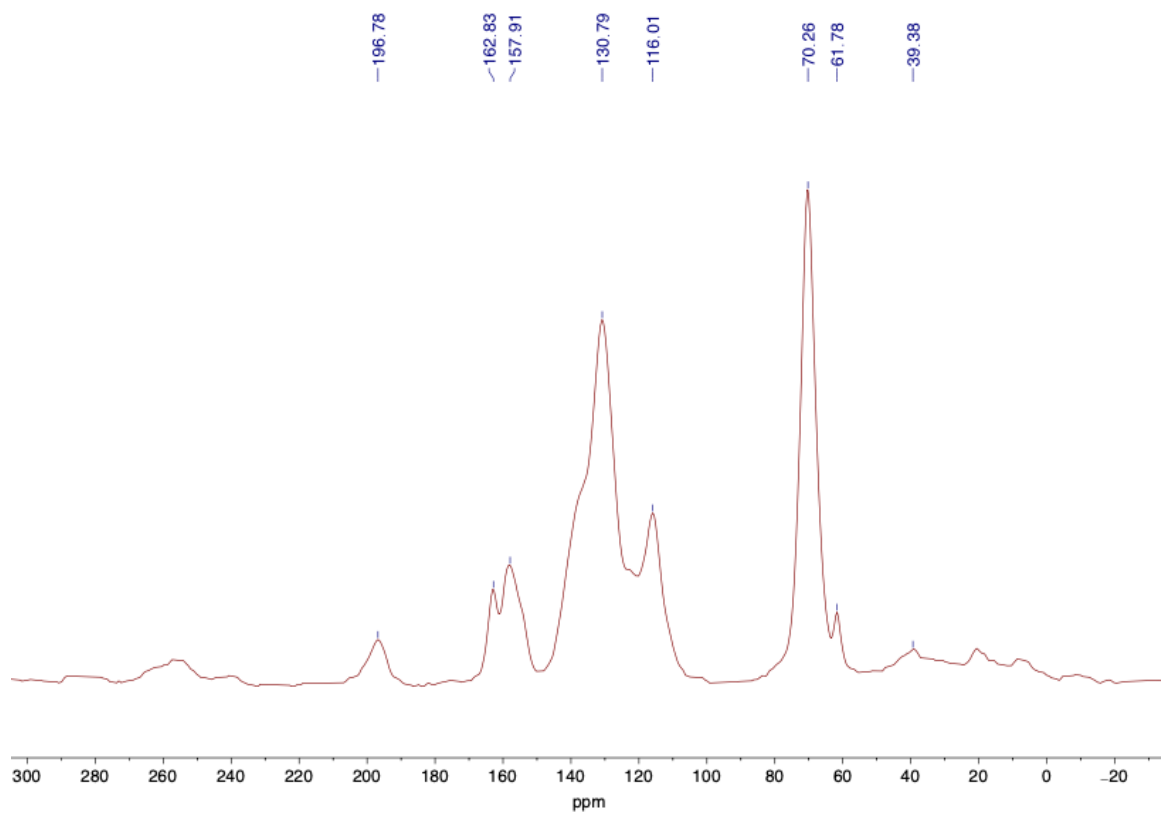
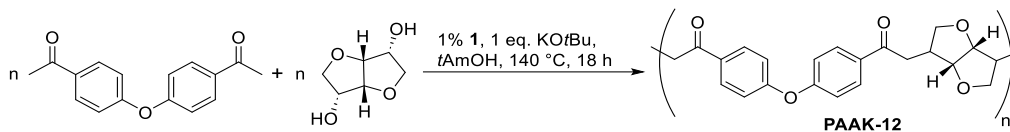


**Figure S99.**  $^{13}\text{C}$  CP MAS NMR spectrum of **PAAK-11** coupling product.

## PAAK-12



D-isosorbide (73 mg, 0.5 mmol) and 4-acetylphenylether (127 mg, 0.5 mmol) were used. The polymer was obtained in 52% yield (94 mg) as an orange solid.

$^{13}\text{C}$  CP MAS NMR (100.6 MHz):  $\delta$  196.4, 158.1, 130.3, 120.5, 75.8, 39.9, 27.0.

IR (ATR-FTIR,  $\text{cm}^{-1}$ ):  $\nu$  2963w (C-H), 1676w (C=O), 1591m (C=C), 1497s, 1231s (C-O), 1161s, 1013m, 827m, 527m.

TGA:  $T_d = 381$  °C

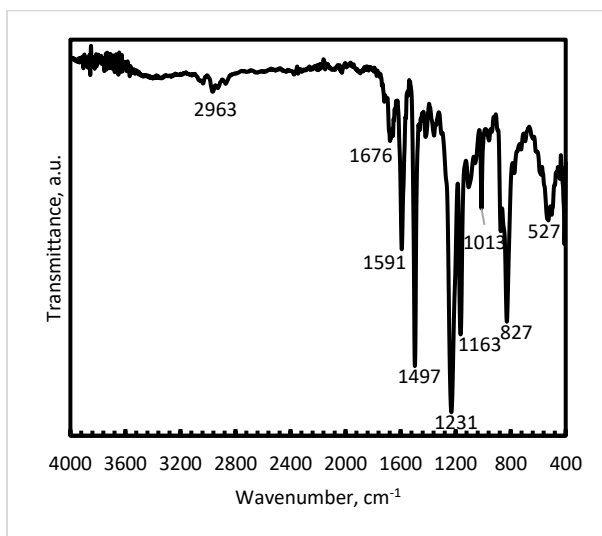


Figure S100. Infrared spectrum (ATR-FTIR) of polyketone PAAK-12.

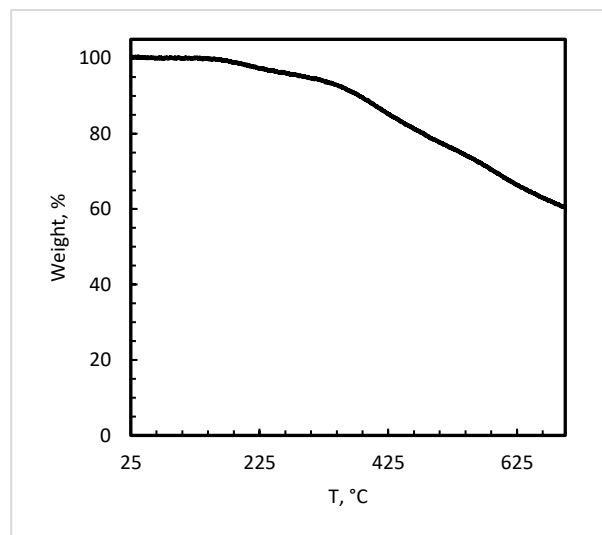
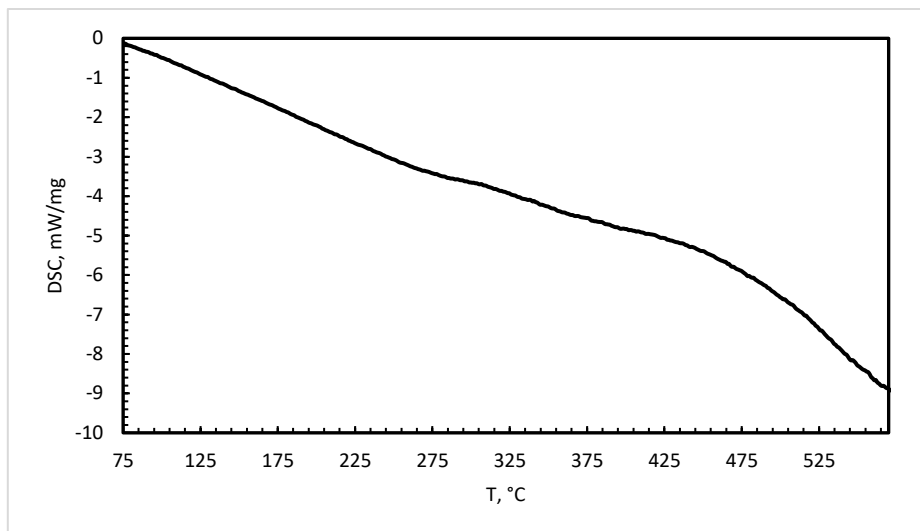
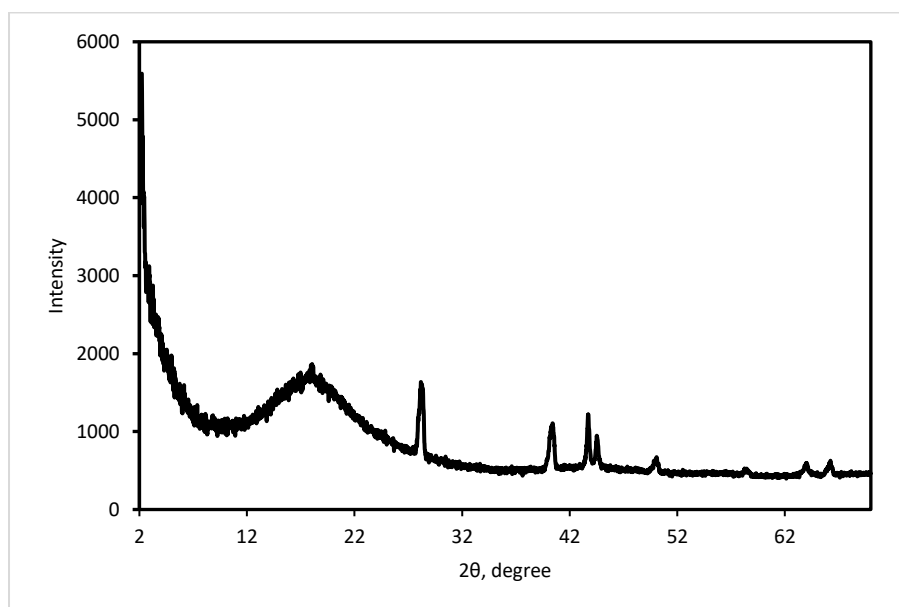


Figure S101. Mass loss as a function of temperature for polyketone PAAK-12.



**Figure S102.** DSC trace corresponding to **PAAK-12**.



**Figure S103.** Experimental powder XRD patterns of **PAAK-12**. Crystalline peaks are either from Teflon substrate or were indexed in the small-volume unit cell which remains unidentified.

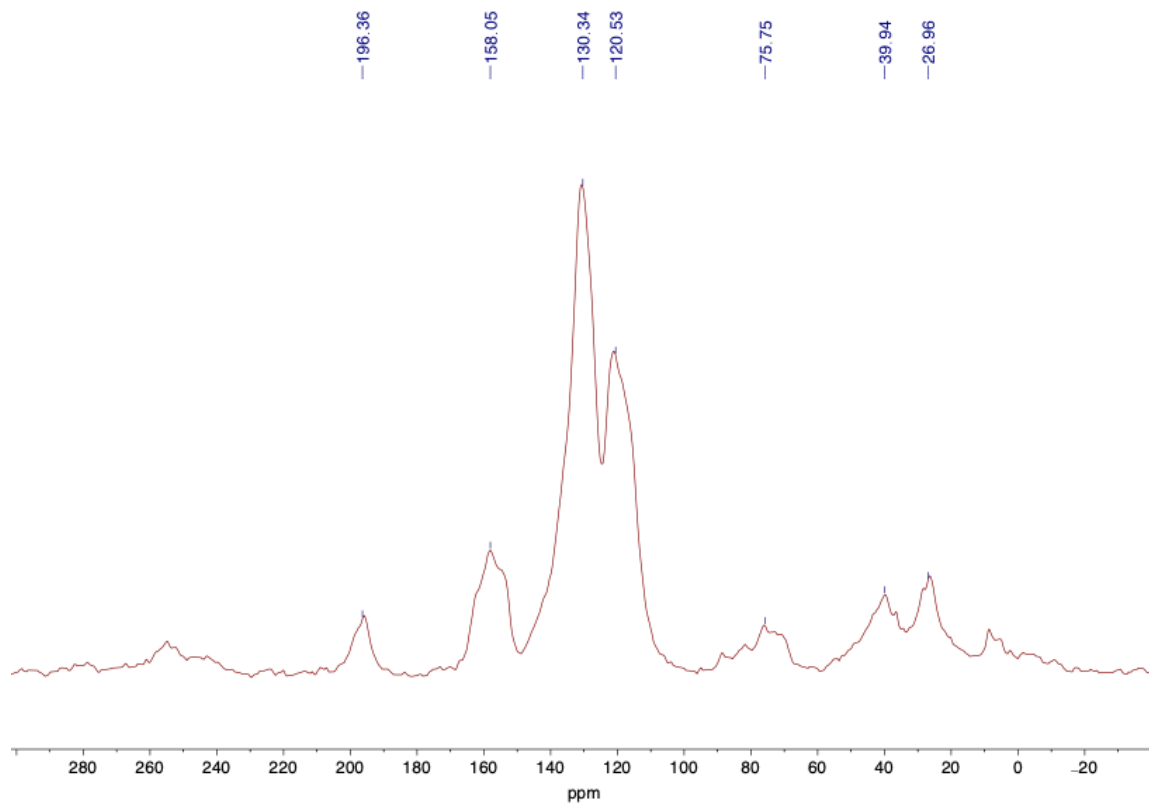
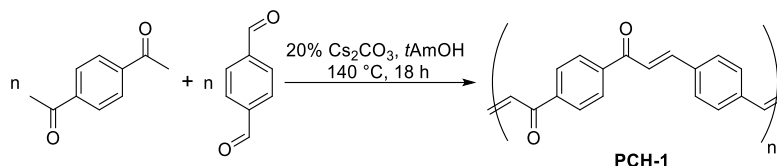


**Figure S104.**  $^{13}\text{C}$  CP MAS NMR spectrum of PAAK-12.

## 1.6 Syntheses of polychalcones from diketones and dialdehydes

A 100 mL ampoule equipped with a J-Young's valve was charged with  $\text{Cs}_2\text{CO}_3$  (33 mg, 0.1 mmol, 20 mol%), dialdehyde (0.5 mmol) and diketone (0.5 mmol). The flask was sealed under an argon atmosphere and *tert*-amyl alcohol (5 mL) was added before heating to 140 °C for 18 h with stirring. After this period, the reaction vessel was allowed to cool to room temperature. To the resulting mixture, 5 mL of water was added and the flask was heated at 90 °C for 1 h. The precipitate was filtered and dried under reduced pressure at 120 °C.

### PCH-1



Terephthalaldehyde (68 mg, 0.5 mmol) and 1,4-diacetylbenzene (81 mg, 0.5 mmol) were used. The polymer was obtained with 93% yield (121 mg) as a yellow solid.

IR (ATR-FTIR,  $\text{cm}^{-1}$ ):  $\nu$  3472w (C-H), 3036w, 2834w, 1657m (C=O), 1599s (C=C), 1566m, 1501w, 1402w, 1327m, 1211s, 980m, 810s.

TGA: Td = 365 °C

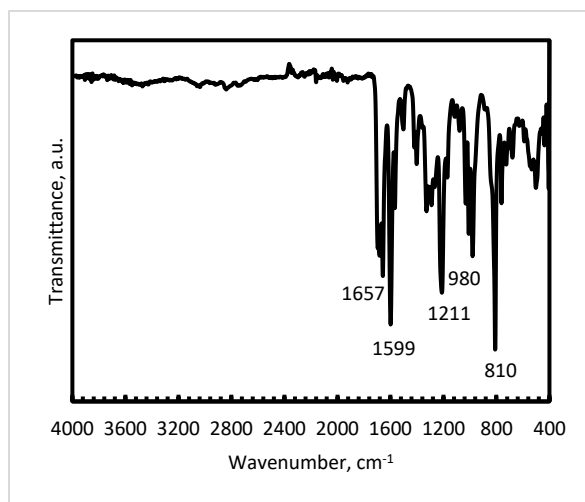


Figure S105. Infrared spectrum (ATR-FTIR) for polychalcone PCH-1.

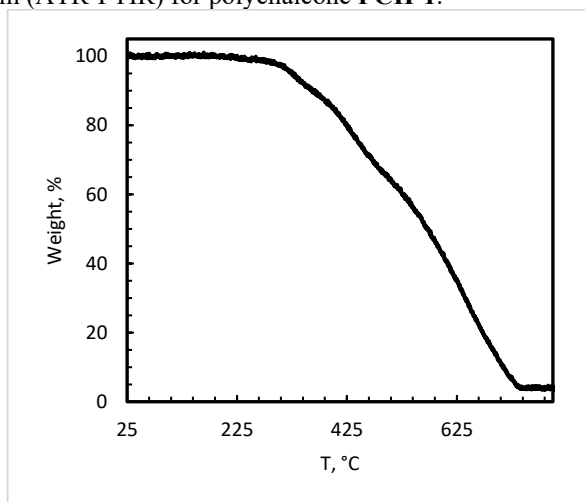


Figure S106. Mass loss as a function of temperature for polychalcone PCH-1.

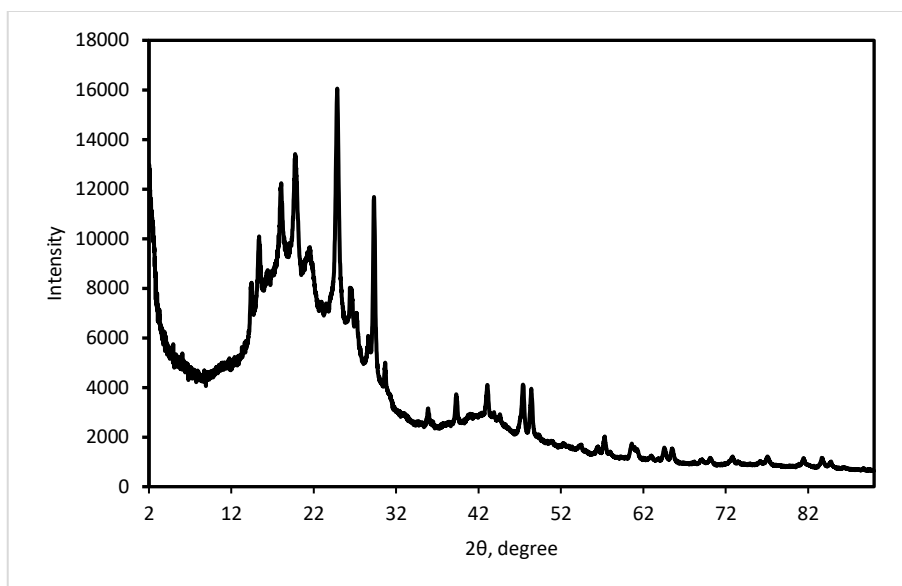
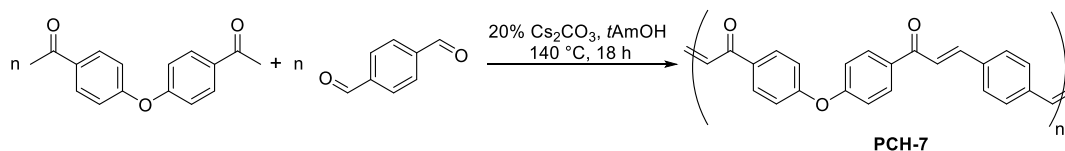


Figure S107. Experimental powder XRD patterns of polychalcone **PCH-1**.

### PCH-7



Terephthalaldehyde (68 mg, 0.5 mmol) and 4-acetylphenyl ether (127 mg, 0.5 mmol) were used. The polymer was obtained in 91% yield (161 mg) as a yellow solid.

IR (ATR-FTIR,  $\text{cm}^{-1}$ ):  $\nu$  3460w (C-H), 3044w, 1657m (C=O), 1589s (C=C), 1499m, 1418w, 1333m, 1215s, 1163s, 978w, 818s, 500m.

TGA: Td = 393 °C

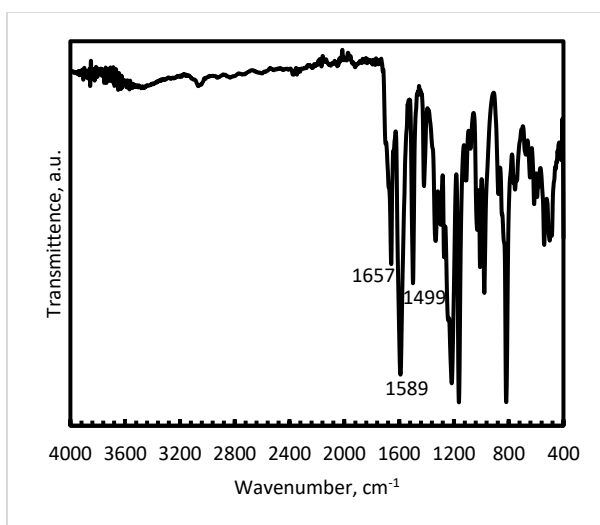


Figure S108. Infrared spectrum (ATR-FTIR) of polychalcone **PCH-7**.

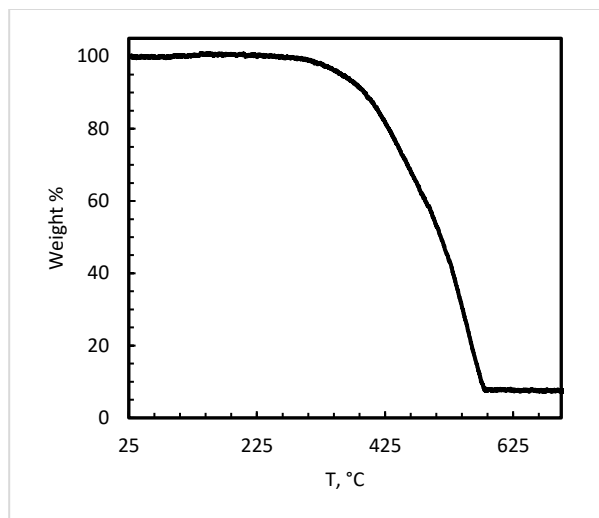


Figure S109. Mass loss as a function of temperature for polychalcone PCH-7.

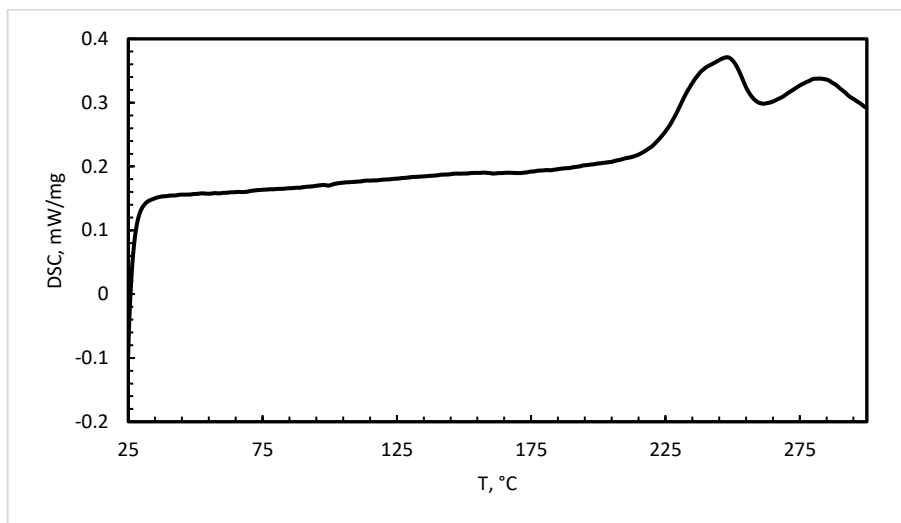


Figure S110. Experimental powder XRD patterns of PCH-7.

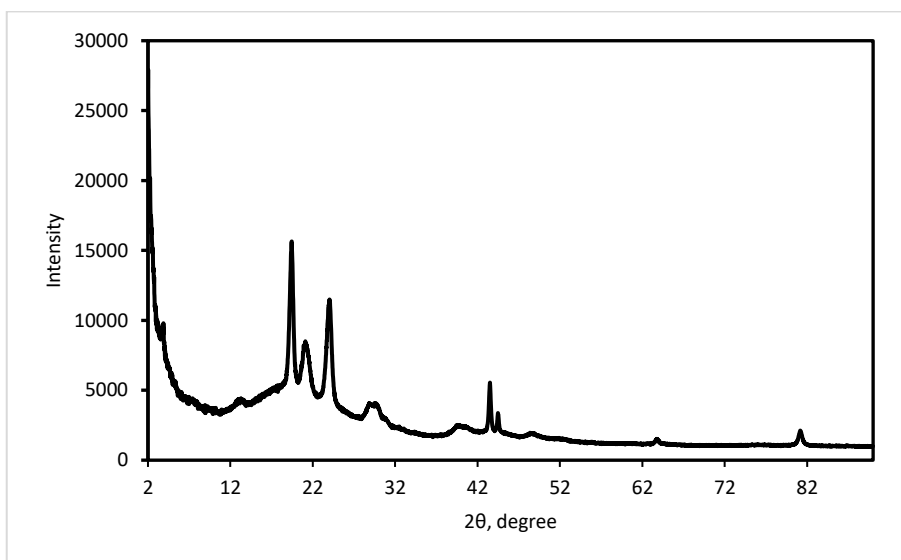


Figure S111. Experimental powder XRD patterns of polychalcone PCH-7.

### 1.7 Reaction 4-acetylphenyl ether and potassium tert-butoxide.

A 50 mL ampoule equipped with a J-Young's valve was charged with KO<sub>t</sub>Bu (56 mg, 0.5 mmol, 1 eq. mol%), 4-acetylphenyl ether (127 mg, 0.5 mmol). The flask was sealed under an argon atmosphere and *tert*-amyl alcohol (5 mL) was added before heating to 140 °C for 18 h with stirring. After this period, the reaction vessel was allowed to cool to room temperature. To the resulting mixture, 5 mL of 1 M solution of HCl was added and the flask was heated at 90 °C for 1 h. The precipitate was filtered, washed with water, acetone and dichloromethane and dried under reduced pressure at 120 °C giving the product (55 mg, 50% yield) as a white solid. The IR and thermal data obtained from this material (as described below) is different from the PAAK-1.

IR (ATR-FTIR, cm<sup>-1</sup>):  $\nu$  1680w, 1591w, 1495s, 1233s, 1163m, 826m, 507w.

TGA: Td = 455 °C

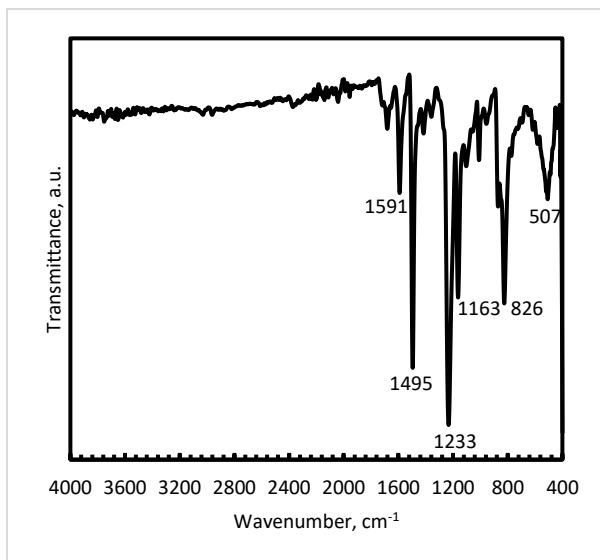


**Figure S112.** Infrared spectrum (ATR-FTIR) of the reaction product of 4-acetylphenyl ether and potassium tert-butoxide.

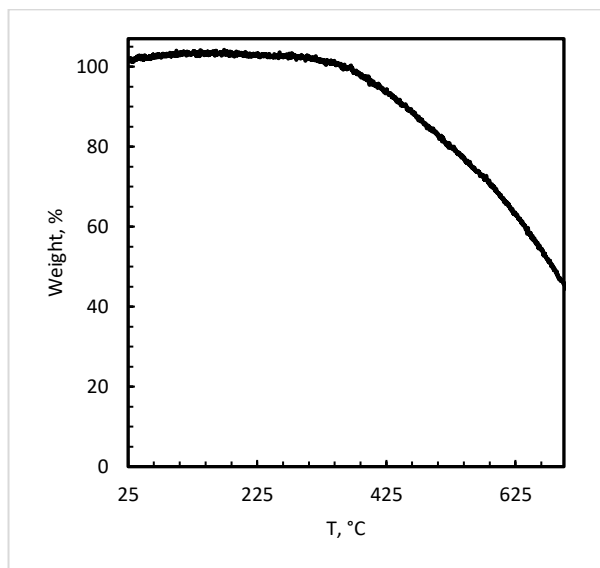


**Figure S113.** Mass loss as a function of temperature for the reaction product of 4-acetylphenyl ether and potassium tert-butoxide.

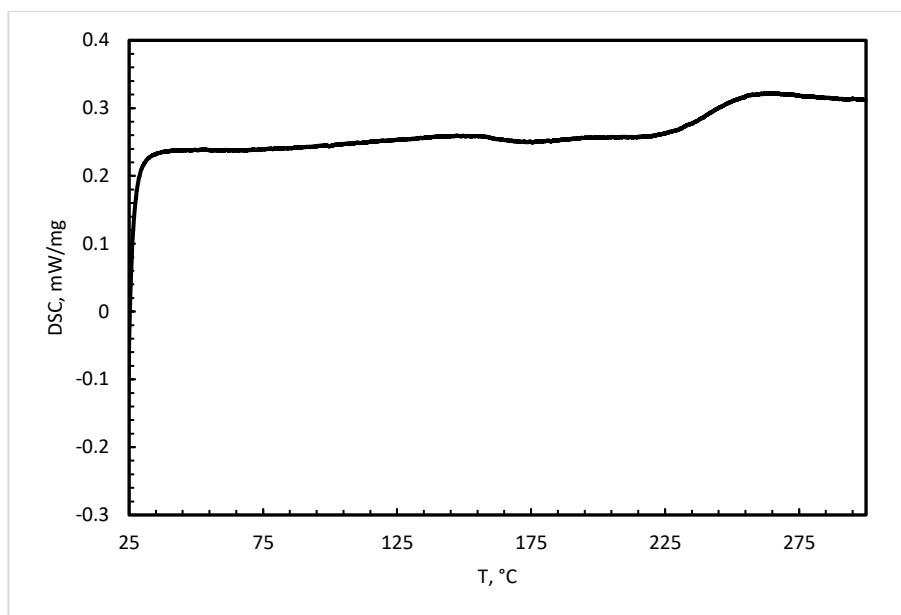


**Figure S114.** DSC trace corresponding to the reaction product of 4-acetylphenyl ether and potassium tert-butoxide.

## 1.8 Syntheses of polyketones in the presence of hydrogen atmosphere.

### *Synthesis of PAAK-1 in the presence of hydrogen atmosphere.*

A 100 mL ampoule equipped with a J-Young's valve was charged with pre-catalyst **1** (2.5 mg, 0.005 mmol, 1 mol%), 1,4-benzenedimethanol (69 mg, 0.5 mmol), 1,4-diacetylketone (81 mg, 0.5 mmol) and  $\text{Cs}_2\text{CO}_3$  (16.5 mg, 0.05 mmol, 10 mol%). *Tert*-amyl alcohol (5 mL) was added and the flask was sealed under a hydrogen atmosphere before heating to 140 °C for 18 h with stirring. After this period, the reaction vessel was allowed to cool to room temperature. To the resulting mixture, 5 mL of 1 M HCl was added and the flask had been heated at 90 °C for 1 h. The yellow precipitate (126 mg, 95% yield) was filtered and dried under reduced pressure at 120 °C.

IR (ATR-FTIR,  $\text{cm}^{-1}$ ):  $\nu$  3476w (O-H), 2920w (C-H), 1676s (C=O), 1605m (C=C), 1510w, 1402m, 1267m, 1211s, 982m, 818s, 550m.

TGA: Td = 397 °C

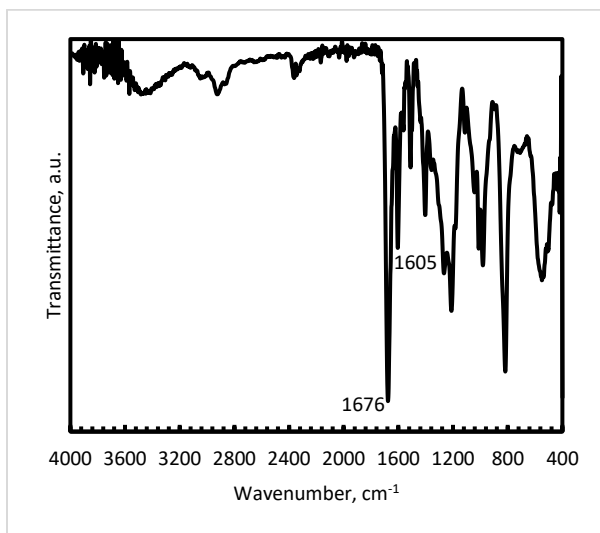


**Figure S115.** Infrared spectrum (ATR-FTIR) of polyketone **PAAK-1** obtained in the atmosphere of hydrogen.

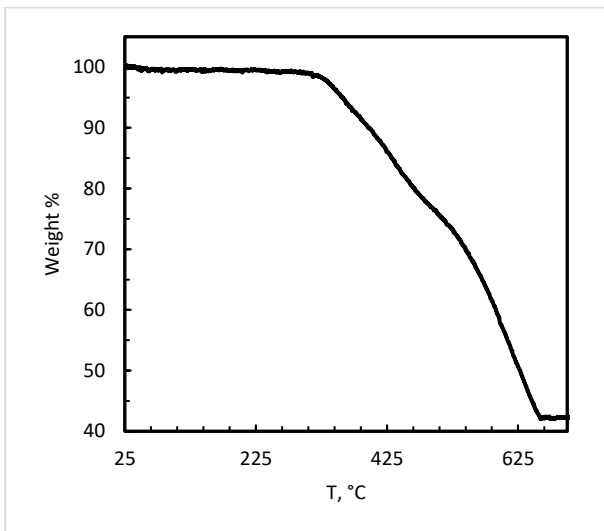


**Figure S116.** Mass loss as a function of temperature for polyketone **PAAK-1** obtained in the atmosphere of hydrogen.

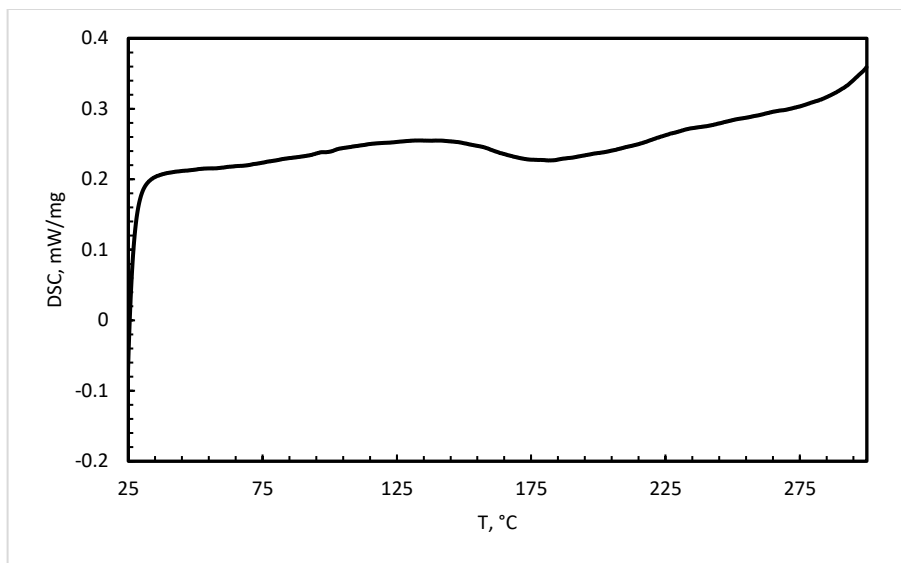


**Figure S117.** DSC trace corresponding to polyketone **PAAK-1** obtained in the atmosphere of hydrogen.

*Synthesis of PAAK-7 in the presence of hydrogen atmosphere.*

A 100 mL ampoule equipped with a J-Young's valve was charged with pre-catalyst **1** (2.5 mg, 0.005 mmol, 1 mol%), 1,4-benzenedimethanol (69 mg, 0.5 mmol), 4-acetylphenyl ether (127 mg, 0.5 mmol) and  $\text{Cs}_2\text{CO}_3$  (16.5 mg, 0.05 mmol, 10 mol%). *Tert*-amyl alcohol (5 mL) was added and the flask was sealed under a hydrogen atmosphere before heating to 140 °C for 18 h with stirring. After this period, the reaction vessel was allowed to cool to room temperature. To the resulting mixture, 5 mL of 1 M HCl was added and the flask had been heated at 90 °C for 1 h. The white precipitate (177 mg, 99% yield) was filtered and dried under reduced pressure at 120 °C.

IR (ATR-FTIR,  $\text{cm}^{-1}$ ):  $\nu$  2914w (C-H), 1674m (C=O), 1585s (C=C), 1497m, 1233s, 1163s, 822m, 548m.

TGA: Td = 371 °C

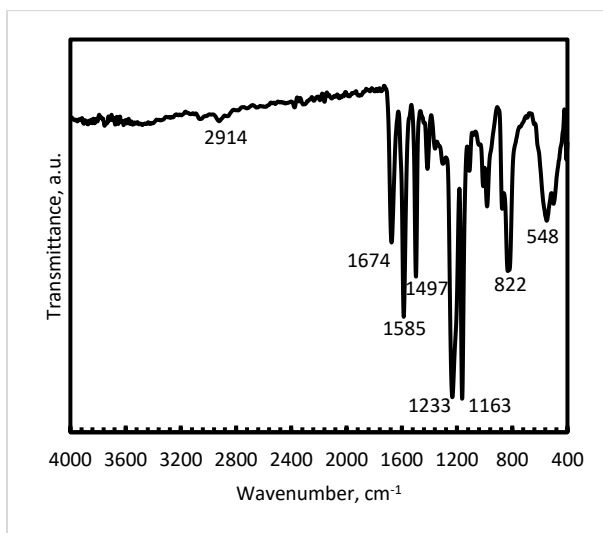


**Figure S118.** Infrared spectrum (ATR-FTIR) of polyketone **PAAK-7** obtained in the atmosphere of hydrogen.

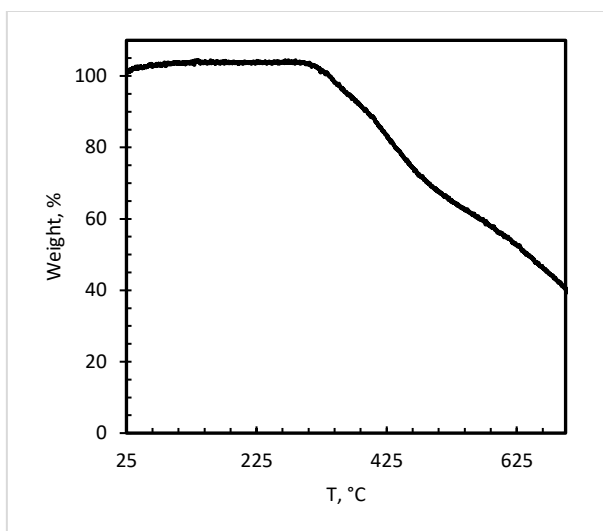


**Figure S119.** Mass loss as a function of temperature for polyketone **PAAK-7** obtained in the atmosphere of hydrogen.

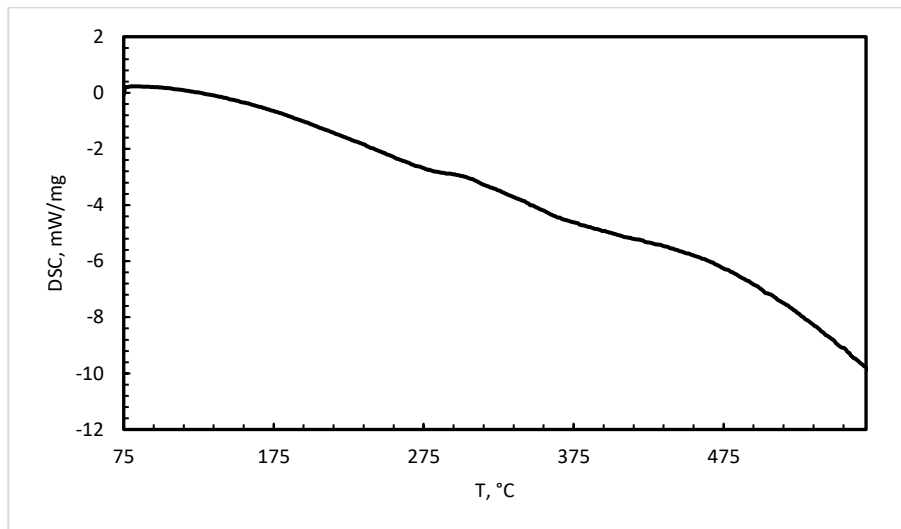


**Figure S120.** DSC trace corresponding to **PAAK-7** obtained in the atmosphere of hydrogen.

*Synthesis of PAAK-9 in the presence of hydrogen atmosphere.*

A 100 mL ampoule equipped with a J-Young's valve was charged with pre-catalyst **1** (2.5 mg, 0.005 mmol, 1 mol%), 1,4-cyclohexanedimethanol (72 mg, 0.5 mmol), 4-acetylphenyl ether (127 mg, 0.5 mmol) and Cs<sub>2</sub>CO<sub>3</sub> (16.5 mg, 0.05 mmol, 10 mol%). *Tert*-amyl alcohol (5 mL) was added and the flask was sealed under a hydrogen atmosphere before heating to 140 °C for 18 h with stirring. After this period, the reaction vessel was allowed to cool to room temperature. To the resulting mixture, 5 mL of 1 M HCl was added and the flask had been heated at 90 °C for 1 h. The white precipitate (178 mg, 98% yield) was filtered and dried under reduced pressure at 120 °C.

IR (ATR-FTIR, cm<sup>-1</sup>): ν 2916w (C-H), 2853w (C-H), 1674m (C=O), 1587m (C=C), 1497m, 1234s, 1163s, 835m.

TGA: T<sub>d</sub> = 384 °C

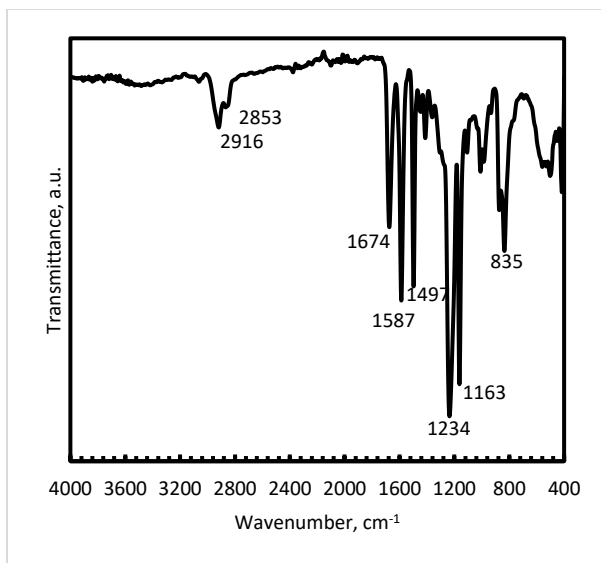


**Figure S121.** Infrared spectrum (ATR-FTIR) of polyketone **PAAK-9** obtained in the atmosphere of hydrogen.

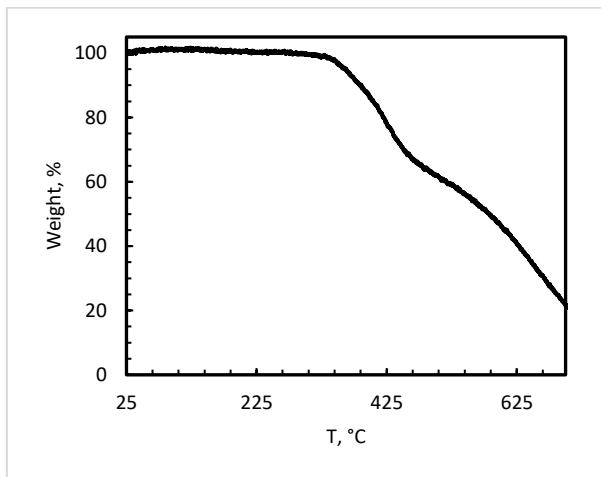


**Figure S122.** Mass loss as a function of temperature for polyketone **PAAK-9** obtained in the atmosphere of hydrogen.

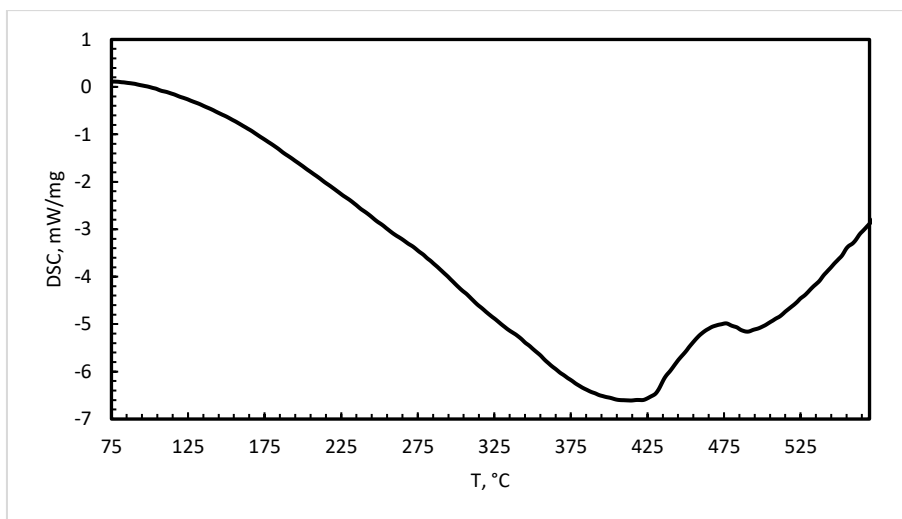


**Figure S123.** DSC trace corresponding to **PAAK-9** obtained in the atmosphere of hydrogen.

*Synthesis of PCH-1 in the presence of hydrogen atmosphere*

A 100 mL ampoule equipped with a J-Young's valve was charged with  $\text{Cs}_2\text{CO}_3$  (16.5 mg, 0.05 mmol, 10 mol%), terephthalaldehyde (68 mg, 0.5 mmol) and 1,4-diacetylbenzene (81 mg, 0.5 mmol). The flask was sealed under a hydrogen atmosphere and *tert*-amyl alcohol (5 mL) was added before heating to 140 °C for 18 h with stirring. After this period, the reaction vessel was allowed to cool to room temperature. To the resulting mixture, 5 mL of water was added and the flask was heated at 90 °C for 1 h. The yellow precipitate (125 mg, 96% yield) was filtered and dried under reduced pressure at 120 °C.

IR (ATR-FTIR,  $\text{cm}^{-1}$ ):  $\nu$  3468w (C-H), 3048w, 2835w, 1657s (C=O), 1597s (C=C), 1566m, 1501w, 1402w, 1327m, 1211s, 978s, 808s, 500m.

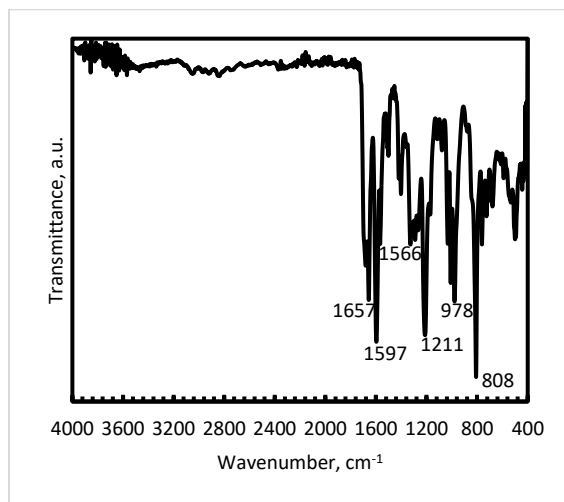


**Figure S124.** Infrared spectrum (ATR-FTIR) of polychalcone **PCH-1** obtained in the atmosphere of hydrogen.

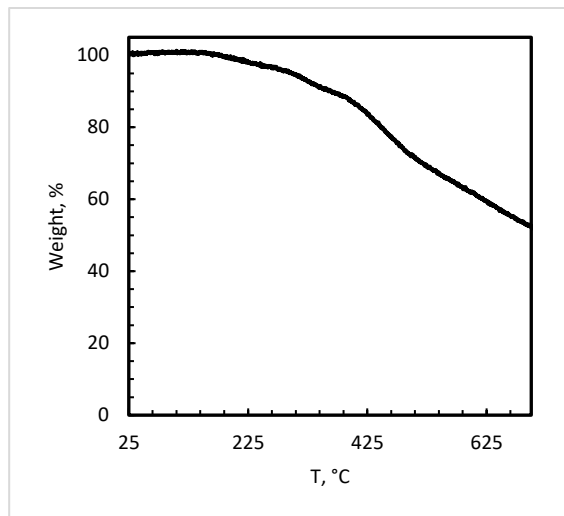


**Figure S125.** Mass loss as a function of temperature for polychalcone **PCH-1** obtained in the atmosphere of hydrogen.

## 1.9 Catalyst reuse experiments.

### Catalyst reuse after synthesis of PAAK-7.

A 100 mL ampoule equipped with a J-Young's valve was charged with pre-catalyst **1** (2.5 mg, 0.005 mmol, 1 mol%) and Cs<sub>2</sub>CO<sub>3</sub> (16.5 mg, 0.05 mmol, 10 mol%), 1,4-benzenedimethanol (69 mg, 0.5 mmol) and 4-acetylphenyl ether (127 mg, 0.5 mmol). The flask was sealed under an argon atmosphere and *tert*-amyl alcohol (5 mL) was added before heating to 140 °C for 2 h with stirring. After this period, the reaction vessel was allowed to cool to room temperature. The reaction mixture consisted of a white precipitate (175 mg, 89%) and a yellowish solution. The ampule was connected to the Schlenk line and the yellowish solution was transferred to another 100 mL ampoule charged with a fresh portion of 1,4-benzenedimethanol (69 mg, 0.5 mmol) and 4-acetylphenyl ether (127 mg, 0.5 mmol) under argon. The freshly charged ampoule was sealed and heated to 140 °C for 2 h with stirring. After this period, the reaction vessel was allowed to cool to room temperature. No precipitate was observed after the second iteration.

### Catalyst reuse after synthesis of PAAK-7 with the addition of base.

A 100 mL ampoule equipped with a J-Young's valve was charged with pre-catalyst **1** (2.5 mg, 0.005 mmol, 1 mol%) and Cs<sub>2</sub>CO<sub>3</sub> (16.5 mg, 0.05 mmol, 10 mol%), 1,4-benzenedimethanol (69 mg, 0.5 mmol) and 4-acetylphenyl ether (127 mg, 0.5 mmol). The flask was sealed under an argon atmosphere and *tert*-amyl alcohol (5 mL) was added before heating to 140 °C for 2 h with stirring. After this period, the reaction vessel was allowed to cool to room temperature. The reaction mixture consisted of a white precipitate (161 mg, 90%) and a yellowish solution. The ampule was connected to the Schlenk line and the yellowish solution was transferred to another 100 mL ampoule charged with a fresh portion of Cs<sub>2</sub>CO<sub>3</sub> (16.5 mg, 0.05 mmol, 10 mol%), 1,4-benzenedimethanol (69 mg, 0.5 mmol) and 4-acetylphenyl ether (127 mg, 0.5 mmol) under argon. The freshly charged ampoule was sealed and heated to 140 °C for 2 h with stirring. After this period, the reaction vessel was allowed to cool to room temperature. To the resulting mixture, 5 mL of 1 M HCl was added and the flask had been heated at 90 °C for 1 h. The precipitate was filtered and dried under reduced pressure at 120 °C giving the product (98 mg, 55% yield) as a white solid.

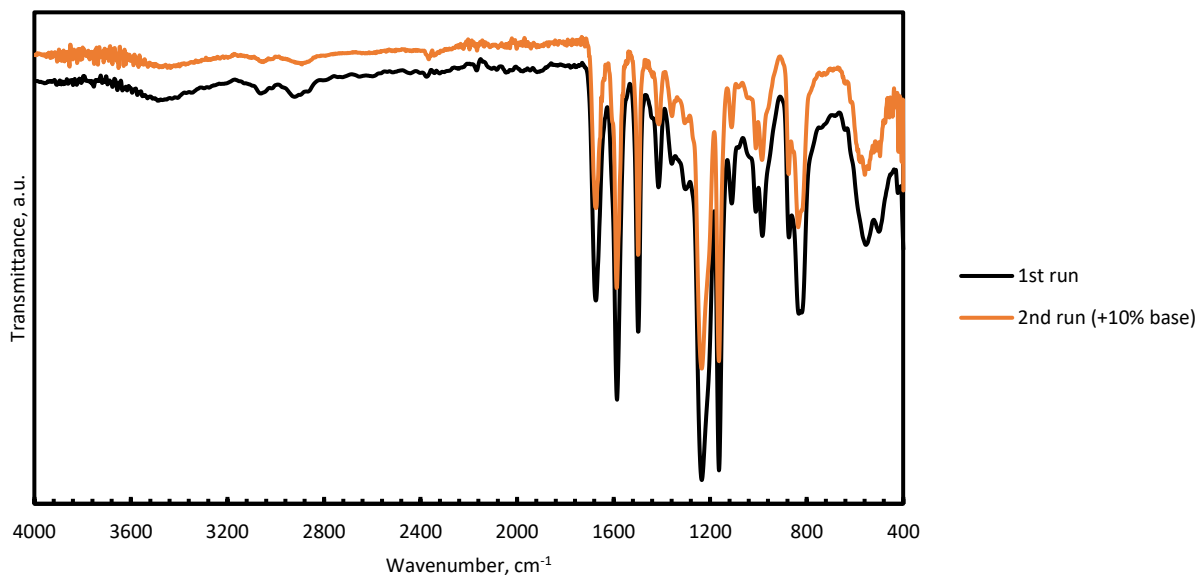


**Figure S126.** Infrared spectrum (ATR-FTIR) of PAAK-7 obtained by fresh catalyst (black) and reused reaction solution with addition of 10% base (orange).

### 1.10 Headspace gas analysis from the synthesis of polyketone PAAK-7.

A 100 mL ampoule equipped with a J-Young's valve was charged with pre-catalyst **1** (2.5 mg, 0.005 mmol, 1 mol%) and Cs<sub>2</sub>CO<sub>3</sub> (16.5 mg, 0.05 mmol, 10 mol%), 1,4-benzenedimethanol (69 mg, 0.5 mmol) and 4-acetylphenyl ether (127 mg, 0.5 mmol). The flask was sealed under an argon atmosphere and *tert*-amyl alcohol (5 mL) was added before heating to 140 °C for 2 h with stirring. After this period, the reaction vessel was allowed to cool to room temperature. A sample of the headspace was extracted using a gas tight syringe and analysed using GC-TCD. It was demonstrated that the injected gas consisted mainly from Hydrogen (from the reaction itself) and Nitrogen (from the reaction inert atmosphere) with some Oxygen originated from the atmosphere during sample preparation and injection (Figure S127).

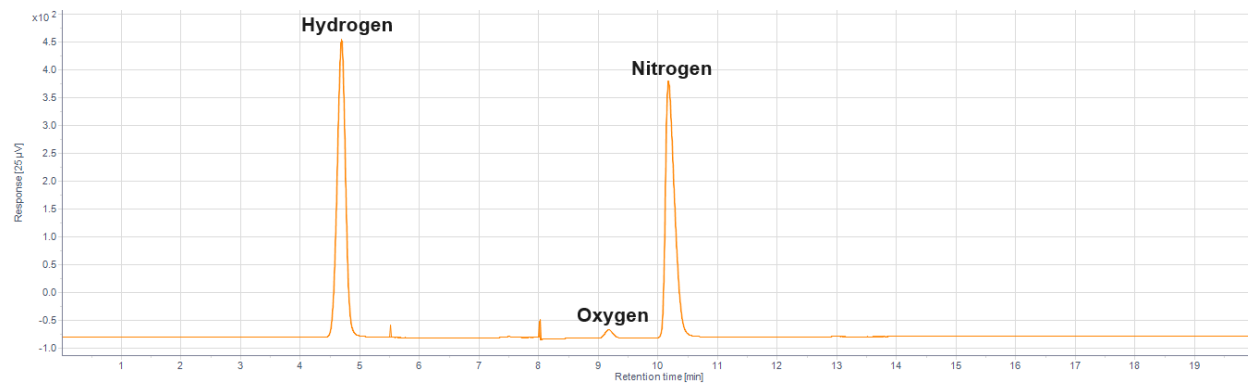
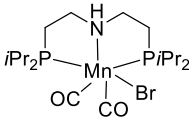
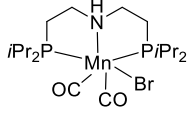
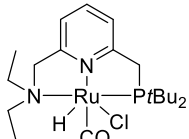


Figure S127. GC-TCD chromatograph of the reaction headspace from synthesis of PAAK-7.

## 1.11 Hydrogenative depolymerization of polyethyleneterephthalate (PET).

**Table S2. Tested conditions for hydrogenative depolymerization of PET.<sup>a</sup>**

Entry	Amount of catalyst	Catalyst	Base	Amount of base	Conversion <sup>b</sup>	Yield of 1,4-benzenedimethanol <sup>c</sup>
1	1%		KOtBu	10%	0%	0%
2	3%		KOtBu	30%	0%	0%
3	2%		KOtBu	10%	quant.	97%

<sup>a</sup> Polyethylene terephthalate (192.2 mg, 1 mmol, 1 eq., taken from a plastic bottle), a catalyst (1–3%) and KOtBu (10–30%), were weighed under air, placed into an 8 mL glass ampoule, a stir bar was added, and the ampule was sealed with a cap, containing a septum. The ampule was backfilled with argon and 5 mL of anhydrous *tert*-amyl alcohol was added via syringe. The ampules were placed inside a 150 mL autoclave with some metal beans to ensure therm conductivity. The autoclave was purged with argon, then sealed, purged with H<sub>2</sub>, pressurized with 50 bar of H<sub>2</sub>, and placed in an oil bath. The reaction was stirred at 140 °C for 88 hours. After that, the autoclave was cooled down to room temperature in an ice bath and carefully vented to the atmosphere. <sup>b</sup> Conversion was calculated as 100% minus amount of unreacted PET flakes. <sup>c</sup> Yield was calculated via <sup>1</sup>H NMR employing mesitylene as an internal standard. Hence, 200–300 mg of the reaction solution and 10 mg mesitylene were weighed in an NMR tube followed by the addition of methanol-d<sub>4</sub> (0.3 mL).

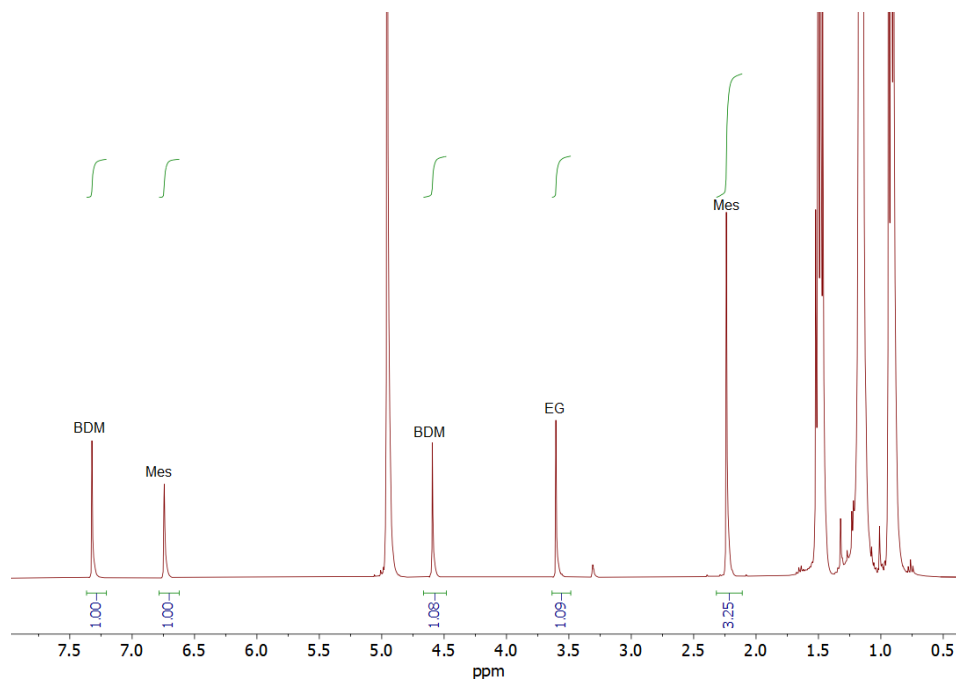
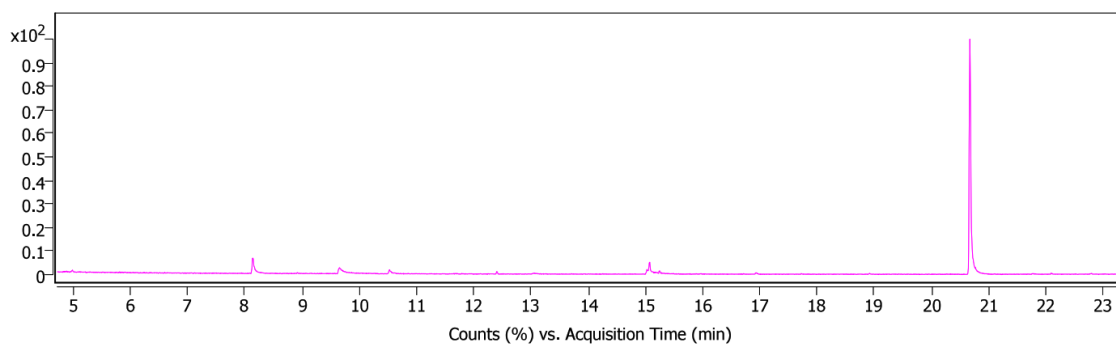


**Figure S128.** <sup>1</sup>H NMR spectrum of reaction mixture from Entry 3 in Table S2 in methanol-d<sub>4</sub> at room temperature. BDM – 1,4-benzenedimethanol, EG – ethylene glycol, Mes – mesitylene. The remaining signals correspond to *tert*-amyl alcohol and methanol-d<sub>4</sub>.

### 1.12 Hydrogenation of *trans*-Chalcone by transfer hydrogenation.

A 100 mL ampoule equipped with a J-Young's valve was charged with **1** (2.5 mg, 0.005 mmol, 1 mol%), 1,4-benzenedimethanol (69 mg, 0.5 mmol), *trans*-chalcone (104 mg, 0.5 mmol) and Cs<sub>2</sub>CO<sub>3</sub> (16.5 mg, 0.10 mmol, 10 mol%). The flask was refilled with argon and *tert*-amyl alcohol (5 mL) was added. The flask was sealed and heated 140 °C for 2 h with stirring. After this period, the reaction vessel was allowed to cool to room temperature and the resulting mixture was analysed with GC-MS and NMR (with CDCl<sub>3</sub> as a solvent) using mesitylene as an internal standard. The yield was estimated to be 46%. The NMR spectrum of 1,3-diphenylpropan-1-one corresponds to the literature data [2].



#### Sample Spectra

##### + Scan (rt: 20.693 min)

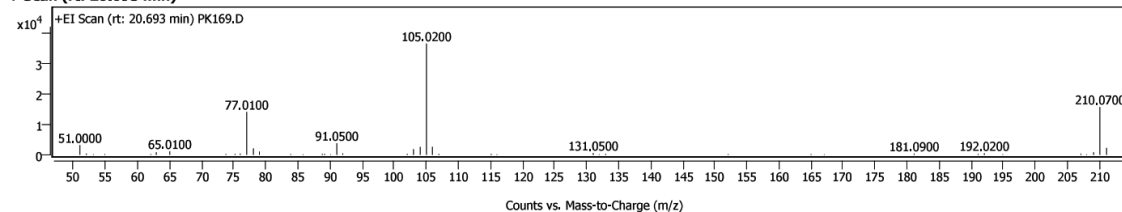


**Figure S129.** GC chromatograph of the products of transfer hydrogenation of *trans*-chalcone (above) and mass spectrum (EI) of 1,3-diphenylpropan-1-one extracted from the chromatogram.

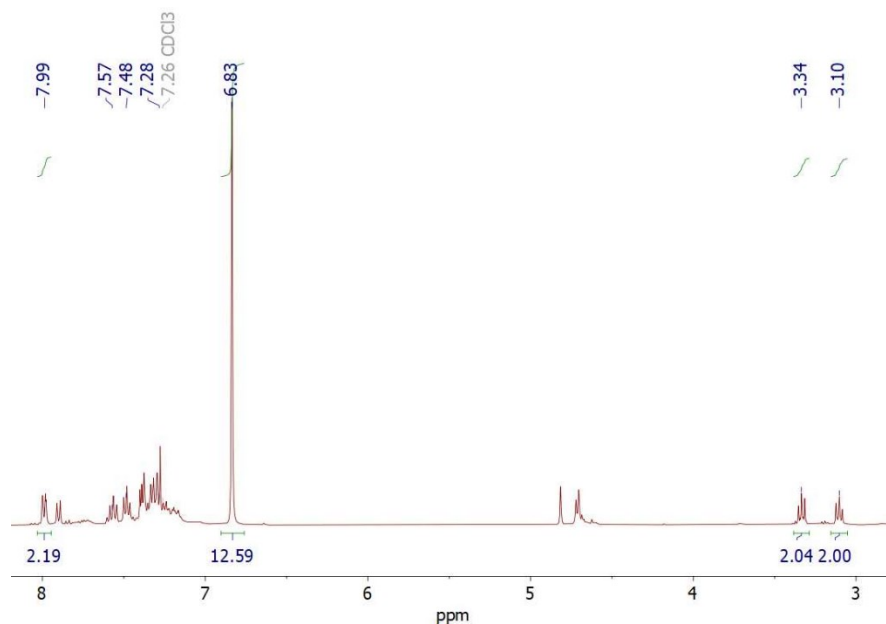


**Figure S130.** Fragment of <sup>1</sup>H NMR (400 MHz, CDCl<sub>3</sub>) of the reaction mixture of transfer hydrogenation of *trans*-chalcone in the presence of 1,4-benzenedimethanol.

### 1.13 Infrared spectra of starting materials and commercially available compounds.

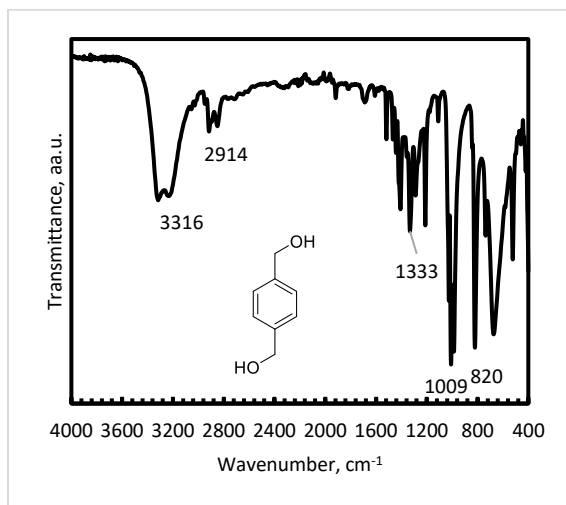


Figure S131. Infrared spectrum (ATR-FTIR) of 1,4-benzenedimethanol.

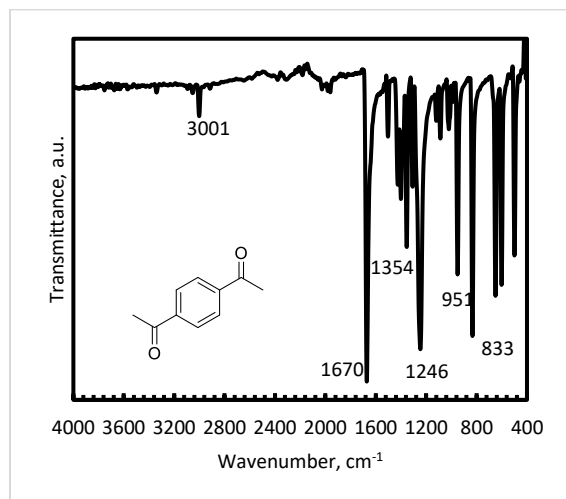


Figure S132. Infrared spectrum (ATR-FTIR) of 1,4-diacetylbenzene.

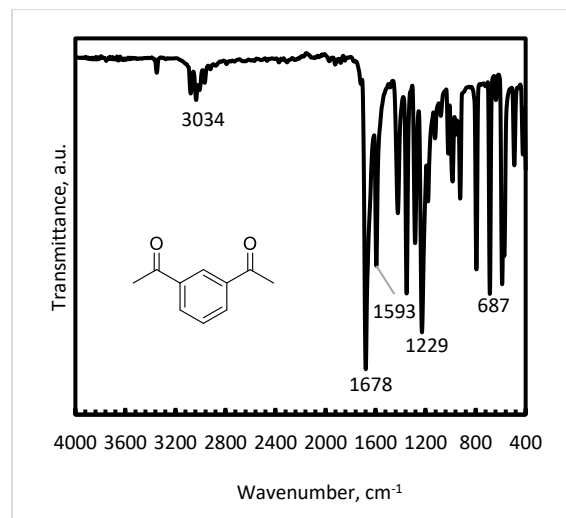


Figure S133. Infrared spectrum (ATR-FTIR) of 1,3-diacetylbenzene.

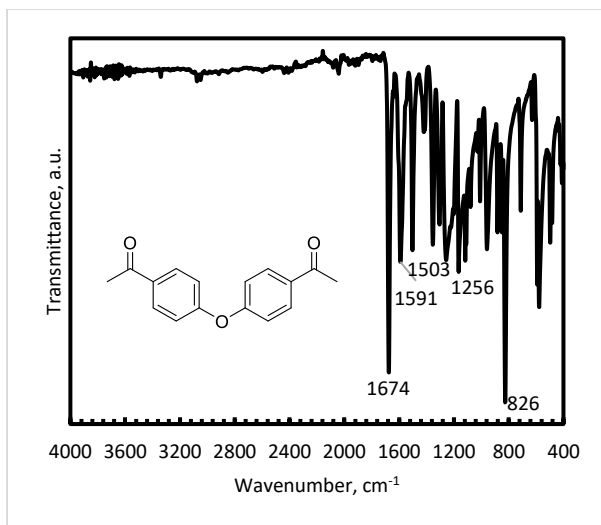


Figure S134. Infrared spectrum (ATR-FTIR) of 4-acetylphenyl ether.

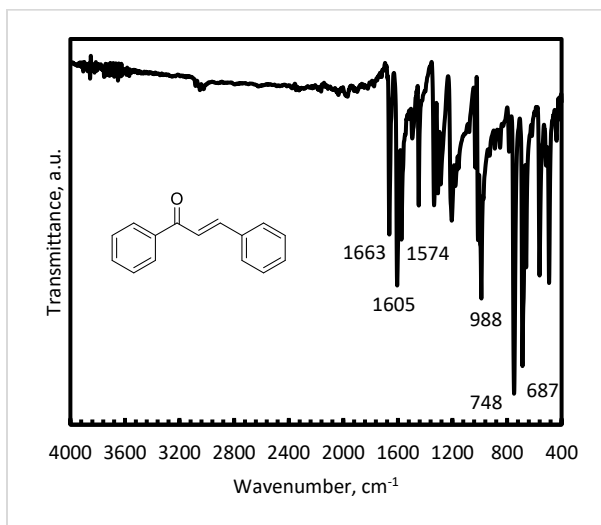


Figure S135. Infrared spectrum (ATR-FTIR) of *trans*-chalcone.

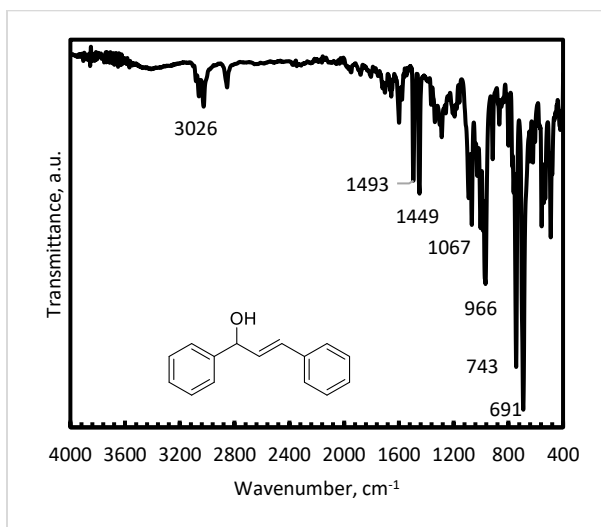


Figure S136. Infrared spectrum (ATR-FTIR) of (*E*)-1,3-diphenylprop-2-en-1-ol.

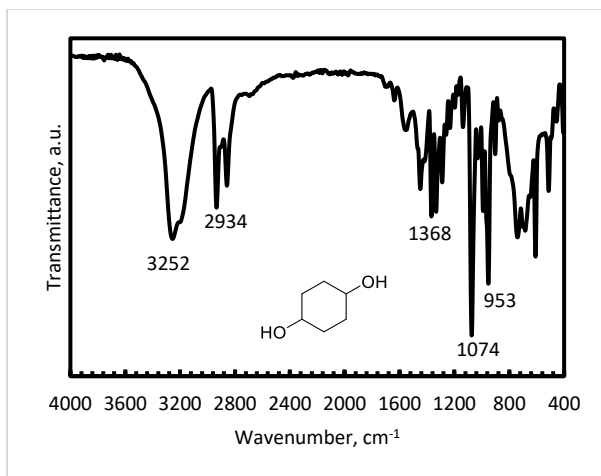


Figure S137. Infrared spectrum (ATR-FTIR) of 1,4-cyclohexanediol.

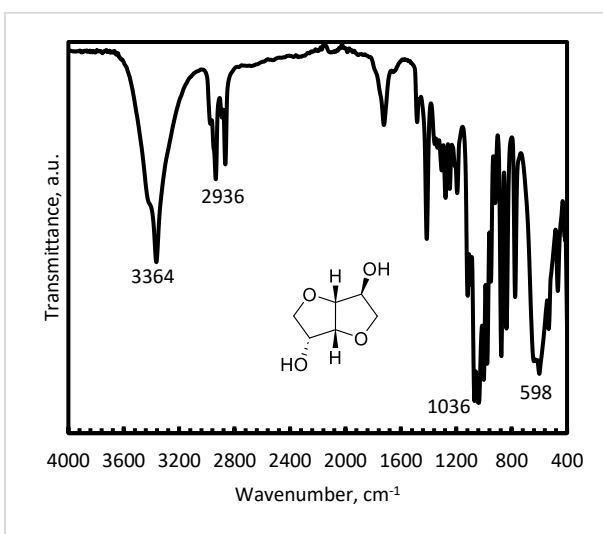


Figure S138. Infrared spectrum (ATR-FTIR) of D-isosorbide.

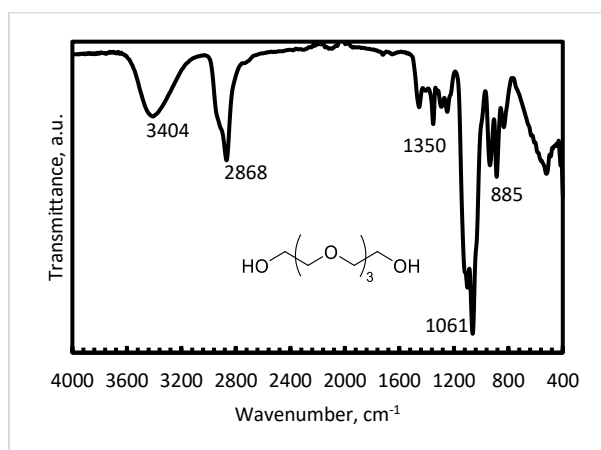


Figure S139. Infrared spectrum (ATR-FTIR) of tetraethylene glycol.

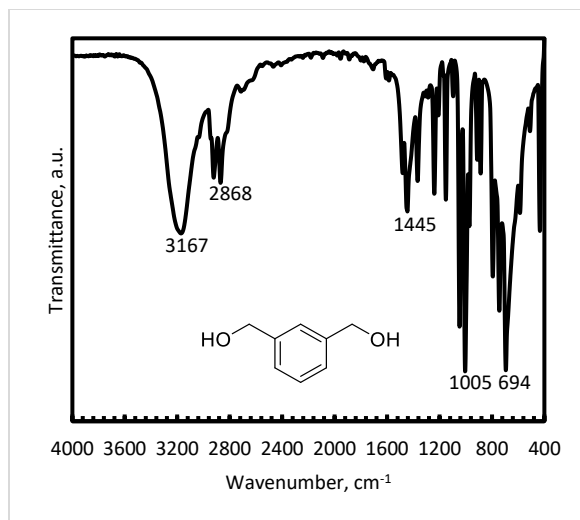


Figure S140. Infrared spectrum (ATR-FTIR) of 1,3-benzenedimethanol.

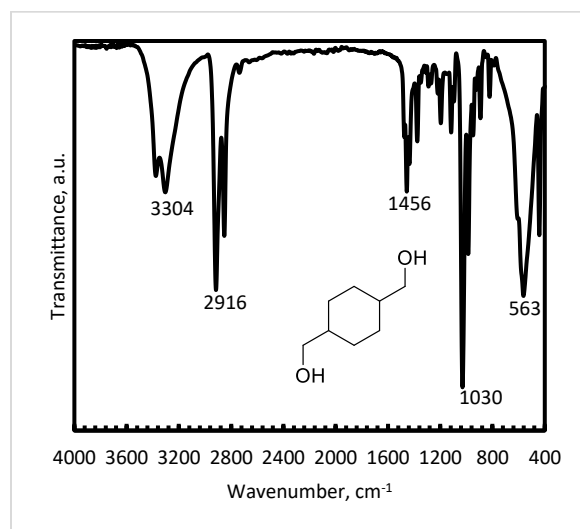


Figure S141. Infrared spectrum (ATR-FTIR) of 1,4-cyclohexanedimethanol.

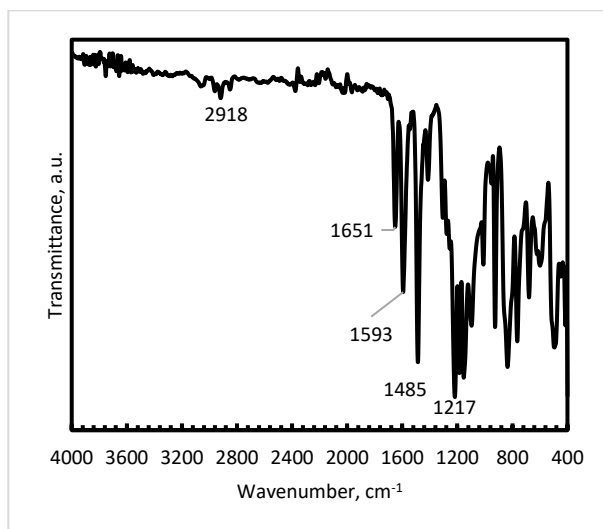


Figure S142. Infrared spectrum (ATR-FTIR) of commercial polymer PEEK.

### 1.14 TGA of commercial PEEK.

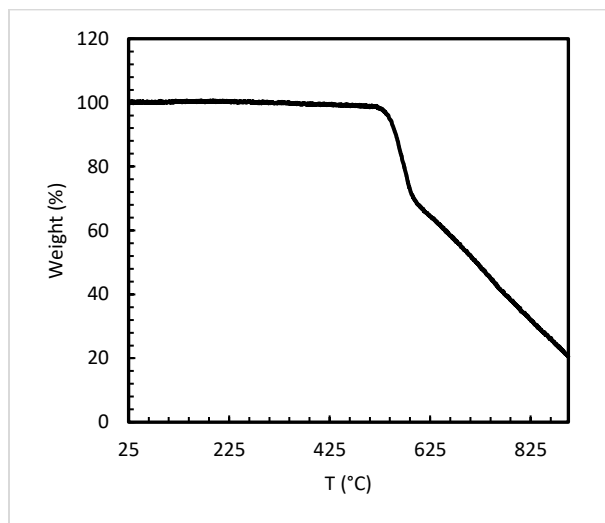


Figure S143. Mass loss as a function of temperature for commercial PEEK.

### 1.15 Powder XRD patterns of starting materials.

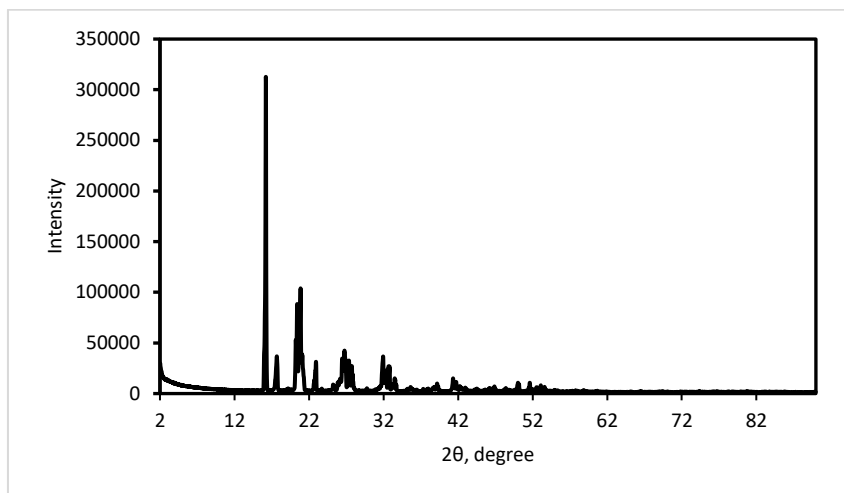


Figure S144. Experimental powder XRD patterns of 1,4-diacetylbenzene.

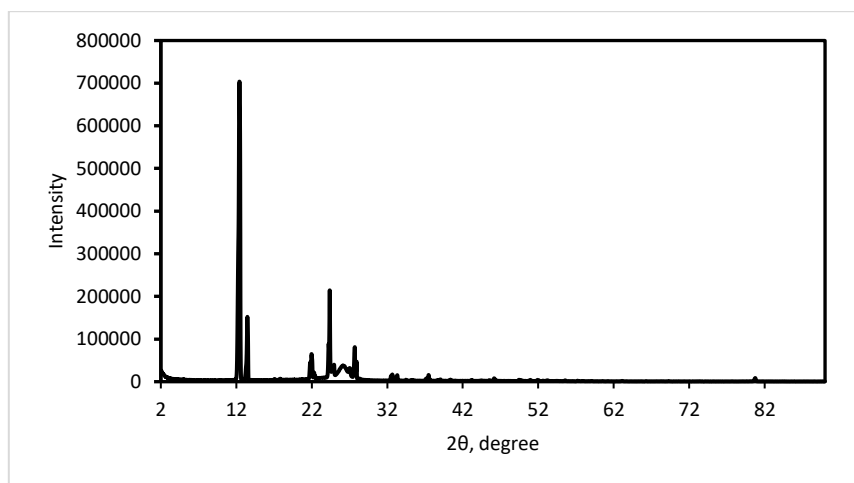


Figure S145. Experimental powder XRD patterns of 1,3-diacetylbenzene.

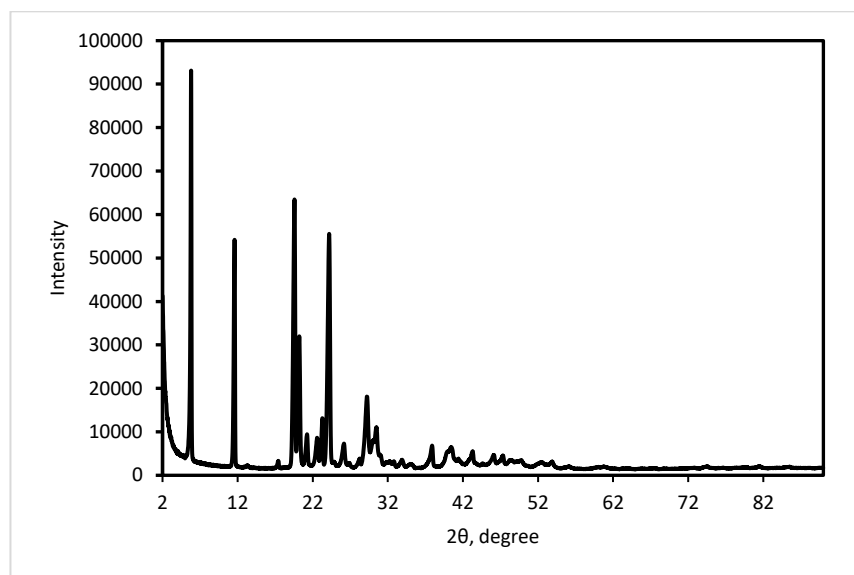
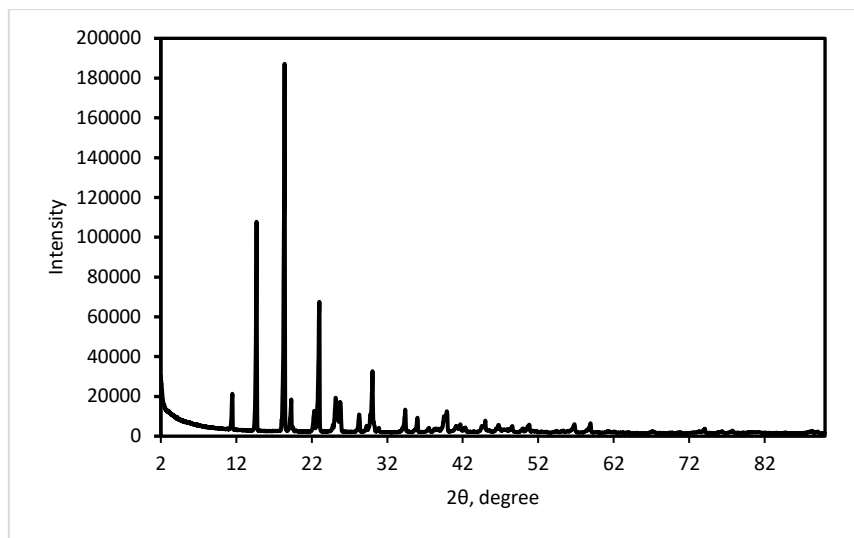
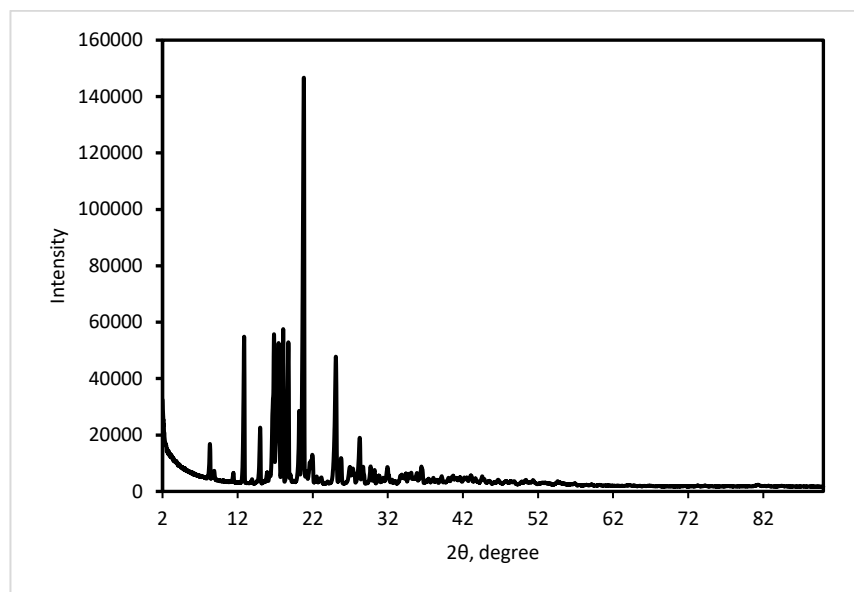


Figure S146. Experimental powder XRD patterns of 4-acetylphenyl ether.



**Figure S147.** Experimental powder XRD patterns of 1,4-benzenedimethanol.



**Figure S148.** Experimental powder XRD patterns of 1,4-cycloheanedimethanol.

## 1.16 Scanning Electron Microscopy

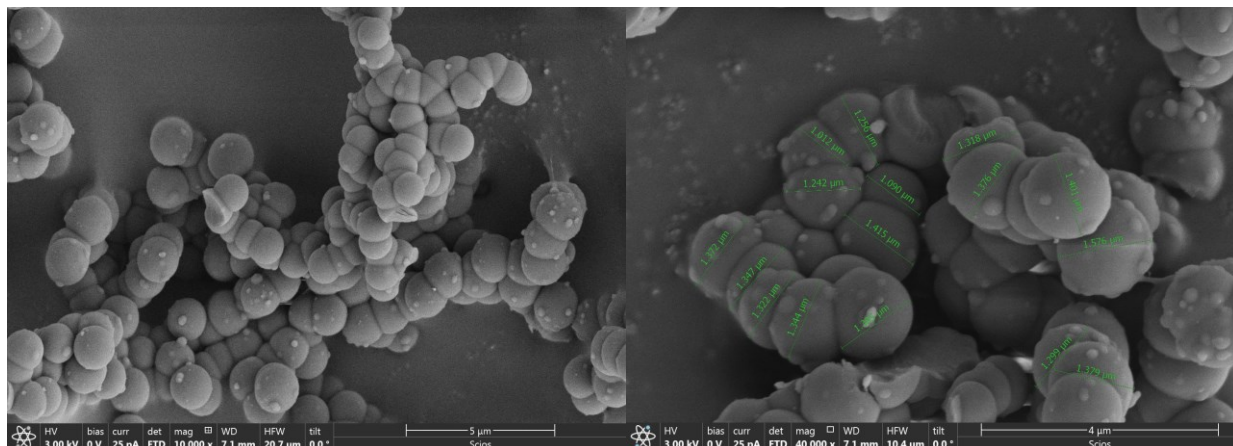


Figure S149. SEM micrographs of polyketone PAAK-1 corresponding to Table S1, Entry 9.

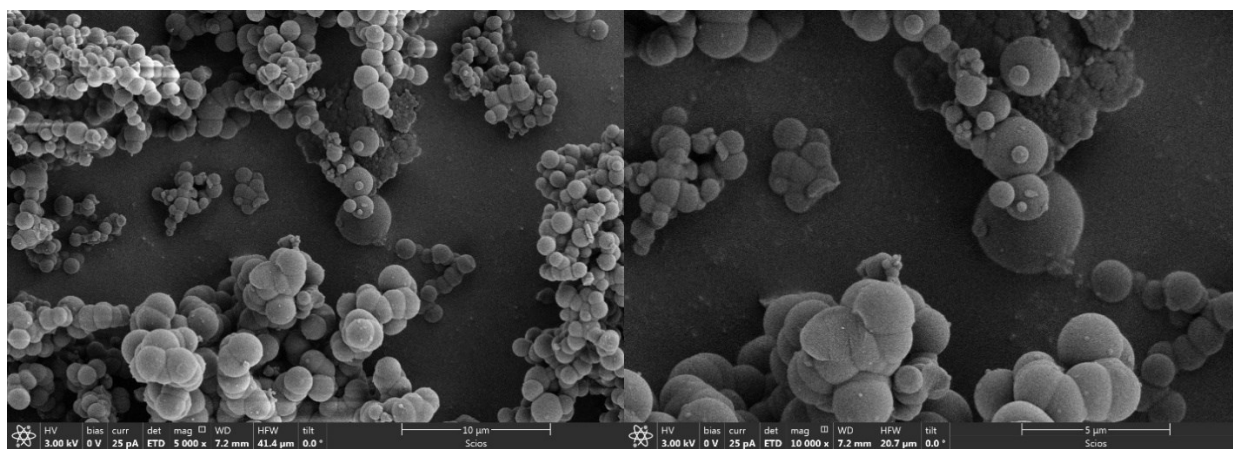


Figure S150. SEM micrographs of polyketone PAAK-2.

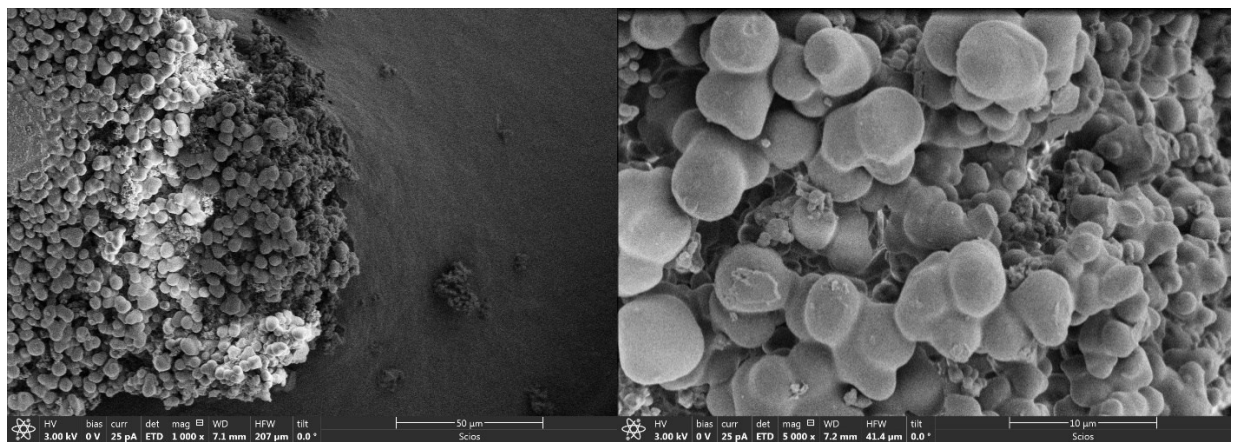
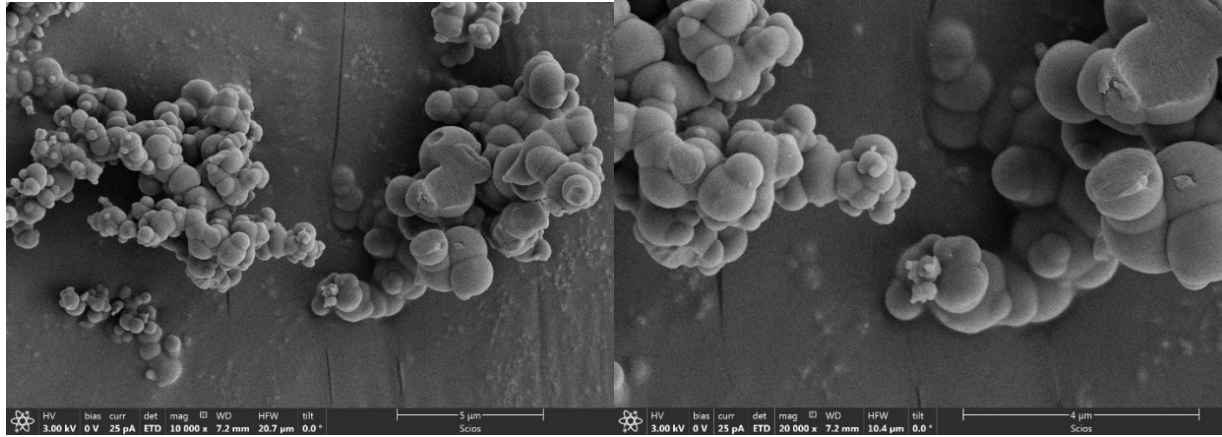
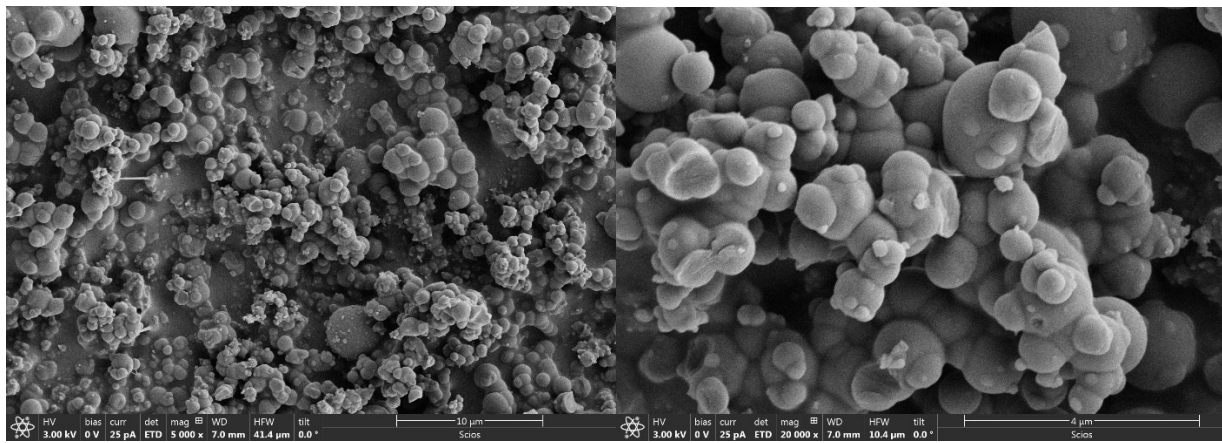


Figure S 151. SEM micrographs of polyketone PAAK-3.



**Figure S152.** SEM micrographs of polyketone PAAK-4.



**Figure S153.** SEM micrographs of polyketone PAAK-5.

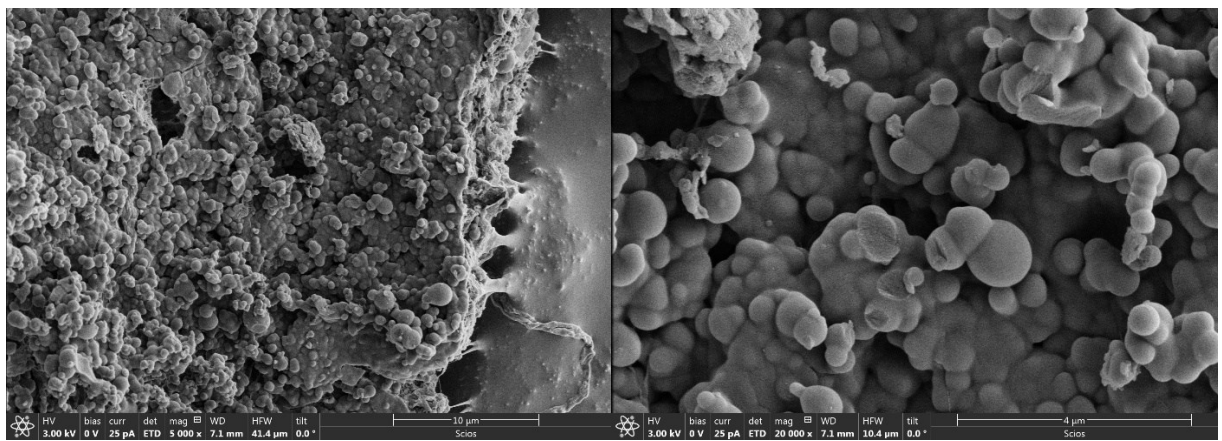


**Figure S154.** SEM micrographs of polyketone PAAK-6.

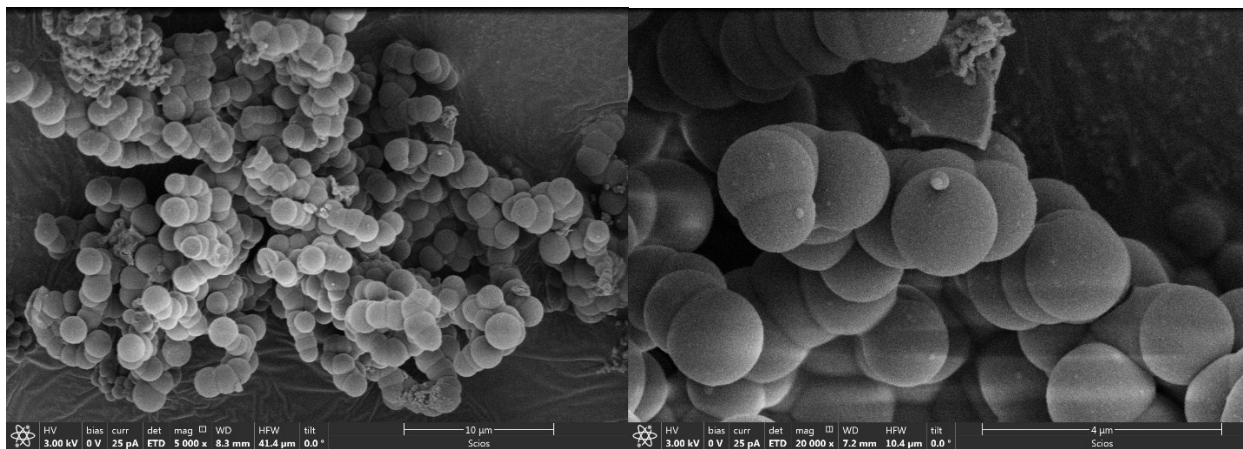


Figure S155. SEM micrographs of polyketone PAAK-7.

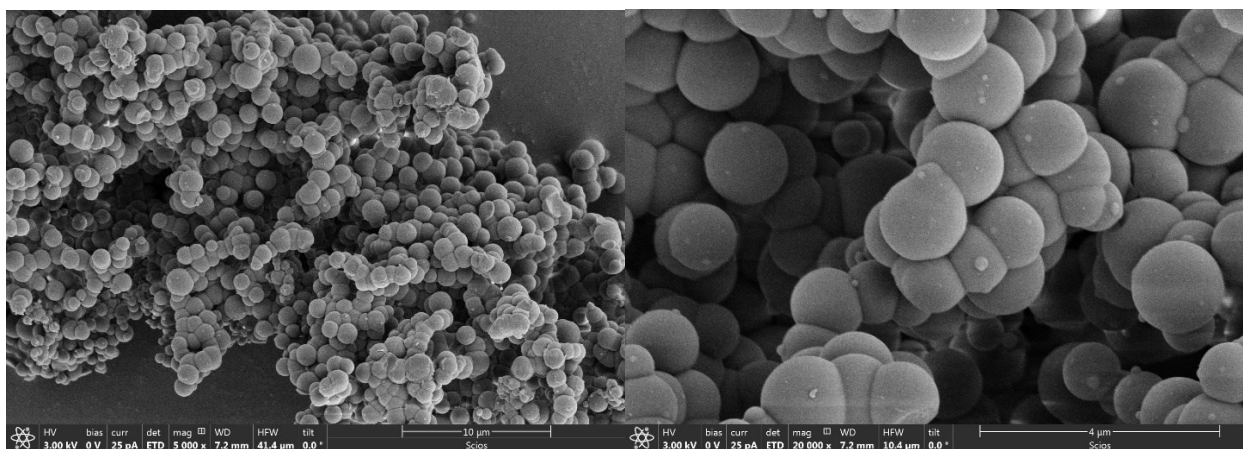


Figure S156. SEM micrographs of polyketone PAAK-8.

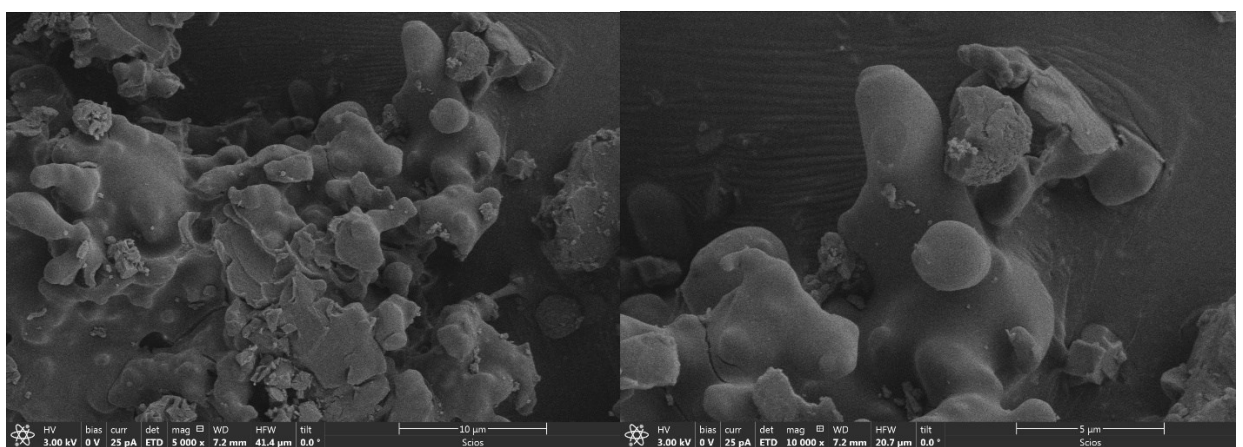
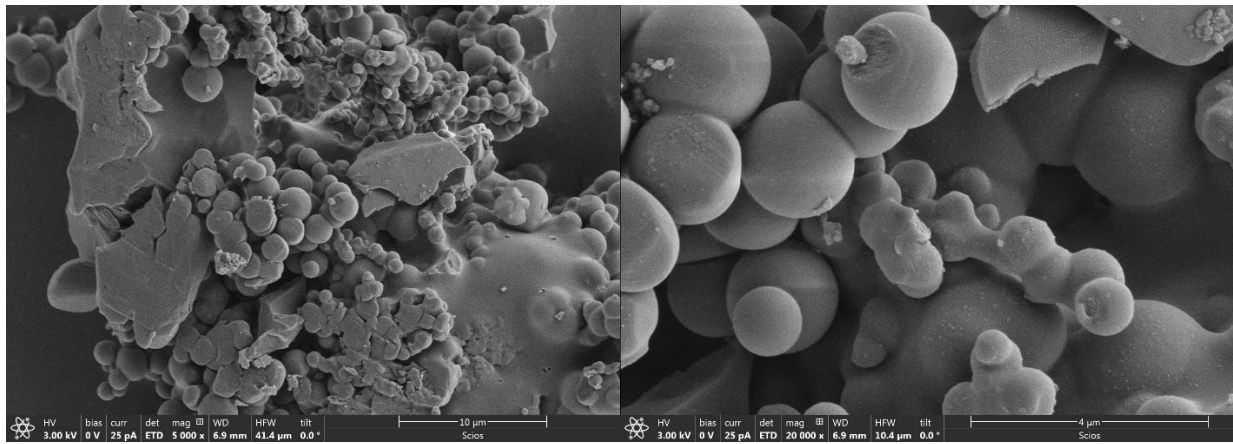
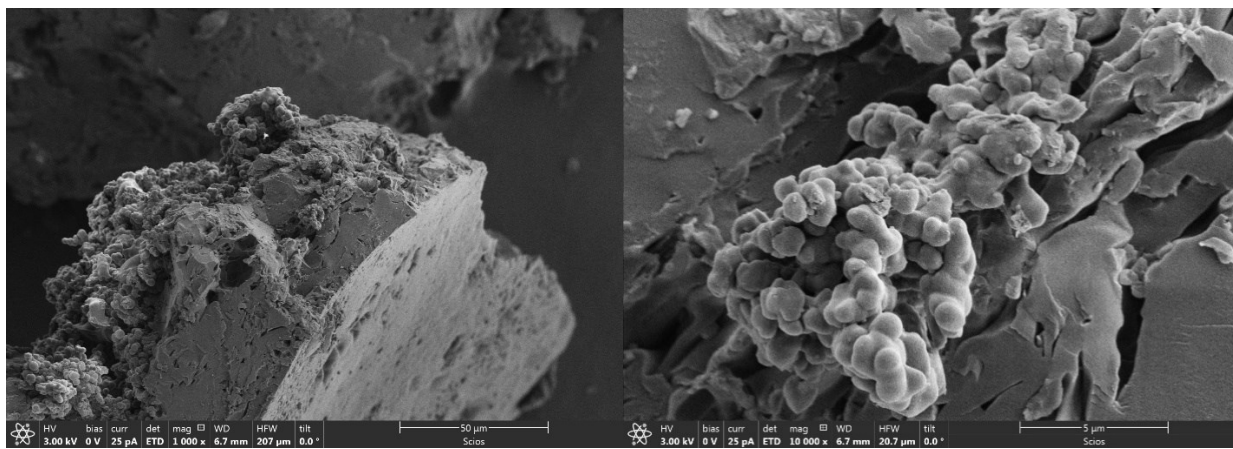


Figure S157. SEM micrographs of polyketone PAAK-9.



**Figure S158.** SEM micrographs of polyketone PAAK-10.



**Figure S159.** SEM micrographs of polyketone PAAK-11.

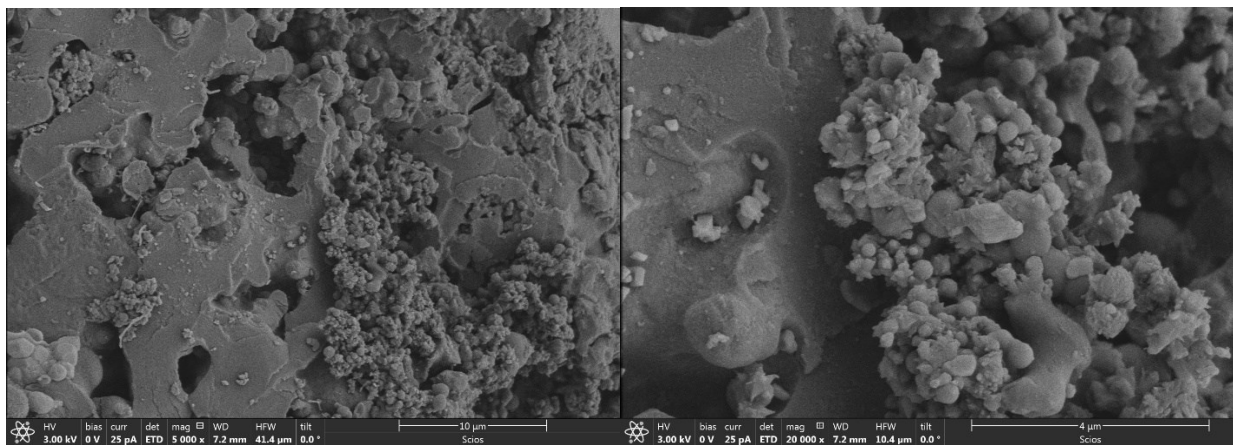


**Figure S160.** SEM micrographs of polyketone PAAK-12.

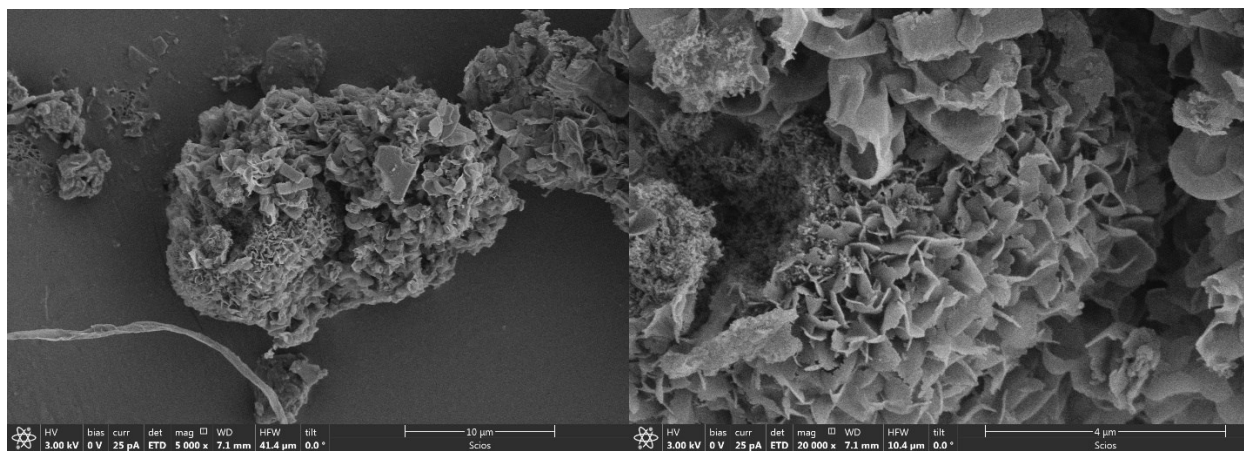


Figure S161. SEM micrographs of polychalcone PCH-1.

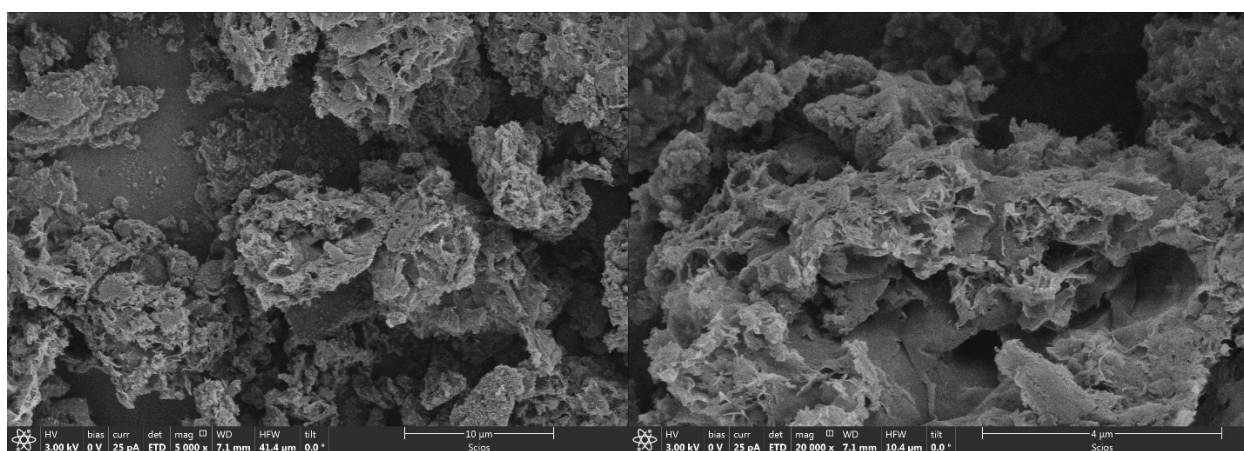


Figure S162. SEM micrographs of polychalcone PCH-7.

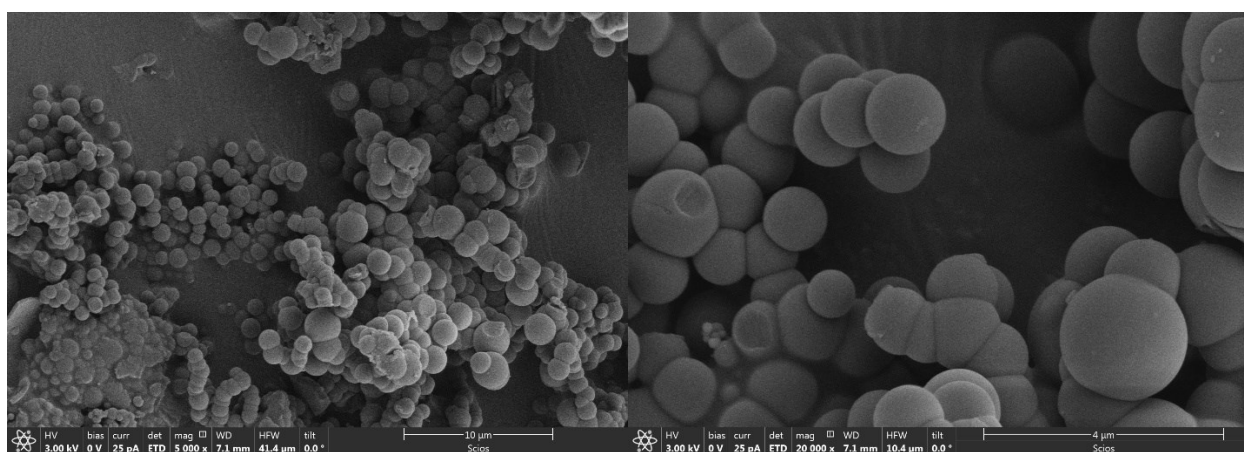


Figure S163. SEM micrographs of polyketone PAAK-1 obtained in atmosphere of hydrogen.

## 1.17 Powder XRD and Scanning Electron Microscopy analysis

**Table S3. Comments on the analysis of the obtained polymers with SEM and pXRD**

Entry	Polymer	SEM	Powder XRD	
			Crystalline state	d-spacing of the largest amorphous bump
1	<b>PAAK-1</b>	Spherical agglomerates (size ~1.5 $\mu\text{m}$ )	Amorphous phase clearly formed; size < 2 nm	4.94 $\text{\AA}$
2	<b>PAAK-2</b>	Spherical agglomerates (size ~0.5 $\mu\text{m}$ )	Amorphous phase clearly formed; size < 2 nm	4.90 $\text{\AA}$
3	<b>PAAK-3</b>	Inhomogeneous agglomerates with spherical particles (size ~3 $\mu\text{m}$ )	Amorphous phase clearly formed; size < 2 nm	5.19 $\text{\AA}$
4	<b>PAAK-4</b>	Spherical agglomerates (0.2-2 $\mu\text{m}$ )	Amorphous phase clearly formed; size < 2 nm	4.51 $\text{\AA}$
5	<b>PAAK-5</b>	Spherical agglomerates (0.1-2 $\mu\text{m}$ )	Amorphous phase clearly formed; size < 2 nm	4.90 $\text{\AA}$
6	<b>PAAK-6</b>	Inhomogeneous agglomerates with spherical particles (0.1-1 $\mu\text{m}$ )	Amorphous phase clearly formed; size < 2 nm	5.02 $\text{\AA}$
7	<b>PAAK-7</b>	Spherical agglomerates (size ~2 $\mu\text{m}$ )	Amorphous phase clearly formed; size < 2 nm	4.88 $\text{\AA}$
8	<b>PAAK-8</b>	Spherical agglomerates (size ~1 $\mu\text{m}$ )	Amorphous phase clearly formed; size < 2 nm	5.18 $\text{\AA}$
9	<b>PAAK-9</b>	Inhomogeneous agglomerates with spherical particles	Amorphous phase clearly formed; size < 2 nm	5.01 $\text{\AA}$
10	<b>PAAK-10</b>	Complex inhomogeneous agglomerates With incorporated spherical agglomerates (size ~2 $\mu\text{m}$ )	Amorphous phase clearly formed; size < 2 nm	4.52 $\text{\AA}$
11	<b>PAAK-11</b>	Complex inhomogeneous agglomerates	Amorphous phase clearly formed; size < 2 nm	4.52 $\text{\AA}$
12	<b>PAAK-12</b>	Complex inhomogeneous agglomerates	Amorphous phase clearly formed; size < 2 nm	4.97 $\text{\AA}$
13	<b>PCH-1</b>	Flakes-like crystallites	Semicrystalline material with large unit cell. Peaks are very broad so not possible to index.	
14	<b>PAAK-1</b> obtained in $\text{H}_2$	Spherical agglomerates (size ~0.7–2.1 $\mu\text{m}$ )	Amorphous phase clearly formed; size < 2 nm	4.84 $\text{\AA}$

## 2. Mechanical properties

PAAK-1 was prepared according to the method described in Table 2, entry 1 (main paper). The commercial sample of PEEK (450g rod, 300 mm length and 6mm diameter) studied here was purchased from the RS (<https://uk.rs-online.com/web/>). The commercial HDPE sample (granule, 2-4 mm particle, density: 0.930 g/cm<sup>3</sup>) studied here was purchased from the Goodfellow (<https://www.goodfellow.com/>).

**Processing of PAAK-1:** The polymer sample was immersed in liquid nitrogen for 30 minutes and pulverised. The polymer was then immersed in THF solvent overnight. Subsequently, the polymer was subjected to vacuum oven drying at 60°C for one hour to achieve complete solvent removal. The dried polymer powder was carefully sandwiched between the bottom and top plates of the mould, ensuring proper alignment. The assembled mould was then transferred to the heated surface of the Specac constant film maker (set to 300 °C). A constant pressure of 1900 N was applied to the mould for a minimum of one minute to induce the film formation. Upon completion of the film formation process, the mould was removed from the heating surface and allowed to cool completely. Once the mould had cooled, the film was carefully peeled off from the plates. The mould was specifically designed to create a cavity between the top and bottom plates, enabling the formation of a 2 mm film of uniform thickness.

Similarly, HDPE granules and PEEK samples were employed to fabricate 2 mm thick films through compression at the respective temperatures.

**Measurement of mechanical properties:** The mechanical properties were estimated using nanoindentation method. Nanoindentation techniques are widely employed to assess the mechanical properties of both materials and thin films. It enables the direct measurement of load applied to a sharp indenter and its displacement as a function of indentation depth. The values of hardness and elastic modulus can be extracted from the load-displacement curves obtained during loading and unloading cycles. All three films were individually mounted on a flat magnetic surface of the Nanoindenter. All measurements were conducted using a Nanoindenter Optics11 Chiaro instrument, employing a continuous stiffness method at a frequency of 25 Hz and a suitable displacement amplitude. A spherical indenter with a diameter of 18 µm and a stiffness of 39.53 N/m was utilised. Prior to the measurements, the equipment was calibrated using spherical indenter. Load-displacement curves were analysed using the Oliver and Pharr method [2] to extract mechanical properties. The elastic modulus was calculated based to the following relation. Further changes in equations are used as discussed in [3].

$$S = 2\beta E \sqrt{\frac{A}{\pi}}$$

where A, E, and S represent the contact area, elastic modulus, and contact stiffness, respectively. The geometric correction factor b was assumed to be unity [4]. Given the direct proportionality between the contact area and the square of the contact depth, its value was estimated through calibration using known polymer properties. The proportionality constant provided both the contact area and contact depth values in accordance with the methodology proposed in [5]. The contact stiffness value was determined by measuring the initial slope of the unloading curve, as depicted in **Figure S162** and **Figure S163**. The computed elastic moduli for each polymer are depicted in **Figure S164**. Additionally, the Vickers hardness (HV) values for each polymer were measured using a Mitutoyo series 810 HM 210/220 instrument and reported in **Figure S165**. The obtained values are consistent with previously reported values [6–9].

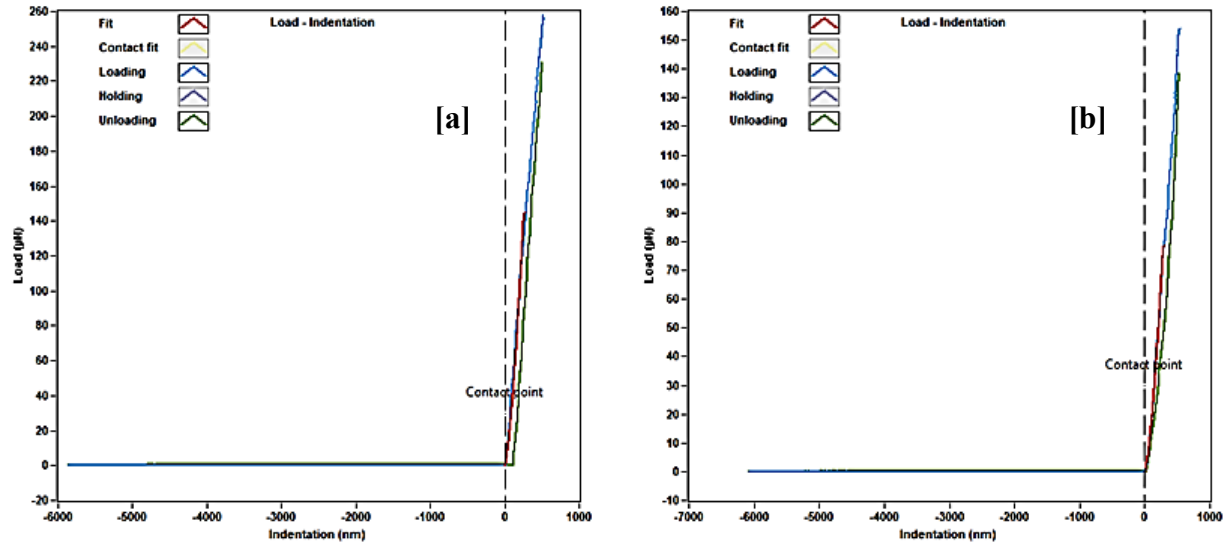


Figure S164. Loading and unloading curves for [a] PEEK and [b] HDPE.

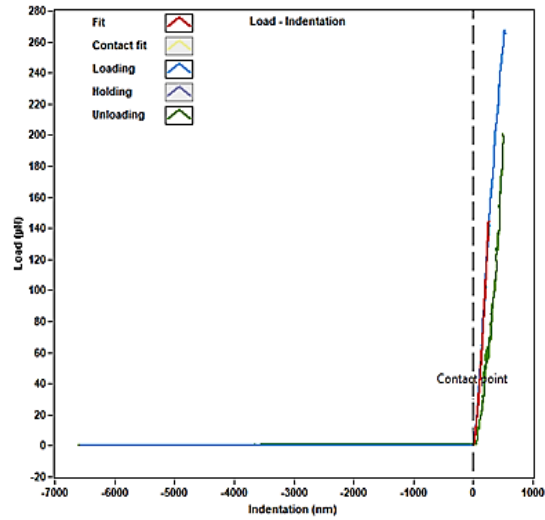


Figure S165. Loading and unloading curves for Polyketone PAAK-1.

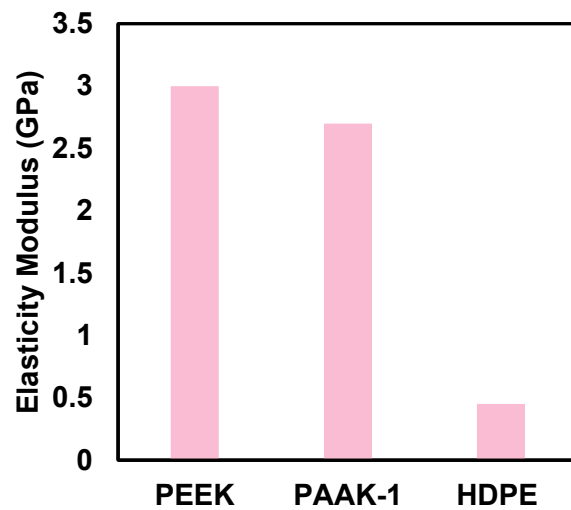


Figure S166. Elasticity modulus of polymers PEEK, PAAK-1 and HDPE.

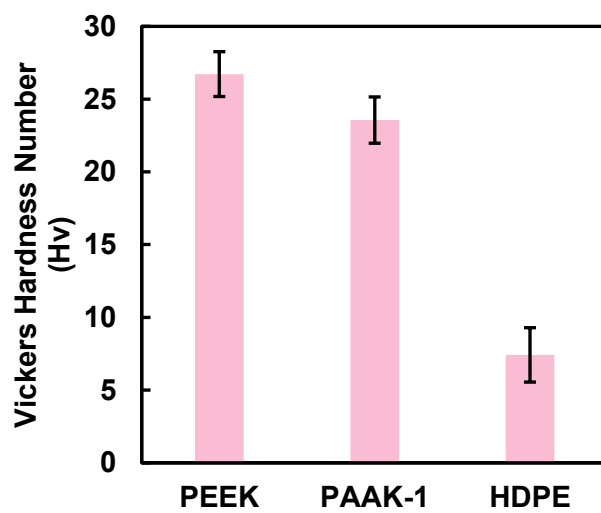


Figure S167. Vickers hardness number of polymers PEEK, PAAK-1 and HDPE.

### 3. References

- [1] M. Peña-López, P. Piehl, S. Elangovan, H. Neumann, M. Beller, “Manganese-Catalyzed Hydrogen-Autotransfer C–C Bond Formation:  $\alpha$ -Alkylation of Ketones with Primary Alcohols.” *Angew. Chem. Int. Ed.* **2016**, 55, 14967.
- [2] J. Liu, K.-F. Hu, J.-P. Qu, and Y.-B. Kang, “Organopromoted Selectivity-Switchable Synthesis of Polyketones” *Organic Letters* **2017** 19 (20), 5593.
- [3] O. C W. Carl, and G. M. Pharr. “An improved technique for determining hardness and elastic modulus using load and displacement sensing indentation experiments.” *Journal of materials research* **1992**, 7(6), 1564.
- [4] A. C. Fischer-Cripps. “Examples of nanoindentation testing.” *Nanoindentation* **2002**, 159.
- [5] G. Hochstetter, A. Jimenez, and J. L. Loubet. “Strain-rate effects on hardness of glassy polymers in the nanoscale range. Comparison between quasi-static and continuous stiffness measurements.” *Journal of Macromolecular Science—Physics* **1999**, 38(5-6), 681.
- [6] L. Chengzhu, Y. Li, and S. C. Tjong. “Polyetheretherketone and its composites for bone replacement and regeneration.” *Polymers* **2020**, 12 (12), 2858.
- [7] Y. Yutao, C. Jiang, Y. Huo, and C. Li. “Preparation and tribological behaviors of lubrication-enhanced PEEK composites.” *Applied Sciences* **2020**, 10 (21), 7536.
- [8] R. T. Tebeta, A. M. Fattahi, and N. A. Ahmed. “Experimental and numerical study on HDPE/SWCNT nanocomposite elastic properties considering the processing techniques effect.” *Microsystem Technologies* **2020**, 26, 2423.
- [9] V. Nectarios, M. Petousis, and A. Maniadi. “Sustainable Additive Manufacturing: Mechanical Response of High-Density Polyethylene over Multiple Recycling Processes.” *Recycling* **2021**, 6(1), 4.